Ispitivanje inačica poboljšanih funkcija zida u simulaciji turbulentnog strujanja

Šutalo, Filip

UNIVERSITY OF ZAGREB

Faculty of Mechanical Engineering and Naval Architecture

MASTER'S THESIS

Filip Šutalo

Zagreb, 2017

UNIVERSITY OF ZAGREB

Faculty of Mechanical Engineering and Naval Architecture

Evaluation of Variants of Enhanced Wall Treatment Wall Function in Turbulent Flow Simulations

Supervisor:

Prof. Hrvoje Jasak, PhD

Student:

Filip Šutalo

Zagreb, 2017

I hereby declare that this thesis is entirely the result of my own work except where otherwise indicated. I have fully cited all used sources and I have only used the ones given in the list of references.

Many people contributed to this work. I express my gratitude to the following people: Gregor, Inno, Robert, Tessa, Vanja, Vuko. Each of them dedicated their time whenever I needed an advice. I would also like to thank Željko Tuković for his endless patience and guidance.

Many thanks to my mentor Hrvoje Jasak for entrusting me with this topic and for discussions about the turbulence modelling.

I express my sincere gratitude to my parents for all the support they have provided me over the years. To my girlfriend Kristina who has motivated me throughout the entire process. Thank you for your patience and for being of such great support.

Finally, and most importantly. This thesis I dedicate to a one person without whom I surely would not even consider pursuing higher education. Thank you for all your support.

To my friend

Vjekoslav Gavrić

SVEUČILIŠTE U ZAGREBU
FAKULTET STROJARSTVA I BRODOGRADNJE
Središnje povjerenstvo za završne i diplomske ispite
Povjerenstvo za diplomske ispite studija strojarstva za smjerove:
procesno-energetski, konstrukcijski, brodostrojarski i inženjersko modeliranje i računalne simulacije

Sveučilište u Zagrebu Fakultet strojarstva i brodogradnje	
Datum	Prilog
Klasa:	
Ur.broj:	

DIPLOMSKI ZADATAK

Student: **Filip Šutalo** Mat. br.: 0035184175

Naslov rada na hrvatskom jeziku: **Ispitivanje inačica poboljšanih funkcija zida u simulaciji turbulentnog strujanja**

Naslov rada na engleskom jeziku: **Evaluation of variants of enhanced wall treatment wall function in turbulent flow simulations**

Opis zadatka:

Industrial simulations of turbulent flows using Computational Fluid Dynamics (CFD) regularly rely on Reynolds Averaged Navier-Stokes (RANS) equations and corresponding turbulence models, with the wall function near-wall treatment, originally developed by Spalding et al. in 1970s. The basic assumption of the near-wall treatment is that the near-wall flow is in equilibrium and unaffected by the mean pressure gradient, wall curvature and other local factors. To remedy its deficiencies, numerous extensions to wall functions have been proposed, claiming ability to capture non-equilibrium near-wall effects.
In this study, the candidate shall provide an overview of model formulations and examine their performance on two canonical flows for most popular combinations of eddy viscosity models and enhanced wall treatment models.

The candidate shall perform the following tasks within this project:

- perform a literature survey of most popular enhanced wall treatments used with the k-epsilon, and k-omega SST models and document their formulation. For models currently unavailable in OpenFOAM CFD software, the candidate shall implement the models within the existing framework. Propose a set of turbulence models and near-wall treatment for validation,
- perform simulations of a steady turbulent incompressible flow around the NACA 4412 airfoil in 2D and compare the results against available experimental data and reference numerical results,
- perform simulations of a steady turbulent incompressible flow around a prolate spheroid geometry in 3D and compare the results against available experimental data and reference numerical results,
- present the comparison of results in terms of accuracy, stability and computational time and propose an appropriate choice of turbulence modelling for the selected cases.

The Thesis shall list the bibliography and any assistance received during this study.

Zadatak zadan:	Rok predaje rada:	Predviđeni datumi obrane:
19. siječnja 2017.	23. ožujka 2017.	29., 30. i 31. ožujka 2017.

Zadatak zadao: Predsjednica Povjerenstva:

Prof. dr. sc. Hrvoje Jasak

Prof. dr. sc. Tanja Jurčević Lulić

Table of Contents

List of Figures

List of Tables

Nomenclature

Greek letters

β_1	Model constant	-
β_2	Model constant	-
γ_1	Model constant	-
γ_2	Model constant	-
β^*	Model constant	-
α	Dimensionless pressure parameter	-
$\alpha_{\omega 1}$	Model constant	-
$\alpha_{\omega 2}$	Model constant	-
$\alpha_{\mathrm{k}1}$	Model constant	-
$\alpha_{\mathrm{k}2}$	Model constant	-
ε	Dissipation rate	m^2/s^3
ε_{BC}	Wall boundary condition for dissipation rate	m^2/s^3
Γ	Argument for Kader blending	-
$\Gamma_{\varepsilon,eff}$	Effective diffusivity for ε	m^2/s
$\Gamma_{\omega,eff}$	Effective diffusivity for ω	m^2/s
$\Gamma_{k,eff}$	Effective diffusivity for k	m^2/s

κ	von Kármán constant	-
ν	Molecular viscosity	m^2/s
ν_t	Eddy viscosity	m^2/s
${\nu_t}^w$	Artificial eddy viscosity	m^2/s
ω	Specific dissipation rate	1/s
ω_{log}	Speciffic dissipation rate in viscous sublayer	1/s
ω_{vis}	Speciffic dissipation rate in viscous sublayer	1/s
$\overset{+}{\omega}_{log}$	Dimensionless specific dissipation rate in logarithmic sublayer	-
$\overset{+}{\omega}_{vis}$	Dimensionless specific dissipation rate in viscous sublayer	-
$\overset{+}{\omega}_{w}$	Dimensionless specific dissipation rate at the wall	-
ρ	Density	kg/m^3
σ_ε	Model constant	-
τ_w	Wall shear stress	N/m^2
τ_{xy}	Component of shear stress tensor	N/m^2
C_μ	Model constant	-
y_v	Turbulent wall shear stress near the wall	N/m^2

Latin letters

a_1	Model constant	-
c_1	Model constant	-
$\mathbf{u}'$	Fluctuating velocity field	m/s
$\overline{\mathbf{u}}$	Mean velocity field	m/s
$\overline{p}$	Mean kinematic pressure field	m^2/s^2

$\mathbf{I}$	Identity tensor	-
$\mathbf{R}$	Reynolds stress tensor	m^2/s^2
$\mathbf{S}$	Strain rate magnitude	1/s
$\mathbf{u}$	Velocity field	m/s
$\overline{u}$	Magnitude of velocity vector parallel to wall	m/s
u^+_{log}	Dimensionless velocity distribution in logarithmic sublayer	-
u^+_{vis}	Dimensionless velocity distribution in viscous sublayer	-
u^*	Velocity scale	m/s
u_τ	Friction velocity	m/s
y^+	Dimensionless distance from the wall	-
y^*	Dimensionless distance from the wall	-
A	Constant for near-wall fluctuating velocity	1/s
arg_1	Argument for function $F1$	-
arg_2	Argument for function $F2$	-
arg_3	Argument for function $F3$	-
B	Constant for near-wall fluctuating velocity	1/ms
B	Constant in law of the wall	-
C	Constant for near-wall fluctuating velocity	1/s
c	Aerofoil chord length	m
c	Integration constant in mean velocity distribution	m/s
C_1	Model constant	-
C_2	Model constant	-

$CD_{k\omega+}$	Positive portion of the cross-diffusion in ω equation	-
$CD_{k\omega}$	Cross-diffusion in ω equation	-
E	Constant in law of the wall	-
F_1	Blending function	-
F_2	Blending function	-
F_23	Blending function	-
F_3	Blending function	-
G	Turbulent kinetic energy production	m^2/s^3
k	Turbulent kinetic energy	m^2/s^2
L	Characteristic length	m
L	Length of prolate spheroid	m
l_m	Mixing length	m
p	Kinematic pressure	m^2/s^2
p'	Fluctuating kinematic pressure field	m^2/s^2
Re	Dimensionless parameter	-
Re_c	Reynolds number based on aerofoil chord length	-
Re_L	Reynolds number based on prolate spheroid length	-
S	Strain rate magnitude	1/s
S_2	Squared modulus of the mean strain rate tensor	$1/s^2$
t	Time	s
U_∞	Freestream velocity	m/s
v_m	Mixing velocity	m/s

y	Normal distance from the wall	m
y_v	Thickness of the viscous sublayer	m
$u_{\tau log}$	Friction velocity in logarithmic sublayer	m/s
$u_{\tau vis}$	Friction velocity in viscous sublayer	m/s

Abbreviations

CFD Computation Fluid Dynamics

DNS Direct Numerical Simulation

LES Large Eddy Simulation

DES Detached Eddy Simulation

RANS Reynolds Averaged Navier-Stokes Equations

EVM Eddy viscosity Model

FVM Finite Volume Method

HRN High Reynolds Number

LRN Low Reynolds Number

NACA National Advisory Committee for Aeronautics

CPU Central processing unit

Abstract

This work presents several treatments of the wall boundary conditions for RANS turbulence models. The focus is the investigation of wall functions suitable for non-equilibrium conditions where the standard wall functions derived from the law-of-the-wall are known to fail.
Although the thesis focuses on wall treatments, for deeper understanding of the problem, knowledge of turbulence modelling is essential. Therefore some key concepts are outlined through a derivation of the law-of-the-wall. Also, analytical solutions for the $k-\varepsilon$ and $k-\omega$ SST model for near-wall regions are given. A property, which defines the treatment of the wall boundary condition, is the asymptotic consistency of turbulence model which is briefly discussed. A general methodology for specifying the wall boundary condition is explained and expressions for each method are presented in detail. Wall treatment for the $k-\omega$ SST model based on pressure sensitised law-of-the-wall [1] is derived in detail and leads to a conclusion that including the convective terms in expressions could improve accuracy.
The wall treatments are implemented in `foam-extend` and compared with standard wall functions on two test cases: flow past the NACA4412 aerofoil and the 6:1 prolate spheroid. A conclusion is reached that certain wall treatments offer an advantage over standard ones implemented in `foam-extend`, although it is emphasised that further investigation on the effects of pressure gradient and convective terms should be conducted.

Key words: CFD, `foam-extend`, turbulence modelling, $k-\varepsilon$ wall functions, $k-\omega$ SST wall treatments, NACA4412, prolate spheroid

Sažetak

Ovaj rad prikazuje implementaciju i rezultate simulacija za zidne funkcije za modele turbulencije s dvije transportne jednadžbe. Fokus je na ispitivanju zidnih funkcija primjerenih u uvjetima neravnotežnog turbulentnog graničnog sloja za koje standardne zidne funkcije izvedene iz zakona zida nisu prikladne.
Iako se rad primarno fokusira na zidne funkcije, za dublje razumijevanje problema nužno je poznavati principe o modeliranju turbulencije. Iz tog razloga, istaknuti su osnovni koncepti pri izvođenju zakona zida. Izrazito važno svojstvo, koje definira postupanje s rubnim uvjetima na zidu, je asimptotska konzistentnost modela turbulencije, koja je ukratko pojašnjena. Generalna metodologija specificiranja rubnih uvjeta na zidu je objašnjena, te su dani izvodi matematičkih izraza za svaku metodu. Tretman rubnih uvjeta na zidu za $k-\omega$ SST model temeljen na izrazu za neravnotežni turbulentni granični sloj [1] izveden je detaljno i vodi k zaključku da uključivanjem konvektivnih članova u izraze može dovesti do poboljšanja u točnosti.
Prikazane zidne funkcije, ugrađene su u `foam-extend` i uspoređeni sa standardnim zidnim funkcijama za dva slučaja: opstrujavanje NACA4412 aeroprofila i opstrujavanje rotacijskog elipsoida. Zaključeno je da određeni tretmani rubnih uvjeta na zidu nude prednost nad trenutačno korištenima u `foam-extendu`, no i da je potrebna daljnja analiza utjecaja gradijenta tlaka i konvektivnih članova.

Ključne riječi: CFD, `foam-extend`, modeliranje turbulencije, $k-\varepsilon$ zidne funkcije, $k-\omega$ SST tretman rubnih uvjeta na zidu, NACA4412, rotacijski elipsoid.

Prošireni sažetak

Turbulencija i dan danas predstavlja izazov i jednu od glavnih izazova u analizi strujanja fluida. Kaotična priroda ovog fizikalnog fenomena otežava znanstvenu analizu stoga i ne čudi da su svi modeli turbulencije zapravo samo aproksimacije koje kada se koriste u numeričkim simulacijama treba koristiti s oprezom. Sljedeći problem u numeričkoj analizi turbulentnog strujanja su područja u blizini zida gdje dominiraju veliki gradijenti pojedinih fizikalnih veličina. Razrješavanje ovog područja uvelike povećava zahtjeve na računalne resurse, stoga je najčešći pristup u područjima blizine zida koristiti takozvane zidne funkcije. One povezuju vrijednosti sa zida sa strujanjem podalje od stijenke, time premošćujući područja velikih gradijenata. Najčešće korištene zidne funkcije temeljene su na zakonu zida koje su izvedene korištenjem pretpostavki o lokalnoj ravnoteži, tj. da su vrijednosti karakterističnih turbulentnih veličina ovisne samo o lokalnim parametrima strujanja te da uzstrujni efekti nisu od velike važnosti. U ovom radu testirane su razne inačice zidnih funkcija od kojih su neke dane i za slučajeve neravnotežnog turbulentnog graničnog sloja.

Jednadžbe nestlačivog turbulentnog strujanja

Turbulencija je potpuno opisana Navier-Stokesovim jednadžbama, no zbog same kompleksne prirode te pojave, rješavanje tih jednadžbi za probleme od industrijskog značaja još uvijek je van dosega trenutno dostupnih računalnih resursa. Umjesto toga, u široj upotrebi su takozvani modeli turbulencije koji uz dodatan set jednadžbi modeliraju utjecaj turbulencije na osrednjene veličine. U ovom radu analizirane su zidne funkcije na Reynoldsovim jednadžbama za nestlačivo strujanje s uključenom Boussinesqovom hipotezom:

$$\frac{\partial \overline{\mathbf{u}}}{\partial t} + \nabla \cdot (\overline{\mathbf{u}} \otimes \overline{\mathbf{u}}) = -\nabla(\overline{p} + \frac{2}{3}k) + \nabla \cdot [(\nu + \nu_t)(\nabla \overline{\mathbf{u}} + \nabla \overline{\mathbf{u}}^T)], \tag{1}$$

u kojima se turbulentna viskoznost ν izražava pomoću dodatne dvije turbulentne veličine za koje se transportne jednadžbe modeliraju. U izrazu (1), $\overline{\mathbf{u}}$ označava osrednjenu brzinu, $\overline{p}$ osrednjeno polje tlaka po jedinici gustoće, k turbulentnu kinetičku energiju i ν kinematsku viskoznost. Za definiranje turbulentne viskoznosti korištena su dva modela, $k-\varepsilon$ i $k-\omega$ SST model čiji su izrazi izloženi u nastavku.

$k-\varepsilon$ model za nestlačivo strujanje

$k-\varepsilon$ model opisuje turbulentne pojave sljedećim izrazima:

- Turbulentna viskoznost:

$$\nu_t = C_\mu \frac{k^2}{\varepsilon}. \tag{2}$$

- Turbulentna kinetička energija:

$$\frac{\partial k}{\partial t} + \nabla \cdot (\overline{\mathbf{u}} k) - k \nabla \cdot \overline{\mathbf{u}} - \nabla \cdot (\Gamma_{k,eff} \nabla k) = G - \varepsilon. \tag{3}$$

- Brzina disipacije turbulentne kinetičke energije:

$$\frac{\partial \varepsilon}{\partial t} + \nabla \cdot (\overline{\mathbf{u}} \varepsilon) - \varepsilon \nabla \overline{\mathbf{u}} - \nabla (\Gamma_{\varepsilon,eff} \nabla \varepsilon) = C_1 \frac{\varepsilon}{k} G - C_2 \frac{\varepsilon^2}{k}. \tag{4}$$

$k-\omega$ SST model za nestlačivo strujanje

Transportne jednadžbe za $k-\omega$ SST model dane su u nastavku.

- Turbulentna viskoznost

$$\nu_t = \frac{a_1 k}{\max(a_1 \omega, b_1 F_{23} S_2)} \tag{5}$$

- Turbulentna kinetička energija

$$\frac{\partial k}{\partial t} + \nabla \cdot (\overline{\mathbf{u}} k) - k \nabla \cdot \overline{\mathbf{u}} - \nabla \cdot (\Gamma_{k,eff} \nabla k) = \min(G, c_1 \beta^* k \omega) - \beta^* k \omega \tag{6}$$

- Brzina disipacije po jedinici turbulentne kinetičke energije

$$\frac{d\omega}{dt} + \nabla \cdot (\overline{\mathbf{u}}\omega) - \omega\nabla \cdot \overline{\mathbf{u}} - \nabla \cdot (\Gamma_{\omega,eff}\nabla\omega) = \gamma \min\left[S2, \frac{c_1}{a_1}\beta^*\omega \max\left(a_1\omega, b_1 F_{23}\sqrt{S_2}\right)\right] - \beta\omega^2 + (1-F_1)CD_{k\omega}. \tag{7}$$

U prethodnim izrazima ε je brzina disipacije turbulentne kinetičke energije, ω brzina disipacije po jedinici turbulentne kinetičke energije, a član G predstavlja produkciju turbulentne kinetičke energije.

Izloženi izrazi predstavljaju modele turbulencije implementirane u `foam-extend` a više detalja o njima može se naći u [2] i[3] za $k-\varepsilon$ models i [4], [5] i [6] za $k-\omega$ SST model, kao i u izvornom kodu `foam-extend` paketa.

Općeniti pristup zidnih funkcija

Najkonzistentniji pristup u slučaju velikih gradijenata u blizini zida je koristiti dovoljno sitnu prostornu diskretizaciju da bi se strujanje uspješno razriješilo. Fizikalno gledajući, prvi volumen na zidu mora biti u viskoznom podsloju, $y^+ < 0.5$, gdje je y^+ predstavlja bezdimenzijsku mjeru udaljenosti od zida definiranu kao:

$$y^+ = \frac{\sqrt{\frac{\tau_w}{\rho}}y}{\nu}, \tag{8}$$

pri čemu τ_w predstavlja predstavlja smično naprezanje na zidu, a y udaljenost prve proračunske točke profila brzine od zida.

Vrlo često u upotrebi je i drugačija definicija za bezdimenzijsku udaljenost:

$$y^* = \frac{{C_\mu}^{1/4}k^{1/2}y}{\nu}. \tag{9}$$

Pristup razriješavanja strujanja u blizini zida uvelike povećava broj kontrolnih volumena u proračunu, vodeći ka duljim vremenima numeričkih simulacija. Nadalje, ovaj pristup je primjeren samo sa modelima turbulencije koji se mogu primjenjivati u viskoznom podsloju, kao

predstavljeni $k-\omega$ SST model. U slučaju $k-\varepsilon$ modela, potrebno je koristiti zidne funkcije ili posebno formulirane modele, npr. Launder-Sharma ili Lam-Bremhorst $k-\varepsilon$ [7] model turbulencije.

Korištenjem zakona zida, računalni zahtjevi uslijed velikih gradijenata na zidu mogu biti znatno smanjeni. Općeniti pristup jest usporediti diskretiziranu vrijednost smičnog naprezanja na zidu: $\tau_w/\rho = \nu(\overline{u}/y)$ sa vrijednošću dobivenom iz zakona zida:

$$\overline{u} = \sqrt{\frac{\tau_w}{\rho}\frac{1}{\kappa}}\ln(Ey^+). \tag{10}$$

U slučaju da razlika u vrijednostima postoji, uveden je dodatan parametar, ${\nu_t}^w$ koji tu diskretiziranu vrijednost korigira:

$$\frac{\tau_w}{\rho} = (\nu + {\nu_t}^w)\frac{\overline{u}}{y}, \tag{11}$$

pri čemu $\overline{u}$ predstavlja iznos vektora osrednjene brzine paralelne sa zidom.
Ovim pristupom izbjegava se razrješavanje velikih gradijenata u blizini zida tako da prostorna diskretizacija u tom dijelu proračuna području ne mora biti fina. No, potrebno je zadovoljiti kriterije za koje je zakon zida valjan. Prva proračunska točka uza zid mora se nalaziti u rasponu: $30 < y^+ < 300$. Također se napominje da je standardni zakon zida izveden uz pretpostavku nultog gradijenta tlaka, tako da se navedeni pristup može koristiti pod uvjetom da je gradijent tlaka u blizini zida umjereno velik.

U slučaju korištenja zidnih funkcija, jednadžbu za turbulentnu kinetičku energiju u prvom volumenu uza stijenku potrebno rješavati s modificiranim članom produkcije G koji u sebi sadrži gradijente brzine. Rubni uvjet na zidu koji se najčešće primjenjuje je $\mathbf{n}\cdot\nabla k = 0$, gdje $\mathbf{n}$ predstavlja vektor normale na zid. Transportne jednadžbe za ε i ω u prvim volumenima se najčešće ne rješavaju. Razlog je u tome da modelirana transportna jednadžba za ε nije primjerena za područja u blizini zida, dok rubni uvjet za ω na zidu ima singularitet, $\omega \to \infty$. Stoga se za obje jednadžbe vrijednosti u prvim volumenima uza stijenku specificiraju pomoću analitičkih izraza koji zapravo predstavljaju rješenja transportnih jednadžbi turbulentnih veličina za područje u blizini zida.

Izrazi koji povezuju vrijednosti sa zida sa strujanjem podalje od stijenke objedinjeni su pod nazivom zidne funkcije i u sljedećim sekcijama su specificirani uz svaku pojedinu metodu.

Standardne zidne funkcije za $k-\varepsilon$ model turbulencije u `foam-extendu`

Izrazi izloženi u ovom odjeljku predstavljaju zidne funkcije za $k-\varepsilon$ model turbulencije u `foam-extendu`.

- Korekcija smičnog naprezanja na zidu:

$$\nu_t{}^w = \begin{cases} 0 & , y^* \leq y^+_{lam} \\ \nu\left(\dfrac{y^*\kappa}{\ln(Ey^*)} - 1\right) & , y^* > y^+_{lam} \end{cases}. \tag{12}$$

- Modificirani član produkcije turbulentne kinetičke energije:

$$G = \begin{cases} 0 & , y^* \leq y^+_{lam} \\ G_{log} & , y^* > y^+_{lam} \end{cases}, \tag{13}$$

$$G_{log} = \frac{[\,(\nu+\nu_t{}^w)\,|\nabla\overline{\mathbf{u}}_w|\,]^2}{\kappa C_\mu{}^{1/4}k^{1/2}y} \quad \text{ili} \quad G_{log} = (\nu+\nu_t{}^w)|\nabla\overline{\mathbf{u}}_w|\frac{C_\mu{}^{1/4}k^{1/2}}{\kappa y}. \tag{14}$$

- Brzina disipacije turbulentne kinetičke energije:

$$\varepsilon = \frac{C_\mu{}^{3/4}k^{3/2}}{\kappa y}. \tag{15}$$

Zidne funkcije za neravnotežne turbulentne granične slojeve za $k-\varepsilon$ model turbulencije

Ponekad, režimi strujanja u blizini stijenke razlikuju se od onih za koje je standardni zakon zida izveden. U slučajevima većih gradijenata tlaka, značajna razlika u odnosu na standardni

zakon zida može nastupiti. Upravo iz tih razloga ovdje su izložene općenitije zidne funkcije koje vrijede i za slučaj neravnotežnog turbulentnog graničnog sloja [8].

- Granica viskoznog podsloja y_v:

$$y_v = \frac{11.225\nu}{{C_\mu}^{1/4}k^{1/2}}. \tag{16}$$

- Korekcija smičnog naprezanja na zidu:

$${\nu_t}^w = \begin{cases} 0 & ,y < y_v \\ \nu\left(\frac{\tilde{U}y^*\kappa}{\overline{u}\ln(Ey^*)} - 1\right) & ,y > y_v \end{cases}. \tag{17}$$

$$\tilde{U} = \overline{u} - \frac{1}{2}\frac{d\overline{p}}{dx}\left[\frac{y_v}{\kappa k^{1/2}}\ln\left(\frac{y}{y_v}\right) + \frac{y - y_v}{\kappa k^{1/2}} + \frac{{y_v}^2}{\nu}\right]. \tag{18}$$

- Modificirani član produkcije turbulentne kinetičke energije:

$$\overline{G} = \begin{cases} 0 & ,y < y_v \\ \frac{((\nu + {\nu_t}^w)|\nabla\overline{\mathbf{u}}_w|)^2\ln(\frac{2y}{y_v})}{2y{C_\mu}^{1/4}k^{1/2}\kappa} & ,y > y_v. \end{cases} \tag{19}$$

- Brzina disipacije:

$$\overline{\varepsilon} = \left\{\frac{1}{2y}\left[\frac{2\nu k_p}{y_v} + \frac{{k_P}^{3/2}{C_\mu}^{3/4}}{\kappa} ln\left(\frac{2y}{y_v}\right)\right] \quad ,y > y_v\,. \right. \tag{20}$$

Zidne funkcije za $k-\omega$ SST model turbulencije u `foam-extendu`

Izrazi dani u nastavku predstavljaju zidne funkcije u `foam-extendu` za $k-\omega$ SST model turbulencije [4].

- Korekcija smičnog naprezanja na zidu:

$${\nu_t}^w = \begin{cases} 0 & ,\ y^* \leq y^+_{lam} \\ \nu\left(\frac{y^*\kappa}{ln(Ey^*)} - 1\right) & ,\ y^* > y^+_{lam} \end{cases}. \tag{21}$$

- Modificirani član produkcije turbulentne kinetičke energije:

$$G = \begin{cases} 0 & , y^* \leq y^+ \\ G_{log} & , y^* > y^+ \end{cases}, \tag{22}$$

$$G_{log} = (\nu + {\nu_t}^w)|\nabla \overline{\mathbf{u}}_w| \frac{{C_\mu}^{1/4} k^{1/2}}{\kappa y}. \tag{23}$$

- Brzina disipacije po jedinici turbulentne kinetičke energije:

$$\omega = \sqrt{\omega_{vis}^2 + \omega_{log}^2}, \tag{24}$$

$$\omega_{vis} = \frac{6\nu}{\beta 1 y^2}\ ,\ \omega_{log} = \frac{k^{1/2}}{{C_\mu}^{1/4}\kappa y}. \tag{25}$$

Modifikacija zidnih funkcija u `foam-extendu` za $k-\omega$ SST model turbulencije

Predstavljeni izrazi su predložena modifikacija na zidne funkcije u `foam-extendu` za $k-\omega$ SST model turbulencije. Razlika je u definiciji člana produkcije turbulentne kinetičke energije koji je ovdje definiran kao kontinuirana funkcija što u konačnici rezultira velikim poboljšanjem rezultata.

- Korekcija smičnog naprezanja na zidu:

$${\nu_t}^w = \begin{cases} 0 & , y^* \leq y^+_{lam} \\ \nu \left(\dfrac{y^* \kappa}{ln(E y^*)} - 1 \right) & , y^* > y^+_{lam} \end{cases}. \tag{26}$$

- Modificirani član produkcije turbulentne kinetičke energije:

$$G_{vis} = \nu_t \left(\frac{d\overline{u}}{dy} \right)^2 = \frac{k}{\omega_{vis}} \left(\frac{\overline{u}}{y} \right)^2. \tag{27}$$

$$G_{log} = (\nu + {\nu_t}^w)|\nabla \overline{\mathbf{u}}_w| \frac{{C_\mu}^{1/4} k^{1/2}}{\kappa y} \tag{28}$$

$$G = G_{vis} e^{\Gamma} + G_{log} e^{1/\Gamma}. \tag{29}$$

- Brzina disipacije po jedinici turbulentne kinetičke energije:

$$\omega = \sqrt{\omega_{vis}^2 + \omega_{log}^2}, \tag{30}$$

$$\omega_{vis} = \frac{6\nu}{\beta 1 y^2} \ , \ \omega_{log} = \frac{k^{1/2}}{{C_\mu}^{1/4} \kappa y}. \tag{31}$$

Automatske zidne funkcije za $k - \omega$ SST model turbulencije

Za modele turbulencije koji se mogu primjenjivati u blizini stijenke, metoda zidnih funkcija može se proširiti. Osnovni princip ove metode je da profinjivanjem mreže, formulacija zakona zida iz logaritamskog podsloja postepeno prelazi u formulaciju viskoznog podsloja korištenjem funkcije miješanja. Sličan pristup koristi se i u zidnim funkcijama u `foam-extendu`, no funkcija miješanja tamo se ne primjenjuje na sve članove. Prikazani izrazi su iz [32] sa promijenjenim članom produkcije turbulentne kinetičke energije iz [14].

- Korekcija smičnog naprezanja na zidu:

$$u_{\tau vis} = \sqrt{\nu \frac{\overline{u}}{y}} \ , \ u_{\tau log} = \frac{\overline{u}\kappa}{\ln(E y^+)}, \tag{32}$$

$$u^* = \sqrt[4]{{u_{\tau vis}}^4 + (\sqrt{a_1 k})^4} \quad , \quad u_\tau = \sqrt[4]{{u_{\tau vis}}^4 + {u_{\tau log}}^4}, \tag{33}$$

$$\frac{\tau_w}{\rho} = u_\tau u^* \ , \ {\nu_t}^w = \frac{\tau_w}{\rho} \frac{y}{\overline{u}} - \nu. \tag{34}$$

- Modificirani član produkcije turbulentne kinetičke energije:

$$G_{vis} = \nu_t (\frac{d\overline{u}}{dy})^2 = \frac{k}{\omega_{vis}} (\frac{\overline{u}}{y})^2 \ , \ G_{log} = (\nu + {\nu_t}^w)|\nabla \overline{\mathbf{u}}_w| \frac{u^*}{\kappa y}, \tag{35}$$

$$G = G_{vis}e^{\Gamma} + G_{log}e^{1/\Gamma}\ ,\ \Gamma = -\frac{0.01(y^+)^4}{1+5y^+}, \tag{36}$$

- Brzina disipacije po jedinici turbulentne kinetičke energije:

$$\omega_{vis} = \frac{6\nu}{\beta_1 y^2}\ ,\ \omega_{log} = \frac{u^{*2}}{a_1\kappa\nu y^+}, \tag{37}$$

$$\omega = \sqrt{{\omega_{vis}}^2 + {\omega_{log}}^2}. \tag{38}$$

Poboljšane zidne funkcije za $k-\omega$ SST model turbulencije

U ovom odjeljku izložene su zidne funkcije za $k-\omega$ SST model turbulencije koje uzimaju u obzir utjecaj gradijenta tlaka na turbulentni granični sloj. Izrazi za profil brzine u viskoznom i logaritamskom podsloju temeljeni su na [10] i [1].

- Bezdimenzijski profil brzine u viskoznom podsloju:

$$u^+_{vis} = \alpha\frac{y^+}{2} + y^+ = y^+\left(1 + \frac{\alpha}{2}y^+\right). \tag{39}$$

- Bezdimenzijski profil brzine u logaritamskom podsloju:

$${u^+}_{log} = \begin{cases} \frac{1}{\kappa}\left[2\sqrt{1+\alpha y^+} + ln\left|\sqrt{1+\alpha y^+}-1\right| - ln\left(\sqrt{1+\alpha y^+}+1\right)\right] + u^+_{t1} & ,y^+ < 60 \\ \frac{1}{\kappa}\sqrt{1+60\alpha}\,ln(y^+) + u^+_{t2} & ,y^+ \geq 60 \end{cases}, \tag{40}$$

$$u^+_{t_2} = \frac{1}{\kappa}\Bigg[2\sqrt{1+60\alpha} + ln\left|\sqrt{1+60\alpha}-1\right| - ln\left(\sqrt{1+60\alpha}+1\right) - \sqrt{1+60\alpha}\,ln(60)\Bigg] + u^+_{t_1}, \tag{41}$$

$$u^+_{t_1} = \frac{1}{\kappa}ln(6E) - \frac{1}{\kappa}\left[2\sqrt{1+6\alpha} + ln\left|\sqrt{1+6\alpha}-1\right| - ln\left(\sqrt{1+6\alpha}+1\right)\right]. \tag{42}$$

- Izraz za bezdimenzijski gradijent tlaka:

$$\alpha = \frac{\nu}{u^{*3}} \frac{d\overline{p}}{dx} \, , \; u^* = {C_\mu}^{1/4} k^{1/2}. \tag{43}$$

- Korekcija smičnog naprezanja na zidu:

$$u_{\tau vis} = \frac{\overline{u}}{{u^+}_{vis}} \, , \; u_{\tau log} = \frac{\overline{u}}{{u^+}_{log}}, \tag{44}$$

$$u_\tau = u_{\tau vis} e^\Gamma + u_{\tau log} e^{1/\Gamma} \, , \tag{45}$$

$$\frac{\tau_w}{\rho} = {u_\tau}^2 \, , \; {\nu_t}^w = \frac{\tau_w}{\rho} \frac{y}{\overline{u}} - \nu. \tag{46}$$

- Modificirani član produkcije turbulentne kinetičke energije:

$$\left(\frac{d\overline{u}}{dy}\right)_{vis} = \frac{\overline{u}}{y} \, , \; \left(\frac{dU}{dy}\right)_{log} = \frac{\sqrt{(\frac{d\overline{p}}{dx} + \overline{\mathbf{u}} \cdot \nabla \overline{u}) y + \frac{\tau_w}{\rho}}}{\kappa y}, \tag{47}$$

$$\frac{d\overline{u}}{dy} = \left(\frac{d\overline{u}}{dy}\right)_{vis} e^\Gamma + \left(\frac{d\overline{u}}{dy}\right)_{log} e^{1/\Gamma}, \tag{48}$$

$$G = \frac{\tau_w}{\rho} \frac{d\overline{u}}{dy}. \tag{49}$$

- Brzina disipacije po jedinici turbulentne kinetičke energije:

$$\omega_{vis} = \frac{6\nu}{\beta_1 y^2} \, , \; \omega_{log} = \frac{1}{{C_\mu}^{1/2}} \left(\frac{d\overline{u}}{dy}\right)_{log} \, , \tag{50}$$

$$\omega = \sqrt{\omega_{vis}^2 + \omega_{log}^2}. \tag{51}$$

Modificirane poboljšane zidne funkcije za $k-\omega$ SST model turbulencije

Nadalje predstavljeni izrazi su predložena modifikacija na poboljšane zidne funkcije koje uz utjecaj gradijenta tlaka na profil brzine, uzimaju u obzir i konvektivne članove. Utjecaj gradijenta tlaka u izrazu za brzinu u viskoznom podsloju je izostavljen jer na finim mrežama uzrokuje velike oscilacije u rezidualima.

- Bezdimenzijski profil brzine za viskozni podsloj:

$$u^{+}{}_{log} = y^{+}. \tag{52}$$

- Bezdimenzijski profil brzine za logaritamski podsloj:

$$u^{+}_{log} = \frac{1}{\kappa}\left[2\sqrt{1+Ay^{+}} + ln\left|\sqrt{1+Ay^{+}}-1\right| - ln\left(\sqrt{1+Ay^{+}}+1\right)\right] + u^{+}{}_{t}, \tag{53}$$

$$u^{+}_{t} = \frac{1}{\kappa}ln(6E) - \frac{1}{\kappa}\left[2\sqrt{1+6A} + ln\left|\sqrt{1+6A}-1\right| - ln\left(\sqrt{1+6A}+1\right)\right]. \tag{54}$$

- Bezdimenzijski parametar A uključuje utjecaj gradijenta tlaka i konvektivnih članova:

$$A = \frac{\nu}{u^{*3}}\left(\frac{d\overline{p}}{dx} + \overline{\mathbf{u}}\cdot\nabla\overline{u}\right),\ u^{*} = C_{\mu}{}^{1/4}k^{1/2}. \tag{55}$$

- Korekcija smičnog naprezanja na zidu:

$$u_{\tau vis} = \sqrt{\nu\frac{\overline{u}}{y}},\ u_{\tau log} = \frac{\overline{u}}{u^{+}{}_{log}}, \tag{56}$$

$$u_{\tau} = u_{\tau vis}e^{\Gamma} + u_{\tau log}e^{1/\Gamma}, \tag{57}$$

$$\frac{\tau_w}{\rho} = u_{\tau}{}^{2},\ \nu_t{}^{w} = \frac{\tau_w}{\rho}\frac{y}{\overline{u}} - \nu. \tag{58}$$

- Modificirani član produkcije turbulentne kinetičke energije:

$$G = \frac{\tau_w}{\rho}\frac{d\overline{u}}{dy}, \tag{59}$$

$$\frac{d\overline{u}}{dy} = \left(\frac{d\overline{u}}{dy}\right)_{vis} e^{\Gamma} + \left(\frac{d\overline{u}}{dy}\right)_{log} e^{1/\Gamma}, \tag{60}$$

$$\left(\frac{d\overline{u}}{dy}\right)_{vis} = \frac{\overline{u}}{y}\,, \left(\frac{dU}{dy}\right)_{log} = \frac{\sqrt{(\frac{d\overline{p}}{dx} + \overline{\mathbf{u}}\cdot\nabla\overline{u})y + \frac{\tau_w}{\rho}}}{\kappa y}. \tag{61}$$

- Brzina disipacije po jedinici turbulentne kinetičke energije:

$$\omega_{vis} = \frac{6\nu}{\beta_1 y^2}\,, \omega_{log} = \frac{1}{{C_\mu}^{1/2}}\left(\frac{d\overline{u}}{dy}\right)_{log}, \tag{62}$$

$$\omega = \sqrt{\omega_{vis}^2 + \omega_{log}^2}. \tag{63}$$

Validacija zidnih funkcija

Zidne funkcije opisane u prethodnim sekcijama implementirane su software otvorenog koda `foam-extend`. Trenutno ugrađene zidne funkcije za $k-\varepsilon$ i $k-\omega$ SST uspoređene su s novo-ugrađenima i eksperimentalnim podacima za dva slučaja. Opstrujavanje NACA4412 aeroprofila pri napadnom kutu of 15° pri Reyoldsovom broju od $3.6\cdot 10^5$ i opstrujavanje rotacijskog elipsoida duljine $L = 1.37$ m, sa 6:1 omjerom velike i male poluosi pri napadnim kutem od 10° pri Reynoldsovom broju $4.2\cdot 10^6$.

Slike 1 - 5 prikazuju usporedbu koeficijenta smičnog naprezanja duž aeroprofila s eksperimentalnim podatcima. Kao što je vidljivo, Najbolji rezultati postignuti su sa $k-\varepsilon$ modelom, i podjednaki su za obje testirane zidne funkcije. U slučaju $k-\omega$ SST modela dobiveni su nešto lošiji rezultati, a najbolji se postižu s modificiranim poboljšanim zidnim funkcijama.

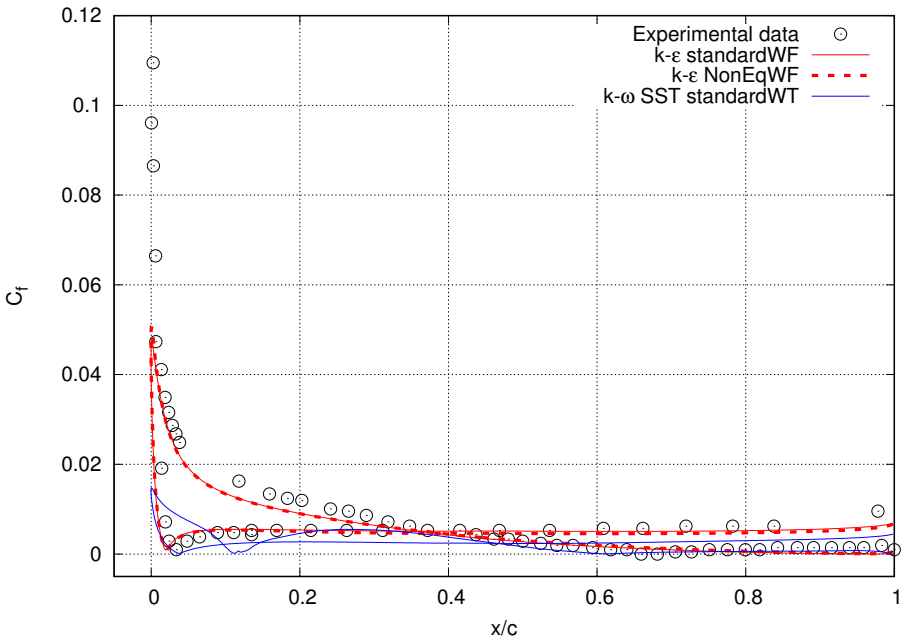

Slika 1: NACA4412: koeficijent smičnog naprezanja za $k-\omega$ SST currentWT u usporedbi sa zidnim funkcijama $k-\varepsilon$ modela

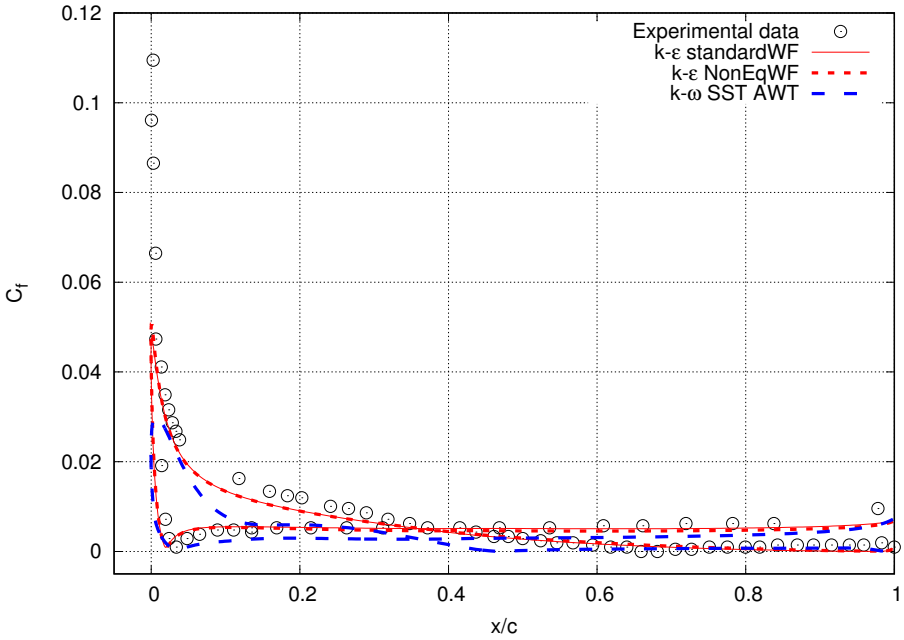

Slika 2: NACA4412: koeficijent smičnog naprezanja za $k-\omega$ SST AWT u usporedbi sa zidnim funkcijama $k-\varepsilon$ modela

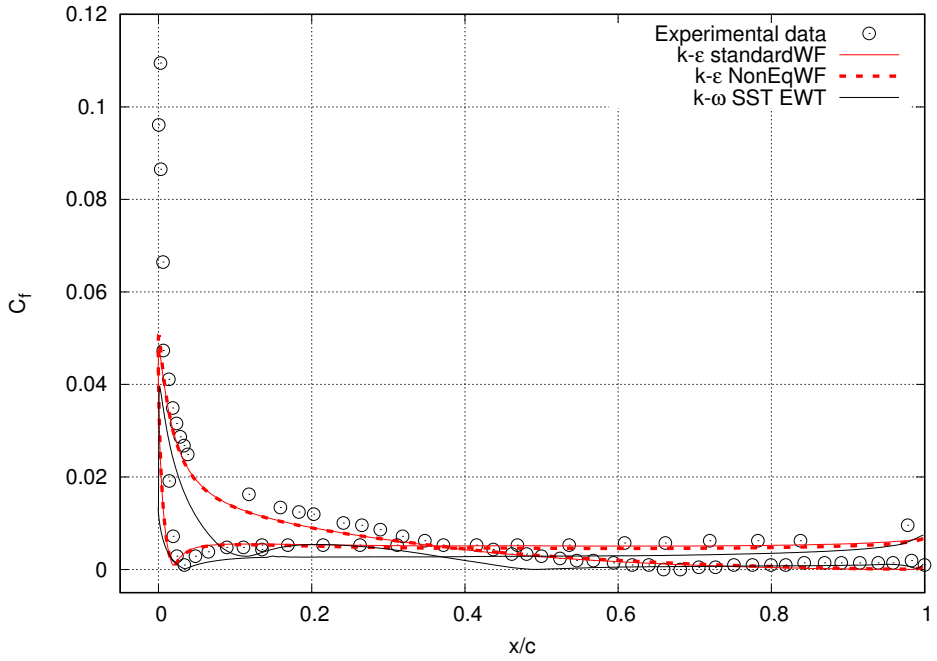

Slika 3: NACA4412: koeficijent smičnog naprezanja za $k-\omega$ SST EWT u usporedbi sa zidnim funkcijama $k-\varepsilon$ modela

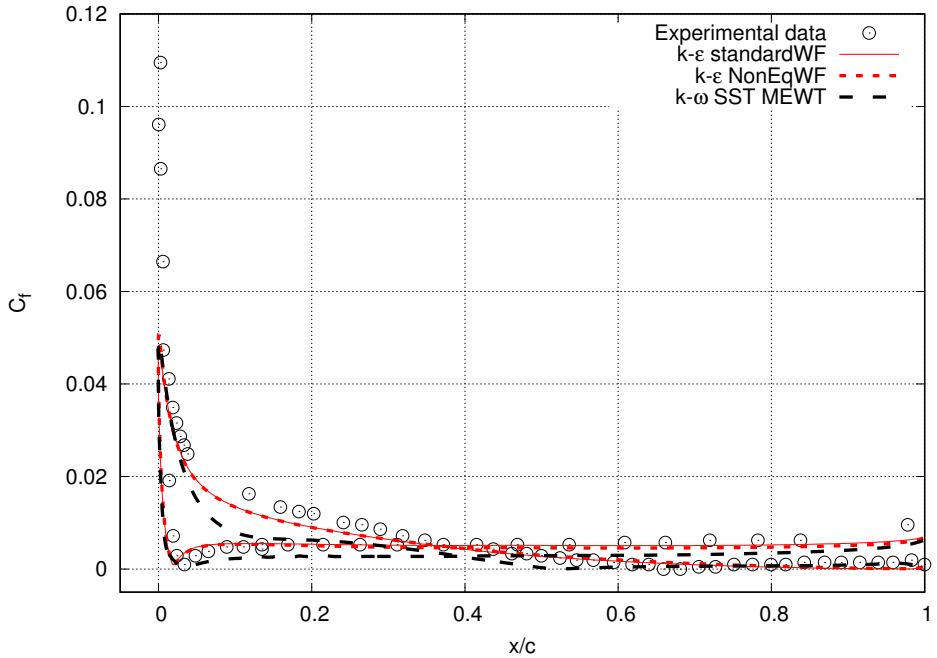

Slika 4: NACA4412: koeficijent smičnog naprezanja za $k-\omega$ SST MEWT u usporedbi sa zidnim funkcijama $k-\varepsilon$ modela

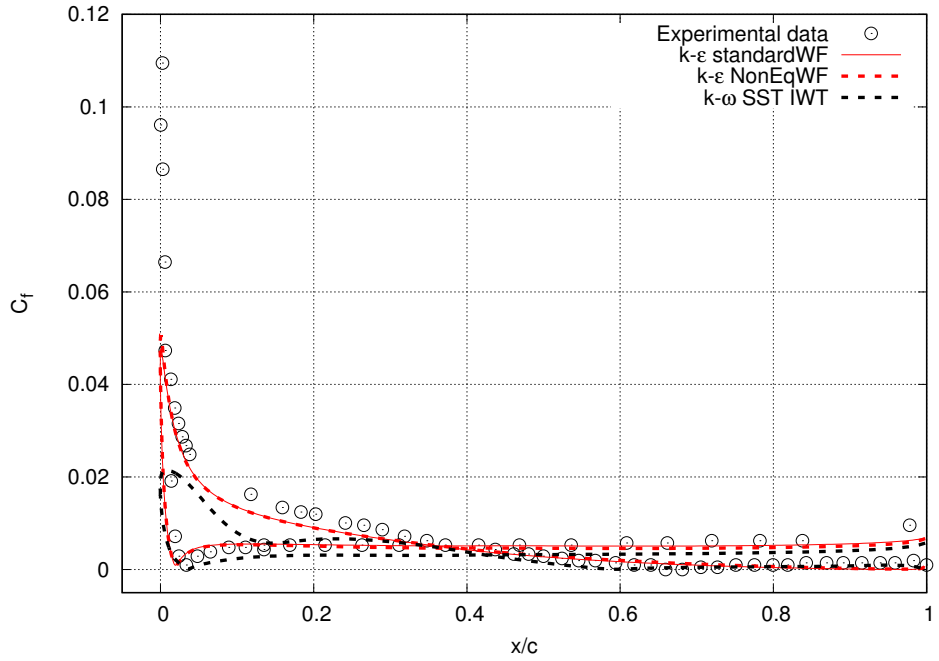

Slika 5: NACA4412: koeficijent smičnog naprezanja za $k-\omega$ SST Gnew u usporedbi sa zidnim funkcijama $k-\varepsilon$ modela

Na slikama 7 i 8 dana je usporedba koeficijenta smičnog naprezanja po obodu rotacijskog elipsoida na presječnim ravninama $x/L = 0.6$ i $x/L = 0.772$. Slika 6 prikazuje koordinatni sustav u odnosu na koji su rezultati prikazani. Iz prikazanog je vidljivo, kako u odnosu na trenutnu formulaciju zidnih funkcija u `foam-extendu`, novo-implementirane metode puno bolje slijede trend eksperimentalnih podataka.

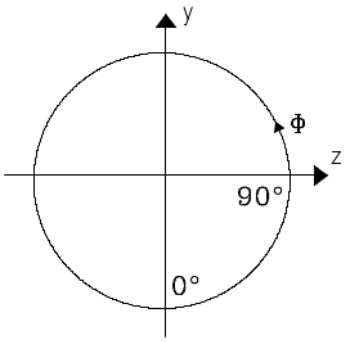

Slika 6: Koordinatni sustav za poprečne presjeke $x/L =$ konst.

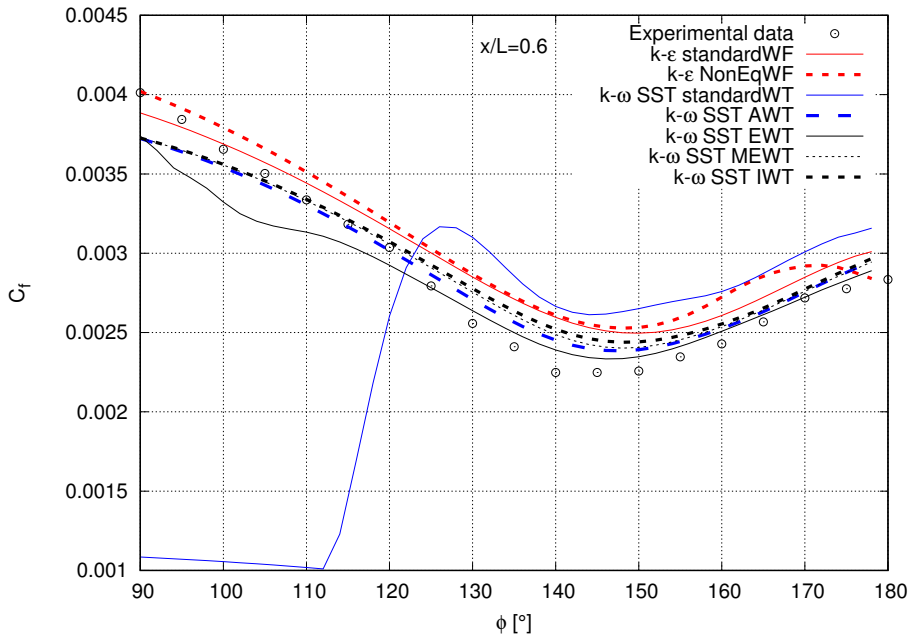

Slika 7: Rotacijski elipsoid: usporedba koeficijenta smičnog naprezanja sa eksperimentalnim podacima na presjeku $x/L = 0.6$.

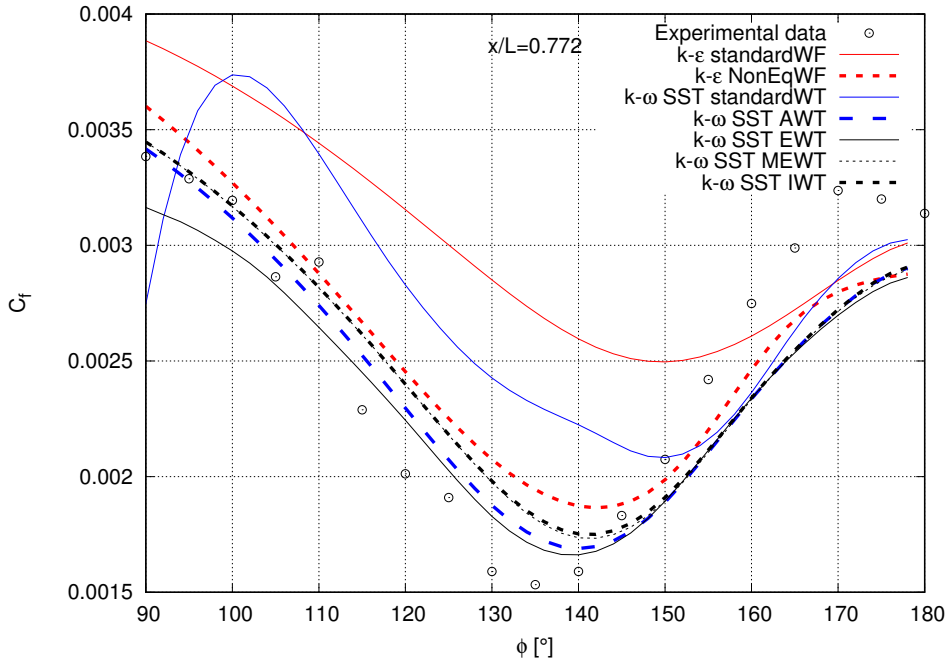

Slika 8: Rotacijski elipsoid: usporedba koeficijenta smičnog naprezanja s eksperimentalnim podacima na presjeku $x/L = 0.772$.

Iz priloženih rezultata vidljivo je kako pojedine implementirane zidne funkcije u `foam-extend` za $k-\varepsilon$ i $k-\omega$ SST model, u odnosu na trenutno ugrađene, pružaju znatno poboljšanje u točnosti. Ovdje se posebno ističu modificirane poboljšane zidne funkcije koje uključuju efekte gradijenta tlaka i konvektivnih članova na profil brzine u blizini zida. Otkriveno je da trenutna implementacija zidnih funkcija za $k-\omega$ SST model podbaci u strujanjima s relativno manjim gradijentima brzine na grubljim mrežama, što je vidljivo na slučaju rotacijskog elipsoida. U slučaju $k-\varepsilon$ modela poboljšanje u točnosti je jedino uočljivo na testu rotacijskog elipsoida. Iako su iz izloženih rezultata poboljšanja očita, naglašava se da je potrebno izvršiti daljnja testiranja kako bi se mogli iznijeti daljnji zaključci.

Chapter 1

Introduction

Computational Fluid Dynamics (CFD) serves as an essential tool in analysing a variety of flows of engineering interest. Successful CFD use requires a deep understanding of the underlying physics and a user should be aware of the modelling assumptions. Since the turbulence is non-deterministic and that all turbulence models are basically just an approximation, simulation of turbulent flows still remains a challenge. Another problem which arises is the substantial increase of computing demands due to the near-wall flow where large gradients prevail. The usual approach is to bypass this region with some other expressions called wall functions [11] which are constructed specifically to capture the effects of turbulent flow near the wall. The most often used wall functions ones are based on the law-of-the-wall which assumes equilibrium flow conditions. In addition, the performance of all turbulence models is determined in large measure by the treatment of the boundary conditions at solid walls. Therefore, a need for a general and economical approach to accurately resolve the near-wall region exists.

1.1 Previous and Related Studies

The first wall functions were proposed by Patankar and Spalding (1967) which employ law-of-the-wall to bridge the values in the near-wall cells and the corresponding quantities on the wall. The original wall functions have been further developed, yielding two approaches which can be distinguished nowadays.

Chieng and Launder [12] employed two-layer approach by splitting the cell into the viscous and logarithmic region, approximating distributions of all quantities in each region and averaging values over the cell. Craft [13] further improved this idea by assuming the variation of eddy viscosity for both viscous and logarithmic region in the first cell which he used to solve the wall-parallel mean momentum equation, thus obtaining the expression for the mean-velocity profile. In the derivation, he retained the effects of a pressure gradient and convection.

The second approach derives expressions for the viscous and logarithmic region for flow properties and employs the blending procedures on for buffer region modelling. Here, the most common blending procedure are presented by Esch and Menter [4] and Kader [14]. The generality of this approach depends on the assumptions taken in deriving the expressions for the viscous and logarithmic region. Popovac and Hanjalic [14], adopted the approach similar to the one of Craft [13], in which they specified the distribution of eddy viscosity only for the logarithmic region, which results in a simpler mathematical expressions for mean flow. For the viscous region, standard viscous-law is used and both relations are blended using Kader blend.

Craft has also developed [15] an efficient numerical method which is used in the wall adjacent cells. After each iteration step on the global mesh, one-dimensional, parabolised, wall parallel equations are integrated on a fine subgrid in the first near wall cells. Tests [16] showed that compared to wall function approach, computational expenses are 60% larger, but still eight times lower than low-Reynolds approach.

In this thesis, the focus is on the two-layer approach for the $k-\varepsilon$ model which takes into account the pressure gradient effects and blending approaches for $k-\omega$ SST model as described in CFX [9] and Fluent [10] theory manual. Furthermore, a modification for Enhanced wall treatment from Fluent is proposed and tested.

1.2 Thesis Outline

The thesis is outlined as follows. Chapter 2 serves as an introduction to the physics of turbulence and highlights the main aspects and difficulties in this area. Chapter 3 presents the equations governing the motion of a fluid, explaining the need for a turbulence model and presenting common approaches in that area. The end of the chapter describes two widely used turbulence models which are the focus of this thesis. In Chapter 4, the topic of turbulence modelling is continued, but with a focus on the treatment of wall boundary conditions in numerical simulations. Upon presenting the general idea, several methods are shown which are then tested in Chapters 5 and 6. Finally, Chapter 7 gives an overview of the thesis with a final conclusion.

Chapter 2

Nature of Turbulence

Turbulence occurs almost everywhere around us. In boundary layers on vehicles, wakes behind vehicles, flow in pipelines, in a smoke rising from the cigarette [20], etc. Laminar flow is an exception which can maintain itself only in special cases. Combining Hinze's [17] and Cebeci's [18] definitions, turbulence can be defined as:

"*Turbulent fluid motion is an irregular condition of flow in which the various quantities show a random variation with time and space coordinates so that statistically distinct average values can be discerned. In addition, turbulence has a wide range of wavelengths...*" meaning that irregular motions appear on a wide range of length and time scales.

Not all irregular flows can be treated as turbulent. To be characterised as turbulent flow, intensive mixing (in the lateral direction of flow) of all fluid properties must be present. This is the most important property of turbulence: enhanced diffusivity. In the context of momentum transport, mixing will cause velocity profile to be smoother, but in a near-wall region, it leads to a large increase of the gradients, Figure 2.1).

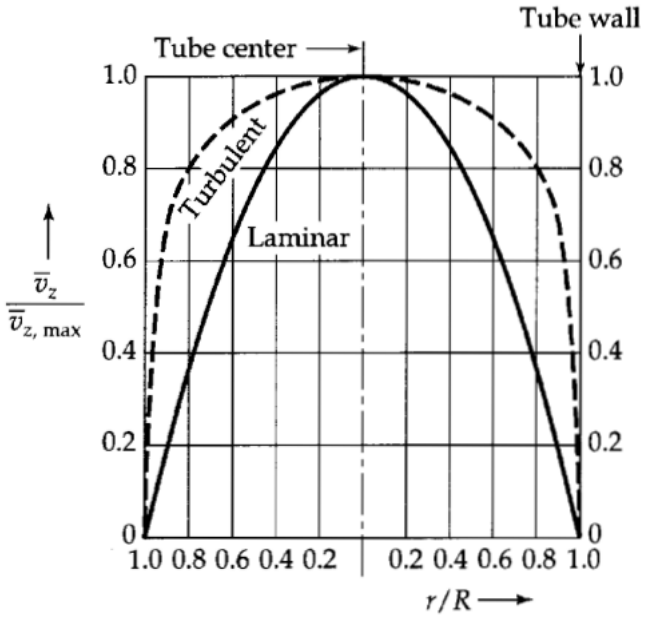

Figure 2.1: Laminar and turbulent velocity profile for pipe flow [19].

The experimental parameter, used in fluid flow, as criteria whether the flow is laminar or turbulent is Reynolds number defined as the ratio of the inertial and viscous forces:

$$Re = \frac{U_\infty L}{\nu}. \tag{2.1}$$

The variables U_∞ and ν are freestream velocity and molecular kinematic viscosity and L is the characteristic length which is associated with the flow domain, e.g. pipe diameter, plate length, chord length.

Turbulence always occurs at large Reynolds numbers, meaning that turbulence manifests itself as an excessive amount of kinetic energy of the fluid. For smaller values, viscous effects are able to damp all the instabilities and laminar flow will maintain itself.

Laminar flow can maintain itself even beyond critical Reynolds number, but only in special-like laboratory conditions. If only the slightest disturbance is applied to flow, it irreversibly passes to a turbulent state. The only way to make it laminar again is to slow down the flow to make viscous effects more dominant over inertial.

Turbulence is a three-dimensional phenomena. Even for the simple flow across the flat plate, turbulent pulsations will occur in all three dimensions, as if the flow contains additional degrees of freedom.

In turbulent flow, vortices are constantly broken up to smaller ones and smaller scales at which they are transferred to heat by viscous effects. In order to maintain turbulent flow, there must be a continuous supply of energy to the largest pulsations from the mean flow. This is a common cascade process associated with turbulence which defines it as a dissipative process.

Non-deterministic nature of turbulence is the main obstacle when it comes to its analysis and it still remains one of the unresolved problems in classical mechanics.

Chapter 3

Governing Equations for Turbulent Flow

The previous chapter introduced the basic phenomena occurring in turbulent flow, while this chapter focuses on its mathematical description. First, basic equations for incompressible fluid flow are presented. Although this set of equations is valid for both flow regimes: laminar and turbulent, the need for a turbulence model is further explained. The methods of Reynolds averaging and Boussinesq assumption are explained and some models based on these methods are presented.

3.1 Navier-Stokes Equations

Fluid flow motion is governed by a set of Navier-Stokes equations. The continuity equation represents the conservation of mass and the momentum equation relates the acceleration of fluid with the pressure, body and viscous forces. Equations are written in spatial coordinates (Eulerian frame) and for an incompressible fluid, they read:

- Continuity equation:

$$\nabla \cdot \mathbf{u} = 0, \tag{3.1}$$

- Momentum equation:

$$\frac{\partial \mathbf{u}}{\partial t} + \nabla \cdot (\mathbf{u} \otimes \mathbf{u}) = -\nabla p + \nabla \cdot [\nu(\nabla \mathbf{u} + \nabla \mathbf{u}^T)], \tag{3.2}$$

where $\mathbf{u}$ and p stand for the velocity field and kinematic pressure respectively, and ν is molecular kinematic viscosity. Body forces are neglected in this work.

The equation for conservation of angular momentum is not solved, but it leads to a condition of symmetric stress tensor which is enforced in linear momentum equation on the constitutive relation for viscous forces. Continuum mechanics, which deals with non-symmetric stress tensor, is called polar (Cosserat) Continuum Mechanics [21] and is not considered in this text.

Due to the nonlinearity of the momentum equation, analytical solutions exist only for few simplified cases. Another problem is that even the existence of a solution cannot be proven for Navier-Stokes equations. Overcoming these problems would be of great significance as Navier-Stokes equations describe the turbulent flow in every detail, and understanding them is the first step in understanding the turbulence. To further illustrate the complexity of the problem, we cite [22] one of the seven "*Millennium Prize problems*" in mathematics with a 1 000 000 $ reward:

"*Prove or give a counter-example of the following statement: In three space dimensions and time, given an initial velocity field, there exists a vector velocity and a scalar pressure field, which are both smooth and globally defined, that solve the Navier–Stokes equations*".

Equations (3.1) and (3.2) describe every detail of underlying turbulence physics and solving them would mean to resolve turbulent velocity field from the largest to the smallest scales. That is why, when using the numerical methods, the requirements for computer resources are immense. From an engineering point of view, solving the problems this way is currently out of reach and it is expected to stay like that for the next few decades. This approach of directly solving the Navier-Stokes equations for turbulent flows is called Direct Numerical Simulation (DNS) and today is used for analysing turbulent flows at lower Reynolds numbers [23].

3.2 Turbulence Modelling

From a practical point of view, the complete history of turbulence phenomena is usually not of interest. Even if we have data for a completely resolved turbulent flow field, we would somehow average the results for practical engineering purposes. Instead of solving the Navier-Stokes equations, the idea is to solve a different set of equations which model the effects of turbulence on the mean flow. This way, we end up with a larger set of equations, but are avoid the calculation of every flow detail, yielding with lower computational requirements.

Two main groups of turbulence models are:

- Reynolds Averaged Navier-Stokes equations - RANS,
- Large Eddy Simulation - LES, or filtered Navier-Stokes equations.

Sometimes, DNS is erroneously added to the list as Navier-Stokes equations do not include any additional assumptions about turbulence.

Each turbulence model has its limitations. When choosing one, the usual choice comes to a compromise between accuracy and computational cost. If the interest is the attached flow over an airfoil and skin friction, simple Algebraic models (a sub-class of RANS models), which are the most simple turbulence models, will suffice. For a highly complex flow field, one would have to resort to a more advanced one, like LES.
LES can be easily described as a method in which small turbulent structures are being modelled, while larger ones are resolved. Compared to RANS models, they are much more expensive, but much more accurate as pulsations at smaller scales are universal and can be modelled accurately. The disadvantage of this approach is that near the wall, computational resources can become similar to those of the DNS [24].
To overcome this, hybrid approaches have been developed, Detached Eddy Simulations - DES. Near the wall, RANS models are used and in the outer flow, LES approach is employed.

When using a turbulence model, it is important to know its range of application and limitation. For example, can the model be applied for swirling flows, or how accurately it can describe curvature effects, high-pressure gradient conditions etc. The best practice is to use ones that are thoroughly tested and for which limitations are well documented.

3.3 Reynolds Averaged Navier-Stokes Equations - RANS

Instead of resolving the complete turbulent flow field with the Navier-Stokes equations, and after analysing and averaging the data, Fig 3.1, one could try to immediately solve the averaged Navier-Stokes equations. The approach Osborne Reynolds took [23] was to decompose each flow property into mean ($^-$) and fluctuating part ($'$):

$$\mathbf{u} = \overline{\mathbf{u}} + \mathbf{u}', \tag{3.3}$$

$$p = \overline{p} + p', \tag{3.4}$$

and substitute it into Navier-Stokes equations:

$$\nabla \cdot (\overline{\mathbf{u}} + \mathbf{u}') = 0, \tag{3.5}$$

$$\frac{\partial(\overline{\mathbf{u}} + \mathbf{u}')}{\partial t} + \nabla \cdot ((\overline{\mathbf{u}} + \mathbf{u}') \otimes (\overline{\mathbf{u}} + \mathbf{u}')) = -\nabla(\overline{p} + p') + \nabla \cdot [\nu((\nabla\overline{\mathbf{u}} + \mathbf{u}') + \nabla(\overline{\mathbf{u}} + \mathbf{u}')^T)]. \tag{3.6}$$

Next, averaging procedure is employed for each term with the operator which satisfies Reynolds conditions [25]:

$$\overline{f + g} = \overline{f} + \overline{g} \tag{3.7}$$

$$\overline{const \cdot f} = const \cdot \overline{f} \tag{3.8}$$

$$\overline{\frac{\partial f}{\partial s}} = \frac{\partial \overline{f},}{\partial s}, \; \overline{\frac{\partial f}{\partial \mathbf{x}}} = \frac{\partial \overline{f},}{\partial \mathbf{x}} \tag{3.9}$$

$$\overline{\overline{f} g} = \overline{f}\,\overline{g}. \tag{3.10}$$

By making an assumption that an average of the mean is the same mean property $\bar{\bar{f}} = \bar{f}$, and that average of fluctuating property vanishes $\overline{f'} = 0$, we obtain:

$$\nabla \cdot \overline{\mathbf{u}} = 0, \tag{3.11}$$

$$\frac{\partial \overline{\mathbf{u}}}{\partial t} + \nabla \cdot (\overline{\mathbf{u}} \otimes \overline{\mathbf{u}}) = -\nabla \overline{p} + \nabla \cdot [\nu(\nabla \overline{\mathbf{u}} + \nabla \overline{\mathbf{u}}^T) - \overline{\mathbf{u}' \otimes \mathbf{u}'}]. \tag{3.12}$$

The resulting form is similar to the original Navier-Stokes equations, with only difference being that the averaging procedure resulted with an additional term, the Reynolds stress tensor $\mathbf{R} = -\overline{\mathbf{u}' \otimes \mathbf{u}'}$. This term results from a convective transport, but historically it has been grouped with shear stresses. The motivation for this approach is explained in the next section. This term is symmetric and introduces six new unknowns that have to be modelled which further illustrates the problem of turbulence modelling. Modelling these six additional components of Reynolds stress tensor leads to Reynolds Stress Models - RSM.

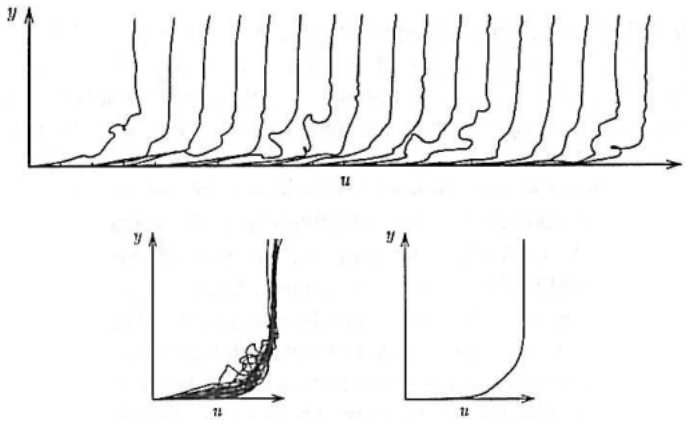

Figure 3.1: Intuitive explanation of Reynolds averaging [18].

Reynolds conditions (3.7) - (3.10) cannot be derived, but operator which does not satisfy them, is not of a much practical use [25]. For the case of stationary turbulence, in which average values does not vary with time, time-average is an appropriate operator [7]:

$$\overline{f} = \lim_{T \to \infty} \frac{1}{T} \int_t^{t+T} f(\mathbf{x}, t)\, dt. \tag{3.13}$$

For the case of non-stationary turbulence, the problem of defining the averaging operator is more complex. Requirements (3.7) and (3.8) imply that operator is linear, which is easy to

satisfy, but the other two conditions, (3.9) and (3.10) are questionable. For the other definitions of averaging, the reader is referred to [7].

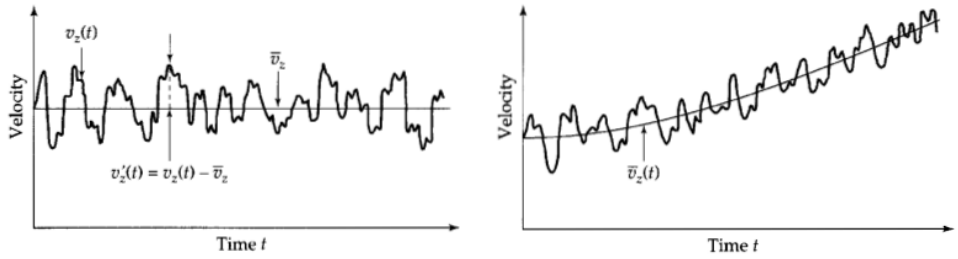

(a) **(b)**

Figure 3.2: (a) stationary and **(b)** non stationary turbulenc [19].

The question is also, whether the assumption of decomposing the velocity and pressure into mean and fluctuating part can be justified. For some flows, it is not possible to distinct between unsteadiness and turbulent pulsations. In those cases the term $\overline{\overline{\mathbf{u}} \otimes \mathbf{u}'}$ in averaging process does not vanish [7], and instead of RANS, LES models need to be used.

3.4 Boussinesq Hypothesis

The most simple approach of closing the system of Reynolds equations follows the hypothesis of Boussinesq [7]. Using the assumption that there is an analogy between chaotic molecular motion (manifested as viscous stresses) and turbulent pulsations, the idea arises that turbulent momentum transport $\overline{\mathbf{u}' \otimes \mathbf{u}'}$ can be modelled as an additional stress acting on the fluid, with an expression which is analogous to Newton's law:

$$-\overline{\mathbf{u}' \otimes \mathbf{u}'} = \nu_t(\nabla\overline{\mathbf{u}} + \nabla\overline{\mathbf{u}}^T) - \frac{2}{3}\mathbf{I}k, \tag{3.14}$$

where $k = \frac{1}{2}\overline{\mathbf{u}' \cdot \mathbf{u}'}$ is turbulent kinetic energy and $\mathbf{I}$ is an identity tensor. The term $2/3\mathbf{I}k$ is added to satisfy the invariant of Reynolds stress tensor $tr(\mathbf{R}) = -\overline{\mathbf{u}' \cdot \mathbf{u}'}$:

$$tr(-\overline{\mathbf{u}' \otimes \mathbf{u}'}) = -\frac{2}{3}tr(\mathbf{I})k = -2k = -2\frac{1}{2}\overline{\mathbf{u}' \cdot \mathbf{u}'} = -\overline{\mathbf{u}' \cdot \mathbf{u}'}. \tag{3.15}$$

Boussinesq's assumption introduces a new parameter, eddy viscosity ν_t which unlike the ν, is not a property of the fluid, but of fluid flow.
Including (3.14) into Reynolds momentum equation (3.12), and regrouping the terms leads to:

$$\frac{\partial \overline{\mathbf{u}}}{\partial t} + \nabla \cdot (\overline{\mathbf{u}} \otimes \overline{\mathbf{u}}) = -\nabla(\overline{p} + \frac{2}{3}k) + \nabla \cdot [(\nu + \nu_t)(\nabla \overline{\mathbf{u}} + \nabla \overline{\mathbf{u}}^T)]. \tag{3.16}$$

The Boussinesq hypothesis is a great simplification which postulates that Reynolds stress tensor is proportional to the strain rate tensor. The first clear deficiency of this assumption is that it postulates that turbulence can be treated as isotropic, e.g. that velocity pulsations are the same in all directions in space. Some cases in which Boussinesq assumption also fails are [7]:

- Flows over curved surfaces,
- Flows with rotation,
- Flows with separation,
- Three-dimensional flows,
- Flows with a sudden increase/decrease in strain rate.

Despite these drawbacks, Eddy Viscosity Models - EVM, are the most common turbulence models today and are a very useful engineering tool.

3.5 Mixing length Model - Law of the Wall

Using the Boussinesq reasoning, Ludwig Prandtl postulated that momentum transfer in turbulent flow can be calculated using the expression from the kinetic theory of gases [19] for molecular momentum transfer:

$$-\overline{u'v'} \sim l_m v_m \frac{d\overline{u}}{dy} \tag{3.17}$$

where l_m is analogous to the mean free path in kinetic theory, and v_m is the mixing velocity [7].

Furthermore, analysing the flow in boundary layer, Prandtl proposed the following relations:

$$v_m = a \cdot l_m \left| \frac{d\overline{u}}{dy} \right| \, , \; l_m = \kappa y. \tag{3.18}$$

Constant a from v_m is absorbed in mixing length l_m and (3.17) transforms into:

$$-\overline{u'v'} = \kappa^2 y^2 \left| \frac{d\overline{u}}{dy} \right| \frac{d\overline{u}}{dy}. \tag{3.19}$$

Next, the mixing-lenght model, expression (3.19), is used to solve turbulent flow over a flat plate. Reynolds equations simplified for boundary layer region are:

$$\frac{\partial \overline{u}}{\partial x} + \frac{\partial \overline{v}}{\partial y} = 0, \tag{3.20}$$

$$\frac{\partial \overline{u}}{\partial t} + \overline{u}\frac{\partial \overline{u}}{\partial x} + \overline{v}\frac{\partial \overline{u}}{\partial y} = -\frac{\partial \overline{p}}{\partial x} + \frac{\partial}{\partial y}\left(\nu \frac{\partial \overline{u}}{\partial y} - \overline{u'v'} \right). \tag{3.21}$$

Restricting to steady, fully developed turbulent flow, with negligible pressure gradient, and including expression (3.19), above equations further reduces to:

$$\frac{d}{dy}\left[\left(\nu + \kappa^2 y^2 \left| \frac{d\overline{u}}{dy} \right| \right) \frac{d\overline{u}}{dy} \right] = 0. \tag{3.22}$$

The above equation implies that trough the boundary layer, shear stresses are constant. Integrating equation 3.22 and setting the integration constant to be the value on the wall leads to:

$$\left(\nu + \kappa^2 y^2 \left| \frac{d\overline{u}}{dy} \right| \right) \frac{d\overline{u}}{dy} = \frac{\tau_w}{\rho}. \tag{3.23}$$

Near the wall, pulsations are damped and turbulent convective transport can be neglected, which leads to the solution for viscous sublayer velocity profile:

$$\nu \frac{d\overline{u}}{dy} = \frac{\tau_w}{\rho} \, , \; \overline{u} = \frac{\tau_w}{\rho \nu} y. \tag{3.24}$$

Away from the wall, it is assumed that convective transport is largely due to mixing, implying that viscous forces can be neglected:

$$\kappa^2 y^2 \left| \frac{d\overline{u}}{dy} \right| \frac{d\overline{u}}{dy} = \frac{\tau_w}{\rho}. \tag{3.25}$$

For a flat plate flow, velocity gradient is positive, $|d\overline{u}/dy|\, d\overline{u}/dy = (d\overline{u}/dy)^2$, further simplifying the expression to:

$$\kappa^2 y^2 \left(\frac{d\overline{u}}{dy}\right)^2 = \frac{\tau_w}{\rho}, \tag{3.26}$$

$$\left(\frac{d\overline{u}}{dy}\right)^2 = \frac{1}{\kappa^2}\frac{\tau_w}{\rho}\frac{1}{y^2}, \tag{3.27}$$

$$\frac{d\overline{u}}{dy} = \frac{1}{\kappa}\sqrt{\frac{\tau_w}{\rho}}\frac{1}{y}. \tag{3.28}$$

The solution for a logarithmic (also called inertial) velocity profile is:

$$\overline{u} = \frac{1}{\kappa}\sqrt{\frac{\tau_w}{\rho}} ln(y) + c. \tag{3.29}$$

Expressions 3.24 and 3.29 are usually transformed into a dimensionless form by dividing them with friction velocity $u_\tau = \sqrt{\tau_w/\rho}$:

$$\frac{\overline{u}}{u_\tau} = u^+_{vis} = y^+, \tag{3.30}$$

$$\frac{\overline{u}}{u_\tau} = u^+_{log} = \frac{1}{\kappa} ln(Ey^+) = \frac{1}{\kappa} ln(y^+) + B, \tag{3.31}$$

with a definition for $y^+ = u_\tau y/\nu$. Value of constants are: $E = 9.8$ or $B = 5$ and $\kappa = 0.41$ are obtained from experimental data [7].

Equations (3.24) and (3.29) relate the value of the wall shear stress with the velocity near the wall, which will prove to be useful in Chapter 4.

The following diagram presents the comparison of derived expressions with measured experimental data. Presented theory is in good agreement for regions $0 < y^+ < 5$ for the viscous sublayer solution (3.30) and $30 < y^+ < 1000$ for the logarithmic sublayer solution (3.31). For buffer layer, $5 < y^+ < 30$, neither of the profiles is valid, as in that region viscous and mixing effects are of the same order. Viscous, buffer and logarithmic part of the boundary layer, called inner part of boundary layer, makes 10-15% of the total thickness of the boundary layer [26].

In the inner part of the turbulent boundary layer, turbulence is mostly dictated by the wall [26] which explains the existence of viscous and logarithmic profiles on other surfaces besides flat

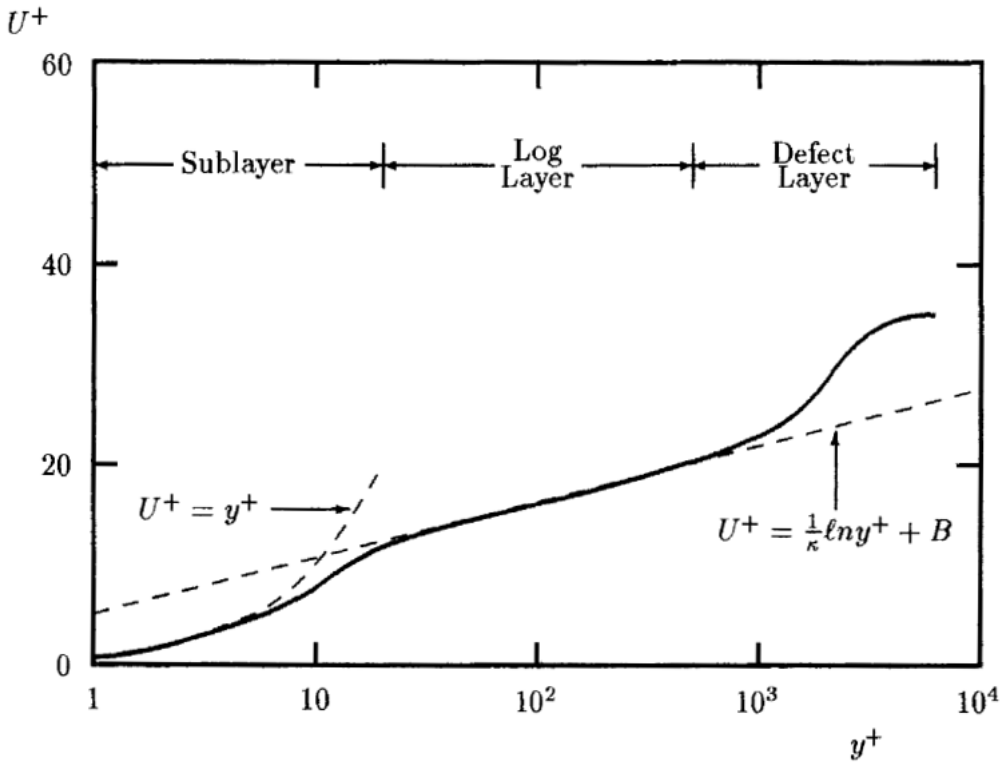

Figure 3.3: Validity of the derived velocity profiles [7] .

plate. Expressions (3.24) and (3.29) can be used on moderately curved surfaces with moderate pressure gradient.

In Chapter 2 the focus was on emphasising the unsteady and three-dimensional nature of turbulence. In this section, we solved it as a two-dimensional steady state problem. This is a direct consequence of Reynolds averaging and Prandtl's mixing-length hypothesis.

3.6 Two-Equation Turbulence Models

The most important consequence of Prandtl's mixing length model is that for effectively defining the turbulent convective transport, a minimum of two scales needs to be provided [7]: turbulent length and turbulent velocity scale. The scales can then be further used in defining the eddy viscosity in the Boussinesq hypothesis. As the turbulent kinetic energy is already introduced by Boussinesq hypothesis, it is natural and common to use it as a turbulent velocity scale. The choice for the second scale is not so straightforward and depends on the turbulence

model. Models which use Boussinesq hypothesis are further classified by the number of additional transport equations introduced for modelling the parameters by which eddy viscosity is defined. Some of them are listed below.

1. *Zero-equation models* are upgraded versions of mixing length models, with the one improvement being the redefinition of mixing length valid trough the whole boundary layer. They do not include any additional transport equations. The examples here are: Cebeci-Smith and Baldwin-Lomax model [7].

2. *One-equation models*, like most models, usually use turbulent kinetic energy for velocity scale. Turbulent length scale can be prescribed with some simple algebraic relation, like in mixing length model, but these models are still incomplete, as the prescription for length scale can be made only for isolated flow regions like boundary layers, mixing planes or jets (planar or round). Exception here is the Spalart-Allmaras turbulence model [7], in which empirical transport equation for eddy viscosity is given.

3. *Two-equation models* represent the simplest class of complete models of turbulence as they provide transport equations for both turbulent velocity scale and turbulent length scale. The choice of turbulent velocity scale usually falls on turbulent kinetic energy. For the turbulent length scale, Wilcox notes [7] that it is equivalent to the dissipation of turbulent kinetic energy. The two most usual choices fall on dissipation rate ε or dissipation per unit turbulence kinetic energy ω, also termed as specific dissipation rate. Here, two main families of two-equation models are branching: $k-\varepsilon$ models and $k-\omega$ models.

For both k and ε exact transport equations can be derived [7], but unfortunately, both of them include additional new terms. So instead of those, the modelled k and ε equations, obtained by modelling these unknown terms using dimensional analysis and including additional closure coefficients (later: model constants), are being used. Equation for ω is completely postulated.

There are many other models, like three and four equation models. Also non-linear, quadratic and cubic, eddy viscosity models, which are not covered here. Ones presented here serve as the base of eddy viscosity models.

3.6.1 $k-\varepsilon$ Turbulence Model

This section covers the $k-\varepsilon$ turbulence model. The model is implemented according to Jones and Launder [2], but with retuned constants of Launder and Sharma [3].

Eddy viscosity, obtained with dimensional analysis and with the inclusion of the addition constant C_μ is:

$$\nu_t = C_\mu \frac{k^2}{\varepsilon}. \tag{3.32}$$

Modelled equation for the turbulent kinetic energy k reads:

$$\frac{\partial k}{\partial t} + \nabla \cdot (\overline{\mathbf{u}} k) - k \nabla \cdot \overline{\mathbf{u}} - \nabla \cdot (\Gamma_{k,eff} \nabla k) = G - \varepsilon. \tag{3.33}$$

Modelled equation for the dissipation rate ε reads:

$$\frac{\partial \varepsilon}{\partial t} + \nabla \cdot (\overline{\mathbf{u}} \varepsilon) - \varepsilon \nabla \overline{\mathbf{u}} - \nabla (\Gamma_{\varepsilon,eff} \nabla \varepsilon) = C_1 \frac{\varepsilon}{k} G - C_2 \frac{\varepsilon^2}{k}. \tag{3.34}$$

The production term G, represents the rate at which kinetic energy is transferred to turbulent velocity fluctuations from the mean flow [7]:

$$G = 2\nu_t \left| \frac{1}{2} (\nabla \overline{\mathbf{u}} + (\nabla \overline{\mathbf{u}})^T) \right|^2. \tag{3.35}$$

Additional relations and model constants,Table 3.1, are:

$$\Gamma_{k,eff} = \nu + \nu_t \ , \ \Gamma_{\varepsilon,eff} = \nu + \frac{\nu_t}{\sigma_\varepsilon}. \tag{3.36}$$

Table 3.1: $k-\varepsilon$ turbulence model constants.

C_μ	C_1	C_2	σ_ε
0.09	1.44	1.92	1.3

The presented set of equations are tuned for free-shear flows [18]. In the near-wall region different expressions, so-called wall functions need to be used. They are derived using the assumption of balanced production and dissipation of turbulent kinetic energy for inertial sub-layer:

$$G = \varepsilon. \tag{3.37}$$

With an additional assumption that the near-wall flow can be regarded as two-dimensional and wall parallel ($G = \nu_t(d\overline{u}/dy)^2$), and if the ε is expressed using eddy viscosity definition $\varepsilon = C_\mu k^2/\nu_t$, we obtain:

$$\nu_t \left(\frac{d\overline{u}}{dy}\right)^2 = C_\mu \frac{k^2}{\nu_t}\ ,\ \left(\nu_t \frac{d\overline{u}}{dy}\right)^2 = C_\mu k^2. \tag{3.38}$$

Assuming constant wall shear stress from law-of-the-wall 3.23 leads to the final expression for k in logarithmic sub-layer:

$$\left(\frac{\tau_w}{\rho}\right)^2 = C_\mu k^2, \tag{3.39}$$

$$k = \frac{\frac{\tau_w}{\rho}}{{C_\mu}^{1/2}} = \frac{{u_\tau}^2}{{C_\mu}^{1/2}}. \tag{3.40}$$

The same expression is obtained using Townsed's observations [7] that in inertial layer following ratio is valid : $\tau_{xy}/(\rho k) \approx 0.3$, and that shear stress is equal to wall shear stress.

Expression for ε is obtained by using the same $G = \varepsilon$ balance assumption and the velocity gradient obtained from law-of-the-wall $d\overline{u}/dy = u_\tau/\kappa y$:

$$\varepsilon = \nu_t \left(\frac{d\overline{u}}{dy}\right)^2 = \frac{\tau_w}{\rho}\frac{d\overline{u}}{dy}, \tag{3.41}$$

$$\varepsilon = \frac{\tau_w}{\rho}\frac{u_\tau}{\kappa y} = \frac{{u_\tau}^3}{\kappa y}. \tag{3.42}$$

A more common expression for ε is obtained by substituting the solution for $k = u_\tau / {C_\mu}^{1/2}$ in (3.42):

$$\varepsilon = \frac{C_\mu^{3/4} k^{3/2}}{\kappa y}. \tag{3.43}$$

3.6.2 $k-\omega$ SST Turbulence Model

The $k-\omega$ model was the first two-equation model proposed by Kolmogorov in 1942 and later redesigned by many other researches. It can be used in the near-wall region and accurately predicts mean flow profile and skin friction [27]. The drawback is that, unlike the $k-\varepsilon$ model, this model has sensitivity on imposed freestream boundary conditions on second transported property, ω.

The approach that Menter [27] took was to combine the preferred characteristics of these two mentioned models. To achieve $k-\varepsilon$ freestream independency and $k-\omega$ ability to resolve the near-wall flow, first ε equation is transformed to ω formulation. According to Wilcox and [28], relation between them is:

$$\varepsilon = \beta^* k \omega, \tag{3.44}$$

$$\frac{d\varepsilon}{dt} = \beta^* k \frac{d\omega}{dt} + \beta^* \omega \frac{dk}{dt} \rightarrow \left(\frac{d\omega}{dt}\right)_{k-\varepsilon} = \frac{1}{\beta^* k}\frac{d\varepsilon}{dt} - \frac{\omega}{k}\frac{dk}{dt}. \tag{3.45}$$

Terms $d\varepsilon/dt$ and dk/dt present modelled equations of $k-\varepsilon$ and $k-\omega$ model. For detailed derivation of above expressions see [28].

Next, transformed ε equation is blended with original ω formulation:

$$\frac{d\omega}{dt} = F_1 \left(\frac{d\omega}{dt}\right)_{k-\omega} + (1-F_1)\left(\frac{d\omega}{dt}\right)_{k-\varepsilon} \tag{3.46}$$

where F_1 is a blending function which in viscous and logarithmic sublayer activates the ω formulation and in the wake region of boundary layer gradually switches to the ε formulation:

$$F_1 = \tanh({arg_1}^4), \tag{3.47}$$

$$arg_1 = \min\left\{\min\left[\max\left(\frac{\sqrt{k}}{\beta^*\omega y}, \frac{500\nu}{y^2\omega}\right), \frac{4\alpha_{\omega 2} k}{CD_{k\omega+} y^2}\right], 10\right\}, \tag{3.48}$$

$$CD_{k\omega+} = \max(CD_{k\omega}, 10^{-10}) \ , \ CD_{k\omega} = 2\alpha_{\omega 2}\frac{\nabla k \cdot \nabla \omega}{\omega}. \tag{3.49}$$

For the k equation this approach is not necessary as the dissipation term in the k equation is simply transformed with $\varepsilon = \beta^* k\omega$.

Second modification is related to eddy viscosity definition in $k-\omega$ formulation: $\nu_t = k/\omega$.

Menter further emphasises that the main information momentum equation receives about the turbulence is through eddy viscosity, which in logarithmic portions of turbulent boundary layer is overestimated and violates important observations of Townsend [27]

$$\frac{\tau_{xy}/\rho}{k} \approx a_1 \ , \ a_1 = 0.31. \tag{3.50}$$

Here, for the value of the ratio $a_1 = 0.31$ is used instead of ${C_\mu}^{1/2} = 0.3$ introduced with the $k-\varepsilon$ model.

Eddy viscosity which would satisfy these observations is:

$$\tau_{xy} = \rho \nu_t \frac{d\overline{u}}{dy} = a_1 \rho k \ , \ \nu_t = \frac{a_1 k}{\frac{d\overline{u}}{dy}}. \tag{3.51}$$

For general flows, instead of $\frac{d\overline{u}}{dy}$, a strain rate magnitude is used:

$$S = \sqrt{S_2} \ , \ S_2 = 2\mathbf{S} : \mathbf{S} \ , \ \mathbf{S} = \frac{1}{2}\left(\nabla \mathbf{u} + \nabla(\mathbf{u})^T\right). \tag{3.52}$$

Expression (3.51) is enforced in the definition of eddy viscosity $\nu_t = k/\omega$ by placing a limiter on the maximum value of ν_t:

$$\nu_t = \min\left(\frac{k}{\omega}, \frac{a_1 k}{F_2\sqrt{S_2}}\right), \tag{3.53}$$

where F_2 is a function that is constructed to have the value of 1 for boundary-layer flows and 0 for free shear layers:

$$F_2 = \tanh({arg_2}^2), \tag{3.54}$$

$$arg_2 = \min\left[\max\left(\frac{2\sqrt{k}}{\beta^*\omega y}, \frac{500\nu}{y^2\omega}\right), 100\right]. \tag{3.55}$$

The name of the model *Shear Stress Transport* is due to the enforced mechanism on eddy viscosity at which shear stresses are being transported $\tau_{xy}/(\rho k) = const$. This modification largely improved the predictions in cases with an adverse pressure gradient.

Implementation of $k-\omega$ SST model in `foam-extend` is given by description from the source code:

"Turbulence model is described in [4], with updated coefficients from [5], but with the consistent production terms from the 2001 paper as form in the 2003 paper is a typo, and the addition of the optional F_3 term for rough walls from [6]".

Eddy viscosity definition reads:

$$\nu_t = \frac{a_1 k}{\max(a_1\omega, b_1 F_{23} S_2)} \tag{3.56}$$

Turbulent kinetic energy equation reads:

$$\frac{\partial k}{\partial t} + \nabla\cdot(\overline{\mathbf{u}}k) - k\nabla\cdot\overline{\mathbf{u}} - \nabla\cdot(\Gamma_{k,eff}\nabla k) = \min(G, c_1\beta^* k\omega) - \beta^* k\omega \tag{3.57}$$

Specific dissipation rate equation reads:

$$\begin{aligned}\frac{d\omega}{dt} + \nabla\cdot(\overline{\mathbf{u}}\omega) - \omega\nabla\cdot\overline{\mathbf{u}} - \nabla\cdot(\Gamma_{\omega,eff}\nabla\omega) = \\ \gamma\min\left[S2, \frac{c_1}{a_1}\beta^*\omega\max\left(a_1\omega, b_1F_{23}\sqrt{S_2}\right)\right] \\ -\beta\omega^2 + (1-F_1)CD_{k\omega}.\end{aligned} \tag{3.58}$$

Additional relations and model constants, Table 3.2 , are:

$$\Gamma_{k,eff} = \alpha_k\nu_t + \nu \ , \ \Gamma_{\omega,eff} = \alpha_\omega\nu_t + \nu, \tag{3.59}$$

$$G = \nu_t S_2, \tag{3.60}$$

$$F_3 = 1 - \tanh({arg_3}^4) \ , \ arg_3 = \min(\frac{150\nu}{y^2\omega}, 10), \tag{3.61}$$

$$F_{23} = \begin{cases} F_2 & \text{default value,} \\ F_2 F_3 & \text{for accounting surface rougness.} \end{cases} \tag{3.62}$$

Table 3.2: k-omega SST turbulence model constants.¡

α_{k1}	α_{k2}	$\alpha_{\omega 1}$	$\alpha_{\omega 2}$	β_1	β_2	β^*	γ_1	γ_2	a_1	b_1	c_1
0.85	1.0	0.5	0.856	0.075	0.0828	0.09	5/9	0.44	0.31	1.0	10.0

Additional model constants: α_k, α_ω, β, γ, collectively noted as φ, result as a blending procedure of ω equation:

$$\varphi = F_1(\varphi_1 - \varphi_2) + \varphi_2. \tag{3.63}$$

Similarly to the $k-\varepsilon$ model, relations for the logarithmic sublayer are derived from the same assumption of balanced generation and dissipation of turbulent kinetic energy, here: $G = \beta^* k\omega$. Solution for the k equation is unchanged as it is the same equation as in $k-\varepsilon$ model:

$$k = \frac{u_\tau^2}{(\beta^*)^{1/2}} = \frac{{u_\tau}^2}{{C_\mu}^{1/2}}. \tag{3.64}$$

Derivation procedure for ω is:

$$\nu_t \frac{d\overline{u}}{dy}\frac{d\overline{u}}{dy} = \beta^*\omega k \,,\ \frac{\tau_w}{\rho}\frac{d\overline{u}}{dy} = \beta^*\omega k \,,\ \omega = \frac{\tau_w/\rho}{k}\frac{1}{\beta^*}\frac{d\overline{u}}{dy}. \tag{3.65}$$

By using $\tau_w/(\rho k) = a_1$ and velocity gradient from the log-law, the final expression for distribution of ω in logarithmic region is:

$$\omega = \frac{a_1}{\beta^*}\frac{d\overline{u}}{dy} \,,\ \omega = \frac{u_\tau}{0.3\kappa y}. \tag{3.66}$$

Value $a_1/\beta^* = 1/0.29$ is replaced either with $1/a_1$ or $1/(\beta^*)^{1/2} = 1/C_\mu^{1/2}$, depending on the choice of the author.

In the case of $k-\omega$ formulation, an additional expression for ω, valid in the viscous region, can be derived. From the assumption of equality of viscous and dissipation terms [29] in that region, we obtain the following differential equation:

$$\frac{d^2\omega}{dy^2} = \frac{\beta}{\nu}\omega^2 \tag{3.67}$$

which has a solution [7]:

$$\omega = \frac{6\nu}{\beta_1 y^2}. \tag{3.68}$$

3.6.3 Low-Reynolds Number Effects

We start this section by analysing the behaviour of turbulent quantities when approaching the wall. For simplicity, the analysis is performed for flow over a flat plate. Taylor series expansion of fluctuating velocity components [19] near the wall reads:

$$u'(y) = u'(0) + \left(\frac{\partial u'}{\partial y}\right)_{y=0} y + \left(\frac{1}{2}\frac{\partial^2 u'}{\partial y^2}\right)_{y=0} y^2 + \cdots, \tag{3.69}$$

$$v'(y) = v'(0) + \left(\frac{\partial v'}{\partial y}\right)_{y=0} y + \left(\frac{1}{2}\frac{\partial^2 v'}{\partial y^2}\right)_{y=0} y^2 + \cdots, \tag{3.70}$$

$$w'(y) = w'(0) + \left(\frac{\partial w'}{\partial y}\right)_{y=0} y + \left(\frac{1}{2}\frac{\partial^2 w'}{\partial y^2}\right)_{y=0} y^2 + \cdots, \tag{3.71}$$

in which it is assumnerd that velocity gradients at $y = 0$ in wall parallel direction are zero. Continuity equation for the fluctuating velocity components at the wall is:

$$\left(\frac{\partial u'}{\partial x}\right)_{y=0} + \left(\frac{\partial v'}{\partial y}\right)_{y=0} + \left(\frac{\partial w'}{\partial z}\right)_{y=0} = 0 \tag{3.72}$$

which by including the $\partial/\partial x = 0$ and $\partial/\partial z = 0$ reduces to:

$$\left(\frac{\partial v'}{\partial y}\right)_{y=0} = 0. \tag{3.73}$$

With the above expressions, and using the no-slip condition, Taylor series can be rewritten as:

$$u'(y) = Ay + \mathcal{O}(y^2,) \tag{3.74}$$

$$v'(y) = By^2 + \mathcal{O}(y^3), \tag{3.75}$$

$$w'(y) = Cy + \mathcal{O}(y^2). \tag{3.76}$$

Distribution of turbulent kinetic energy near the wall is:

$$\begin{aligned} k &= \frac{1}{2}\overline{\mathbf{u}' \cdot \mathbf{u}'} = \frac{1}{2}[\overline{(u')^2 + (v')^2 + (w')^2}] \\ &= \frac{1}{2}(\overline{A^2 + C^2})y^2 + \mathscr{O}(y^3) \approx \frac{1}{2}(A^2 + C^2)y^2, \end{aligned} \tag{3.77}$$

and near-wall distribution of dissipation rate [7] can be rewritten as:

$$\begin{aligned} \varepsilon &= \nu\overline{\nabla\mathbf{u}' : \nabla\mathbf{u}'} = \nu\overline{\left(\frac{\partial u}{\partial y}\right)^2 + \left(\frac{\partial w}{\partial y}\right)^2 + \cdots} \\ &= \nu(A^2 + C^2) + \mathscr{O}(y) \approx \nu(A^2 + C^2). \end{aligned} \tag{3.78}$$

Combining expressions (3.77) and (3.78), a relation is obtained in which finding the value of constants A and C is avoided:

$$\frac{\varepsilon}{k} = \frac{2\nu}{y^2} \rightarrow \varepsilon = \frac{2\nu k}{y^2}. \tag{3.79}$$

Using $\varepsilon = \beta^* k\omega$, a relation for near-wall ω can also be found:

$$\omega = \frac{2\nu}{\beta^* y^2}. \tag{3.80}$$

Comparing the $\varepsilon = \nu(A^2 + C^2) + \mathscr{O}(y)$ and $k = 0.5(A^2 + C^2)y^2 + \mathscr{O}(y^3)$ another expression can be deduced:

$$\varepsilon = 2\nu\left(\frac{\partial\sqrt{k}}{\partial y}\right)^2. \tag{3.81}$$

Final expression valid for ε in near-wall region follows from k equation and assumption that near the wall diffusion and dissipation terms are balanced:

$$\varepsilon = \nu\frac{dk^2}{dy^2}. \tag{3.82}$$

Models which are following the derived distribution of turbulent quantities in near-wall region are said to be asymptotically consistent.

Historically, in modelling the transport equations for turbulence, two approaches can be discerned. In the first approach, a model is tuned for the regions distanced from the wall, characterised by local High Reynolds Numbers - HRN models. The near-wall region is characterised

by high gradients, and computational resources at the time of development of these models were insufficient to deal with them. Instead, when these models are used, near-wall regions are covered by wall functions. Typically, presented $k-\varepsilon$ model is of this class of turbulence models.

In the second approach, viscous effects of the near-wall region are taken into account by multiplying each term of the right-hand side of HRN models with damping functions which are activated in the near-wall region (value below 1) to damp the high-Reynolds formulation. Damping functions are constructed to match the DNS distribution and asymptotic consistency of turbulent quantities as accurately as possible and to retrieve the additive constant B of the law-of-the-wall. To achieve this, a significant number of damping functions has been developed. Models following this approach are termed as Low-Reynolds Number - LRN models. Wilcox [7] points that it is misleading to expect that this approach corrects the bad performance of $k-\varepsilon$ in the case of adverse pressure gradient flows [7].

Later, performance of $k-\omega$ clarified some uncertainties of two-equation models. It showed that the problem was not in the damping functions but in the choice of the second transported variable. This model allows its use in the near wall region, and although it is not asymptotically consistent (compare (3.80) and (3.68)) it reproduces reasonable mean flow profiles ($B = 5.1$ [7]).

Finally, Menter in his SST model showed that direct modification to eddy viscosity has a greater effect than matching the distribution of k and ε with DNS or experimental data. He even argues that it is unclear why matching turbulence variables with the DNS data should result in improved eddy viscosity distribution.

Therefore, $k-\omega$ and $k-\omega$ SST are not real low-Reynolds turbulence models but are often referred as such. This is a misconception since additional variants of $k-\omega$ and $k-\omega$ SST with the damping functions exist.

3.7 Closure

This chapter covered turbulence modelling from the engineering perspective. The main emphasis was on RANS modelling of which two models were presented in detail, $k-\varepsilon$ and $k-\omega$ SST model. Both of them are based on the Boussinesq hypothesis, but also on the conclusions of the mixing length model which was derived in detail. The end of the chapter introduced some limitations of the presented two-equation models. The focus was on the region near the wall, since later on the wall function will be explained and other methods used as a part of near-wall treatment.

Chapter 4

Numerical Modeling of Turbulent Flows

In the previous chapter it was noted that analytical solution to the Navier-Stokes equations exists only for a few special cases. After the Reynolds averaging and Boussinesq assumption, the semi-analytical solution exists only for a wall limited flow region. When two additional transport equations which desribe the eddy viscosity are added to the set, the analytical solution is impossible to obtain. To find a solution for more complex problems of practical interest, numerical procedures are often employed. Specifying the domain of interest with boundary and initial conditions, these methods will provide an approximate solution in the predefined set of points of the domain.

As a part of numerical solution procedure, boundary conditions for each transported variable need to be prescribed. The boundary conditions for an incompressible flow are:

- Freestream boundary conditions such as inlet and outlet,
- Periodic boundary conditions,
- Wall boundary conditions - wall treatment,
- Symmetry plane.

A commonly used numerical method in Computational Fluid Dynamics is the Finite Volume Method and the wall treatment will be explained pertinent to it. The logic which all methods follow is explained in the first section and each following section gives more detail for each specific method. More detail on the specified numerical method can be seen in [30] and [31].

4.1 General Approach to Wall Treatment

In Chapter 2 it was pointed out that the main characteristic of turbulence is its enhanced mixing which in near wall region causes an increase of gradients. From a computational point of view, most natural way to deal with this would be to use sufficiently fine mesh to completely resolve the flow. Physically, first computational point must fall in the viscous sublayer, $y^+ < 0.5$. This approach is called the Low-Reynolds Number approach and requires turbulence models that can be integrated through viscous sublayer, such as LRN models, or in our case $k-\omega$ SST. This procedure dramatically increases the number of cells leading to a high computational time and large memory requirements. Consequently, resolving high gradients makes convergence rate much slower. Also, high-Reynolds models cannot be used on such meshes, such as the introduced $k-\varepsilon$ model. Because of these disadvantages a different method needs to be used.

The first idea would be to use the findings of the standard law-of-the-wall and set the value of velocity in wall adjacent cells. This way, a problem of high gradients is avoided but it is only applicable to the case of a flat plate flow. A more general way would be to obtain the value of wall shear stress from the law-of-the-wall and compare it with the discretised one: $\nu\overline{u}/y$. For cases where values differ, additional viscosity ${\nu_t}^w$ is introduced in the discretised form of wall shear stress for correction:

$$\frac{\tau_w}{\rho} = (\nu + {\nu_t}^w)\frac{\overline{u}}{y}. \tag{4.1}$$

Physically, eddy viscosity at the wall is zero. Still, this notation is adopted as it is used in `foam-extend`. The term $\overline{u}$ stands for the magnitude of velocity vector parallel to the wall and for the case of a moving wall, magnitude of relative velocity vector parallel to the wall. In the context of Finite Volume Method, y is the normal distance of first cell centre from the wall. In order to present the final implementation of wall treatments in `foam-extend`, in final expressions velocity gradient will be consistently written as $\overline{u}/y = |\nabla\overline{\mathbf{u}}_w|$.

Standard law-of-the-wall is derived using the assumption of negligible convection and pressure gradient effects, meaning that for complex flows the obtained wall shear stress will at best be just an approximation. Other expressions, which include effects of pressure gradient and convection exist, and some of them will be shown in the next sections.

The advantage of the wall functions is that the need for a large number of grid nodes points near the wall is eliminated. In this way, resolving the near wall high gradients is avoided making the computation more efficient. Furthermore, accounting for the viscous effects in turbulence models through damping functions is avoided. But, the method is not completely satisfactory. Numerical solutions are sensitive to the placement of the first node. Strictly speaking, wall functions are limited by the validity of expression for wall shear stress, e.g. for law-of-the-wall y^+ must be between 30 and 300. The upper limit is not strictly defined, and depends on the Reynolds number.

Turbulent kinetic energy equation follows a similar procedure. The value for k in first cell centre can be set using the expression derived for the log-layer:

$$k = \frac{{u_\tau}^2}{{C_\mu}^{1/2}}, \tag{4.2}$$

or a more general approach would be to solve the transport equation with a modified production and destruction term. Both terms have large gradients and need to be modified in order to achieve an accurate solution on coarse meshes. For turbulent kinetic energy, two boundary conditions are valid, $k = 0$ and $\nabla k|_n = 0$ (see (3.77)). Using the $\nabla k|_n = 0$ sets the diffusion term to zero and is much more often used than $k = 0$.

For ε, specifying the boundary condition is not straightforward. Asymptotic analysis implies a fixed value of ε on the wall:

$$\varepsilon = \nu(A^2 + C^2), \tag{4.3}$$

but the constants A and C are unspecified. Instead, a definition for dissipation equation is altered to $\tilde{\varepsilon}$ for which the wall-boundary condition: $\tilde{\varepsilon} = 0$ is applied and the relation for dissipation

term in k equation is given by:

$$\tilde{\varepsilon} = \varepsilon - \varepsilon_{BC}. \tag{4.4}$$

Where ε_{BC} is the expression valid as wall boundary condition, derived from the asymptotic analysis, with the possibility of being:

$$\varepsilon_{BC} = \frac{2\nu k}{y^2} \quad \text{or} \quad \varepsilon_{BC} = 2\nu \left(\frac{\partial \sqrt{k}}{\partial y} \right)^2 \quad \text{or} \quad \varepsilon_{BC} = \nu \frac{\partial^2 k}{\partial y^2}. \tag{4.5}$$

In their version of the Low-Reynolds $k-\varepsilon$ model, Lam and Bremhorst [7] solve ε equation and impose $\nu \partial^2 k / \partial y^2$ as wall boundary condition.

Note that this procedure is only meaningful for the Low-Reynolds versions of $k-\varepsilon$ model. In the case of our standard $k-\varepsilon$ model, ε equation prohibits the use of model near the wall, and above mentioned methods for specifying the boundary condition cannot be used. Instead, value is prescribed in wall adjacent cell using derived wall function:

$$\varepsilon = \frac{C_\mu^{3/4} k^{3/2}}{\kappa y}, \tag{4.6}$$

or some other expression, which will be covered in next sections.

Wall boundary condition for $\omega = \frac{6\nu}{\beta_1 y^2}\Big|_{y=0}$ at the wall has singularity and from a numerical point of view cannot be used. Instead, value is set in wall adjacent cell centre using the solution either for viscous or log-layer, depending of the placement of first cell centre. Menter [27] alters expression for ω in viscous layer (3.68) which can be used as boundary condition:

$$\omega = 10 \frac{6\nu}{\beta_1 y^2}. \tag{4.7}$$

The use of above expression is valid for $y^+ < 3$.

4.2 Wall Functions for $k-\varepsilon$ Model

4.2.1 Standard Wall Functions

In this section, wall functions of Launder and Spalding are presented. As they state [11], they: "*represent the best practice of the Imperial College group*" and are given for $k-\varepsilon$ turbulence model. Wall shear stress is obtained from law-of-the-wall in which $u^* = {C_\mu}^{1/4}k^{1/2}$ is used as the velocity scale instead of $u_\tau = \tau_w/\rho$:

$$\overline{u} = \frac{u^*}{\kappa} ln\left(E\frac{u^* y}{\nu}\right) \ , \ u^* = \frac{\overline{u}\kappa}{ln(Ey^*)} \ , \ u^* = \frac{\overline{u}\kappa}{ln(Ey^*)} \ \Big/ \cdot u^* \ , \tag{4.8}$$

$$u^{*2} = \frac{u^*\overline{u}\kappa}{ln(Ey^*)} \ , \ \frac{\tau_w}{\rho} = \frac{{C_\mu}^{1/4}k^{1/2}\overline{u}\kappa}{ln(Ey^*)}. \tag{4.9}$$

New velocity scale u^* follows from the Townsend observations: $\tau_w/\rho = {C_\mu}^{1/2}k$ (here ${C_\mu}^{1/2}$ is used insted a_1) and improves the performance [32] in separation and reattachment points of the law-of-the-wall. Also, by replacing u_τ with u^*, new non-dimensional distance parameter is introduced, $y^* = u^* y/\nu$.

Turbulent kinetic energy is calculated from transport equation, setting the diffusion term to zero. The modified production term is calculated from the original definition, which for a 2D case reduces to:

$$G = \nu_t\left(\frac{d\overline{u}}{dy}\right)^2 = \nu_t\left(\frac{d\overline{u}}{dy}\right)\left(\frac{d\overline{u}}{dy}\right) = \frac{\tau_w}{\rho}\left(\frac{d\overline{u}}{dy}\right) = \frac{\tau_w}{\rho}\frac{\tau_w}{\kappa\rho{C_\mu}^{1/4}k^{1/2}y}. \tag{4.10}$$

The final expression (4.10) for G follows from the assumption of near-wall constant shear stress $\nu_t(d\overline{u}/dy) = \tau_w/\rho$, and velocity gradient derived from law-of-the-wall (4.8) which is redefined with new velocity scale u^*:

$$\frac{d\overline{u}}{dy} = \frac{u^*}{\kappa y} \ , \ \frac{d\overline{u}}{dy} = \frac{u^*}{\kappa y}\cdot\frac{u^*}{u^*} = \frac{u^{*2}}{\kappa u^* y} = \frac{\frac{\tau_w}{\rho}}{\kappa{C_\mu}^{1/4}k^{1/2}y}. \tag{4.11}$$

High gradients of dissipation term can be taken into account by the averaging procedure. However, performing the integration:

$$\overline{\varepsilon} = \frac{1}{2y}\int_0^{2y}\frac{{C_\mu}^{3/4}k^{3/2}}{\kappa y}dy, \tag{4.12}$$

leads to the mathematical singularity at the wall. This happens as the expression $\varepsilon = {C_\mu}^{3/4} k^{3/2}/\kappa y$ is valid only in logarithmic portion of turbulent boundary layer. Instead, the modified dissipation term is found from regular production = dissipation balance in the inertial layer. The averaging is performed up to the first wall-grid point, and not throughout the whole control volume:

$$\int_0^y \varepsilon dy = \int_0^y G dy = \int_0^y \frac{\tau_w}{\rho} \left(\frac{d\overline{u}}{dy} \right) dy. \tag{4.13}$$

Using the assumption of constant wall shear stresses leads to:

$$\int_0^y \varepsilon dy = \frac{\tau_w}{\rho} \int_0^y \left(\frac{d\overline{u}}{dy} \right) dy = \frac{\tau_w}{\rho} \Delta\overline{u}, \tag{4.14}$$

$$\Delta\overline{u} = \overline{u}_2 - \overline{u}_1 = \frac{u^*}{\kappa} \ln(Ey^*) - \overline{u}_1. \tag{4.15}$$

In the expression (4.15), $\Delta\overline{u}$ is obtained using the value from the law-of-the-wall and boundary condition for velocity. If the wall boundary condition for velocity is zero, and expression (4.15) is back-substituted to (4.14), after averaging, the final expression is:

$$\frac{1}{y} \int_0^y \varepsilon dy = \frac{1}{y} \frac{\tau_w}{\rho} \frac{u^*}{\kappa} \ln(Ey^*) = \frac{1}{y} \frac{{u^*}^3}{\kappa} \ln(Ey^*) = \frac{1}{y} \frac{{C_\mu}^{3/4} k^{3/2}}{\kappa} \ln(Ey^*). \tag{4.16}$$

In the original paper [11], for the above expression C_μ is used rather than ${C_\mu}^{3/4}$. As it is noted in [28], it is probably a typographical error.

Finally, transport equation for ε is not solved and instead the value at the wall adjacent cell centre is prescribed using the expression:

$$\varepsilon = \frac{{C_\mu}^{3/4} k^{3/2}}{\kappa y}. \tag{4.17}$$

In `foam-extend` this is the default wall function for k-epsilon model. Expressions in the form in which they are implemented will be covered in section 4.4. Similar wall functions can be derived for the $k-\omega$ SST model. As this model has additional property that can be used through viscous sublayer, a more general method can be developed in which wall functions are just a part of wall treatment. This is presented in section 4.3.

4.2.2 Non-Equilibrium Wall Functions

Sometimes, near-wall flows are subjected to conditions that differ from the ones for which standard law-of-the-wall is derived. For favourable pressure gradient, major differences can occur from the so-called universal inner-law velocity distribution, meaning that standard wall functions will be less reliable. For this reason, a more general wall functions that account for those non-equilibrium effects are presented here. The law-of-the-wall, modified for accounting the pressure gradient [8] is:

$$\frac{\tilde{U}{C_\mu}^{1/4}k^{1/2}}{\tau_w/\rho} = \frac{1}{\kappa}\ln(Ey^*), \tag{4.18}$$

$$\tilde{U} = \overline{u} - \frac{1}{2}\frac{d\overline{p}}{dx}\left[\frac{y_v}{\kappa k^{1/2}}\ln\left(\frac{y}{y_v}\right) + \frac{y-y_v}{\kappa k^{1/2}} + \frac{{y_v}^2}{\nu}\right], \tag{4.19}$$

in which $d\overline{p}/dx$ is the wall parallel kinematic pressure gradient. Physical viscous sublayer thickness y_v, denotes the edge of the viscous sublayer ${y^*}_v = 11.225$ as the intersection of viscous law $u^+ = y^+$ and log-law $u^+ = \frac{1}{\kappa}\ln(Ey^+)$. Different values for ${y^*}_v$ are reported in different sources. The actual solution of the resulting nolinear equation $y^+ = \frac{1}{\kappa}ln(Ey^+)$ is $y^+ = 11.5301$.

$${y^*}_v = \frac{{C_\mu}^{1/4}k^{1/2}y_v}{\nu}\ , \ y_v = \frac{11.225\nu}{{C_\mu}^{1/4}k^{1/2}}. \tag{4.20}$$

As already pointed out, two distinct regions with different structures near the wall exist, the viscous and inertial sublayer. However, previous wall functions eliminated the influence of the viscous sublayer, which may be significant for the solution. For improving the accuracy, a more complete model of near-wall turbulence is required. Approximated variations of turbulent quantities across the wall adjacent cell are:

$$\tau_t = \begin{cases} 0 & ,y < y_v \\ \tau_w & ,y > y_v \end{cases}, \ k = \begin{cases} (\frac{y}{y_v}^2) & ,y < y_v \\ k_P & ,y > y_v \end{cases}, \ \varepsilon = \begin{cases} \frac{2\nu k}{y^2} & ,y < y_v \\ \frac{{C_\mu}^{3/4}k^{3/2}}{\kappa y} & ,y > y_v \end{cases}, \tag{4.21}$$

where k_P denotes the value in the cell centre.

Artificial wall eddy viscosity ${\nu_t}^w$ for cells in turbulent region is computed by equating the wall shear stress by its discretised value:

$$\frac{\tau_w}{\rho} = \frac{\tilde{U}{C_\mu}^{1/4}k^{1/2}\kappa}{\ln(Ey^*)} = (\nu + {\nu_t}^w)\frac{\overline{u}}{y}, \tag{4.22}$$

$${\nu_t}^w = \frac{y}{\overline{u}}\frac{\tilde{U}{C_\mu}^{1/4}k^{1/2}\kappa}{\ln(Ey^*)} - \nu = \nu\left(\frac{\tilde{U}\kappa}{\overline{u}\,\ln(Ey^*)}\frac{{C_\mu}^{1/4}k^{1/2}y}{\nu} - 1\right) = \nu\left(\frac{\tilde{U}\,y^*\kappa}{\overline{u}\ln(Ey^*)} - 1\right). \tag{4.23}$$

Using the prescribed variation of turbulent shear stresses (4.21), wall eddy viscosity for the whole near-wall region is defined as:

$${\nu_t}^w = \begin{cases} 0 & ,y < y_v \\ \nu\left(\frac{\tilde{U}y^*\kappa}{\overline{u}ln(Ey^*)} - 1\right) & ,y > y_v \end{cases}. \tag{4.24}$$

Here, modified terms for turbulent kinetic energy equation, averaged production and dissipation terms are including the effects of viscous layer by averaging the assumed variation over first wall adjacent cell. Given procedure is valid only for quadrilateral and hexahedral cell types:

$$\begin{aligned}\overline{G} &= \frac{1}{2y}\int_0^{2y}\frac{\tau_t}{\rho}\frac{d\overline{u}}{dy}dy = \frac{1}{2y}\left(\int_0^{y_v}0\,dy + \int_{y_v}^{2y}\frac{\tau_w}{\rho}\frac{d\overline{u}}{dy}dy\right) = \frac{1}{2y}\int_{y_v}^{2y}\frac{\tau_w}{\rho}\frac{\tau_w}{\kappa\rho{C_\mu}^{1/4}{k_p}^{1/2}y}dy \\ &= \frac{1}{2y}\left(\frac{\tau_w}{\rho}\right)^2\frac{1}{\kappa{C_\mu}^{1/4}{k_p}^{1/2}}\ln\left(\frac{2y}{y_v}\right) = \frac{((\nu+{\nu_t}^w)\,|\nabla\overline{\mathbf{u}}_w|)^2}{2y\,{C_\mu}^{1/4}k^{1/2}\kappa}\ln\left(\frac{2y}{y_v}\right),\end{aligned} \tag{4.25}$$

$$\begin{aligned}\overline{\varepsilon} &= \frac{1}{2y}\int_0^{2y}\varepsilon\,dy = \frac{1}{2y}\left(\int_0^{y_v}\frac{2\nu k_P}{{y_v}^2}dy + \int_{y_v}^{2y}\frac{{k_P}^{3/2}{C_\mu}^{3/4}}{\kappa y}dy\right) \\ &= \frac{1}{2y}\left[\frac{2\nu k_P}{{y_v}^2}y_v + \frac{{k_P}^{3/2}{C_\mu}^{3/4}}{\kappa}\ln\left(\frac{2y}{y_v}\right)\right] = \frac{1}{2y}\left[\frac{2\nu k_p}{y_v} + \frac{{k_P}^{3/2}{C_\mu}^{3/4}}{\kappa}\ln\left(\frac{2y}{y_v}\right)\right].\end{aligned} \tag{4.26}$$

Final form of the averaged terms reads:

$$\overline{G} = \begin{cases} 0 & ,y < y_v \\ \frac{((\nu+{\nu_t}^w)|\nabla\overline{\mathbf{u}}_w|)^2\ln(\frac{2y}{y_v})}{2y{C_\mu}^{1/4}k^{1/2}\kappa} & ,y > y_v \end{cases}, \overline{\varepsilon} = \begin{cases} \frac{1}{2y}\left[\frac{2\nu k_p}{y_v} + \frac{{k_P}^{3/2}{C_\mu}^{3/4}}{\kappa}\ln\left(\frac{2y}{y_v}\right)\right] & \\ \frac{2\nu k_P}{{y_v}^2} & ,y > y_v \end{cases}. \tag{4.27}$$

Comparing this with the expression derived for velocity gradient, it is evident that in averaged production term, pressure gradient is only partially included in velocity gradient. Assuming that $d\overline{p}/dx$ is constant:

$$\overline{u} = \frac{\tau_w}{\rho}\frac{1}{\kappa {C_\mu}^{1/4} k^{1/2}} ln\left(E\frac{{C_\mu}^{1/4}k^{1/2}y}{\nu}\right) + \frac{1}{2}\frac{d\overline{p}}{dx}\left[\frac{y_v}{\kappa k^{1/2}} ln\left(\frac{y}{y_v}\right) + \frac{y-y_v}{\kappa k^{1/2}} + \frac{{y_v}^2}{\nu}\right], \tag{4.28}$$

$$\frac{d\overline{u}}{dy} = \frac{\tau_w}{\rho}\frac{1}{\kappa {C_\mu}^{1/4} k^{1/2}}\frac{1}{y} + \frac{1}{2}\frac{d\overline{p}}{dx}\left[\frac{y_v}{\kappa k^{1/2}}\frac{1}{y} + \frac{1}{\kappa k^{1/2}}\right]. \tag{4.29}$$

As it was the case with the standard wall functions with ε equation, value is prescribed in the wall adjacent cells, but here using the assumed variation (4.21):

$$\varepsilon = \begin{cases} \frac{2\nu k}{y^2} & , y < y_v \\ \frac{{C_\mu}^{3/4}k^{3/2}}{\kappa y} & , y > y_v \end{cases}. \tag{4.30}$$

4.3 Wall Treatments for $k-\omega$ SST Model

4.3.1 Automatic Near-Wall Treatment

For turbulence models that allow integration up to the wall, a more general method of wall treatment can be applied. If the first cell volume falls in the logarithmic region, a wall function approach is preferred, effectively avoiding the sharp gradients near the wall. For cells in the viscous region, it would be reasonable to make use of a relation which is valid there, expressions 3.30 and 3.68. When refining the near-wall mesh, it would be desirable to have a function that gradually switches from the wall function expressions to expressions for the viscous layer, making them appropriate even for the buffer region. Something similar is used with non-equilibrium wall functions (section 4.2.2), although there, with a sharp switching behaviour at $y^+ = 11.225$.

The method here is presented for the $k-\omega$ SST model, but other turbulence models, which allow integration through viscous sublayer, use the same logic too.

Esch and Menter's [4] proposition for wall treatment is presented here.

- Blending for shear stresses $\frac{\tau_w}{\rho} = {u_\tau}^2$ reads:

$$u_\tau = \sqrt[4]{{u_{\tau vis}}^4 + {u_{\tau log}}^4}, \tag{4.31}$$

$$u^+ = y^+ \ , \ \frac{\overline{u}}{u_{\tau vis}} = \frac{u_{\tau vis} y}{\nu} \ , \ {u_{\tau vis}}^2 = \nu \frac{\overline{u}}{y}, \tag{4.32}$$

$$u^+ = \frac{1}{\kappa} ln(Ey^+) \ , \ \frac{\overline{u}}{u_{\tau log}} = \frac{1}{\kappa} ln(Ey^+) \ , \ u_{\tau log} = \frac{\overline{u}\kappa}{ln(Ey^+)}, \tag{4.33}$$

- Blending for the specific dissipation rate ω:

$$\omega = \sqrt{{\omega_{vis}}^2 + {\omega_{log}}^2}, \tag{4.34}$$

$$\omega_{vis} = \frac{6\nu}{\beta_1 y^2}, \quad \omega_{log} = \frac{u_\tau}{{C_\mu}^{1/2} \kappa y}. \tag{4.35}$$

For low y values the $1/y^2$ in ω_{vis} will dominate and for larger y values $\frac{1}{y}$ from ω_{log} will prevail. Similar obseravtions hold for friction velocity blending. For small y, $1/y$ values prevail over $|1/ln(y)|$ while the opposite is for larger y.
Also, another very common method is Kader blending [14]:

$$\phi = \phi_{vis} e^\Gamma + \phi_{log} e^{1/\Gamma} \ , \ \Gamma = -\frac{0.01(y^+)^4}{1+5y^+}, \tag{4.36}$$

where ϕ can be any flow property for which a value is required in the wall adjacent cell, e.g. : G, $\frac{d\overline{u}}{dy}$, ω, τ_w...

Wall treatment, that will be tested in the next chapter, is based on Menter's blend, but with a more detailed implementation, as given in [32]. Although they refer to [33], formulations are not the same. Furthermore, similar expressions are given in [9], but without any reference to the source. Additionally, production term is altered according to [14].

- Wall shear stress with different definition: $\frac{\tau_w}{\rho} = u_\tau u^*$, is computed as:

$$u^* = \sqrt[4]{{u_{\tau vis}}^4 + (\sqrt{a_1 k})^4} \quad , u_\tau = \sqrt[4]{{u_{\tau vis}}^4 + {u_{\tau log}}^4} \tag{4.37}$$

- Specific dissipation rate $\omega = \sqrt{{\omega_{vis}}^2 + {\omega_{log}}^2}$ is blended with altered expression for log-layer. Instead of the usual ${C_\mu}^{1/2} = 0.3$ constant, here $a_1 = 0.31$ is used, and also u_τ is replaced with u^*:

$$\omega_{vis} = \frac{6\nu}{\beta_1 y^2}, \tag{4.38}$$

$$\omega_{log} = \frac{u_\tau}{a_1 \kappa y} = \frac{u_\tau}{a_\kappa y}\frac{u_\tau}{u_\tau}\frac{\nu}{\nu} = \frac{{u_\tau}^2}{a_1 \kappa \nu \frac{u_\tau y}{\nu}} = \frac{{u_\tau}^2}{a_1 \kappa \nu y^+} = \frac{{u^*}^2}{a_1 \kappa \nu y^+}. \tag{4.39}$$

This wall treatment uses a combination of derived and empirical values. Caution should be taken in (4.39) as u^* is now a blended (4.37) value.

Solution procedure stays the same as with the wall functions. For the momentum equation, ${\nu_t}^w$ is obtained from equality:

$$\frac{\tau_w}{\rho} = u_\tau u^* = (\nu + {\nu_t}^w)|\nabla \overline{\mathbf{u}}_w| \ , \ {\nu_t}^w = \frac{u_\tau u^*}{|\nabla \overline{\mathbf{u}}_w|} - \nu. \tag{4.40}$$

ω is set in wall adjacent cell according to (4.38), and the same value is used when solving the k equation. The modified production term is prescribed as:

$$G_{log} = \frac{\tau_w}{\rho}\left(\frac{d\overline{u}}{dy}\right) = (\nu + {\nu_t}^w)|\nabla \overline{\mathbf{u}}_w|\frac{u^*}{\kappa y}, \tag{4.41}$$

where for the wall shear stress $\tau_w/\rho = u_\tau u^* = (\nu + {\nu_t}^w)|\nabla \overline{\mathbf{u}}_w|$ is used, and velocity gradient is from the log-law $d\overline{u}/dy = u^*/\kappa y$, but now with u^* as a blended value.

Although the wall shear stress appearing in (4.41) is blended-value applicable for the whole near-wall region, due to the velocity gradient $d\overline{u}/dy = u^*/\kappa y$, the final result should be applicable only for log-region. It is shown in [14] that the similar expression to (4.41) gives reasonable representation of G through the whole near-wall region, but for better asymptotic consistency in viscous region, G_{log} should be blended with a definition for viscous layer $G_{vis} = \nu_t(d\overline{u}/dy)^2 = k/\omega_{vis}(\overline{u}/y)^2$. For that purpose Kader, blending is used:

$$G = G_{vis}e^{\Gamma} + G_{log}e^{1/\Gamma}. \tag{4.42}$$

In [14] a different turbulence model is used, but we expect to achieve similar behaviour the with $k-\omega$ SST model.

4.3.2 Enhanced Wall Treatment

In this section, we pursue to improve automatic wall treatment method, in order to make it more accurate by taking into account the effects of the pressure gradient. Derivation of the expressions follows the notes from [10], and the original paper [1] upon which the wall treatment is based.

The starting point is the simplified averaged wall parallel momentum equation:

$$\frac{\partial \overline{u}}{\partial t} + \overline{\mathbf{u}} \cdot \nabla \overline{u} = -\frac{1}{\rho}\frac{\partial \overline{p}}{\partial x} + \frac{\partial}{\partial y}\left(\nu \frac{\partial \overline{u}}{\partial y} - \overline{u'v'}\right). \tag{4.43}$$

Neglecting the unsteady and convective terms and performing the integration while keeping the pressure gradient constant results with the following:

$$\left(\nu \frac{d\overline{u}}{dy} - \overline{u'v'}\right) = \frac{d\overline{p}}{dx} y + C. \tag{4.44}$$

The same approach is used in deriving the law-of-the-wall, the only difference being that the pressure gradient term is retained. At the wall, shear stress is equal to wall shear stresses, which leads to the value for the integration constant $(\nu d\overline{u}/dy - \overline{u'v'}) = \tau_w/\rho = C$:

$$\left(\nu \frac{d\overline{u}}{dy} - \overline{u'v'}\right) = \frac{d\overline{p}}{dx} y + \frac{\tau_w}{\rho}. \tag{4.45}$$

Near the wall, viscous effects are dominant and turbulent shear stress $\tau_t/\rho = -\overline{u'v'}$ can be neglected:

$$\nu \frac{d\overline{u}}{dy} = \frac{d\overline{p}}{dx} y + \frac{\tau_w}{\rho}. \tag{4.46}$$

Equation is further transformed into dimensionless form:

$$\nu \frac{d\overline{u}}{dy} = \frac{d\overline{p}}{dx} y + \frac{\tau_w}{\rho} : \Big/ \frac{\tau_w}{\rho} \ , \ \frac{\nu}{\tau_w/\rho}\frac{d\overline{u}}{dy} = \frac{1}{\tau_w/\rho}\frac{d\overline{p}}{dx} y + 1, \tag{4.47}$$

$$\frac{\nu}{{u_\tau}^2}\frac{d\overline{u}}{dy} = \frac{1}{{u_\tau}^2}\frac{d\overline{p}}{dx} y \frac{u_\tau}{u_\tau}\frac{\nu}{\nu} + 1 \ , \ \frac{\nu}{u_\tau u_\tau}\frac{d\overline{u}}{dy} = \alpha y^+ + 1, \tag{4.48}$$

$$\frac{d(\frac{\overline{u}}{u_\tau})}{d(\frac{u_\tau y}{\nu})} = \alpha y^+ + 1 \ , \ \frac{du^+}{dy^+} = \alpha y^+ + 1, \tag{4.49}$$

with introduced pressure gradient parameter $\alpha = \nu/{u_\tau}^3 (d\overline{p}/dx)$. Note that the pressure is divided by the density. Integrating over y^+ and setting the integration constant from the no-slip

condition, leads to the solution for the velocity profile near the wall:

$$u^+_{vis} = \alpha\frac{y^+}{2} + y^+ = y^+\left(1 + \frac{\alpha}{2}y^+\right). \tag{4.50}$$

Setting $\alpha = 0$, expression (4.50) reduces to the standard viscous law-of-the-wall $u^+ = y^+$. Note that Fluent's definition of α is based on u^*:

$$\alpha = \frac{\nu}{u^{*3}}\frac{d\overline{p}}{dx}. \tag{4.51}$$

Away from the wall, turbulent shear stresses prevail over viscous stresses (4.45), and for modelling them Prandtl's mixing length model is used: $-\overline{u'v'} = \kappa^2 y^2 \left|d\overline{u}/dy\right| d\overline{u}/dy$:

$$\kappa^2 y^2 \left|\frac{d\overline{u}}{dy}\right| \frac{d\overline{u}}{dy} = \frac{d\overline{p}}{dx}y + \frac{\tau_w}{\rho}. \tag{4.52}$$

Assuming that the right hand side is non-negative, which puts a lower limit on the value of the pressure gradient $d\overline{p}/dyy \geq -\tau_w$, the term $\left|d\overline{u}/dy\right| d\overline{u}/dy$ can be replaced with $\left(d\overline{u}/dy\right)^2$:

$$\kappa^2 y^2 \left(\frac{d\overline{u}}{dy}\right)^2 = \frac{d\overline{p}}{dx}y + \tau_w\,,\ \left(\frac{d\overline{u}}{dy}\right)^2 = \frac{\frac{d\overline{p}}{dx}y + \frac{\tau_w}{\rho}}{\kappa^2 y^2}. \tag{4.53}$$

Taking the square root:

$$\frac{d\overline{u}}{dy} = \frac{\sqrt{\frac{d\overline{p}}{dx}y + \frac{\tau_w}{\rho}}}{\kappa y}\,,\ \frac{d\overline{u}}{dy} = \frac{\sqrt{\frac{d\overline{p}}{dx}y + \frac{\tau_w}{\rho}}}{\kappa y} \Bigg/ \cdot\frac{\frac{1}{u_\tau}}{\frac{u_\tau}{\nu}}\,, \tag{4.54}$$

$$\frac{d(\frac{\overline{u}}{u_\tau})}{d(\frac{u_\tau y}{\nu})} = \frac{\sqrt{\frac{1}{{u_\tau}^2}\frac{d\overline{p}}{dx}y + \frac{\tau_w}{\rho}\frac{1}{{u_\tau}^2}}}{\kappa\frac{u_\tau y}{\nu}} = \frac{\sqrt{\frac{1}{{u_\tau}^2}\frac{d\overline{p}}{dx}y\frac{u_\tau}{u_\tau}\frac{\nu}{\nu} + 1}}{\kappa y^+}, \tag{4.55}$$

$$\frac{du^+}{dy^+} = \frac{\sqrt{\frac{1}{{u_\tau}^2}\frac{d\overline{p}}{dx}\frac{\nu}{u_\tau}\frac{u_\tau y}{\nu} + 1}}{\kappa y^+} = \frac{\sqrt{\frac{\nu}{{u_\tau}^3}\frac{dp}{dx}y^+ + 1}}{\kappa y^+}, \tag{4.56}$$

$$\frac{du^+}{dy^+} = \frac{\sqrt{\alpha y^+ + 1}}{\kappa y^+}, \tag{4.57}$$

leads to differential equation which can be solved by the following substitution:

$$t = \alpha y^+ + 1, \tag{4.58}$$

$$dt = \alpha\, dy^+, \tag{4.59}$$

$$u^+ = \int \frac{\sqrt{\alpha y^+ + 1}}{\kappa y^+} dy^+ = \frac{1}{\kappa} \int \frac{\sqrt{t}}{(t-1)} dt. \tag{4.60}$$

Making an additional substitution ($t = p^2, dt = 2p\,dp$) yields :

$$\begin{aligned} u^+ = \frac{1}{\kappa} \int \frac{\sqrt{p^2}}{p^2-1} 2p\,dp &= \frac{1}{\kappa} \int \frac{p\,2p}{p^2-1} dp = \frac{1}{\kappa} \int \frac{2p^2}{p^2-1} dp \\ &= \frac{1}{\kappa} \left[\int \frac{2p^2-2}{p^2-1} dp + \int \frac{2}{p^2-1} dp \right] \\ &= \frac{1}{\kappa} \left[\int 2dp + \int \frac{2}{p^2-1} dp \right] \\ &= \frac{1}{\kappa} \left[\int 2dp + \int \left(\frac{1}{p-1} - \frac{1}{p+1} \right) dp \right] \\ &= \frac{1}{\kappa} \left[2p + \int \frac{1}{p-1} dp - \int \frac{1}{p+1} dp \right] + u^+_{t_1} \\ &= \frac{1}{\kappa} \left[\, 2p + \ln|p-1| - \ln|p+1| \,\right] + u^+_{t_1}. \end{aligned} \tag{4.61}$$

Back substituting the $p = \sqrt{t}$, $t = \alpha y^+ + 1$ and simplifying the expression with $\left|\sqrt{1+\alpha y^+} + 1\right| = \sqrt{1+\alpha y^+} + 1$ leads to:

$$u^+ = \frac{1}{\kappa} \left[2\sqrt{1+\alpha y^+} + \ln\left|\sqrt{1+\alpha y^+} - 1\right| - \ln\left(\sqrt{1+\alpha y^+} + 1\right) \right] + u^+_{t_1}. \tag{4.62}$$

As the (4.62) is not defined at the wall, $y^+ = 0$, the constant of integration, $u^+_{t_1}$ is treated as a slip velocity. Its value is obtained following the same approach as in [1], by matching the profile (4.62) with standard law-of-the-wall at the point $y^+ = 6$:

$$\frac{1}{\kappa} \ln(6E) = \frac{1}{\kappa} \left[2\sqrt{1+6\alpha} + \ln\left|\sqrt{1+6\alpha} - 1\right| - \ln\left(\sqrt{1+6\alpha} + 1\right) \right] + u^+_{t_1}, \tag{4.63}$$

$$u^+_{t_1} = \frac{1}{\kappa} \ln(6E) - \frac{1}{\kappa} \left[2\sqrt{1+6\alpha} + \ln\left|\sqrt{1+6\alpha} - 1\right| - \ln\left(\sqrt{1+6\alpha} + 1\right) \right]. \tag{4.64}$$

Analysis of (4.65) shows that for $\alpha \to 0$, enhanced law-of-the-wall reduces to $1/\kappa \ln(Ey^+)$:

$$u^+ = \frac{1}{\kappa}\left[2\sqrt{1+\alpha y^+} + \ln\left|\sqrt{1+\alpha y^+}-1\right| - \ln\left(\sqrt{1+\alpha y^+}+1\right)\right] + \frac{1}{\kappa}\ln(6E) - \frac{1}{\kappa}\left[2\sqrt{1+6\alpha} + \ln\left|\sqrt{1+6\alpha}-1\right| - \ln\left(\sqrt{1+6\alpha}+1\right)\right], \quad (4.65)$$

$$u^+ = \frac{1}{\kappa}\left[2\sqrt{1+\alpha y^+} + \ln\left|\frac{\sqrt{1+\alpha y^+}-1}{\sqrt{1+6\alpha}-1}\right| - \ln\left(\sqrt{1+\alpha y^+}+1\right)\right] + \frac{1}{\kappa}\ln(6E) - \frac{1}{\kappa}\left[2\sqrt{1+6\alpha} - \ln\left(\sqrt{1+6\alpha}+1\right)\right], \quad (4.66)$$

$$\lim_{\alpha\to 0} u^+ = \frac{1}{\kappa}\ln\left(\lim_{\alpha\to 0}\frac{0}{0}\right) + \frac{1}{\kappa}\ln(6E) = \frac{1}{\kappa}\ln\left(\frac{y^+}{6}\right) + \frac{1}{\kappa}\ln(6E) = \frac{1}{\kappa}\ln(Ey^+). \quad (4.67)$$

For indeterminate form $\frac{0}{0}$, L'Hospital's rule is used:

$$\lim_{\alpha\to 0}\frac{\sqrt{1+\alpha y^+}-1}{\sqrt{1+6\alpha}-1} = \lim_{\alpha\to 0}\frac{\frac{d}{d\alpha}(\sqrt{1+\alpha y^+}-1)}{\frac{d}{d\alpha}(\sqrt{1+6\alpha}-1)} = \lim_{\alpha\to 0}\frac{\frac{1}{2}\frac{y^+}{\sqrt{1+\alpha y^+}}}{\frac{1}{2}\frac{6}{\sqrt{1+6\alpha}}} = \frac{y^+}{6}. \quad (4.68)$$

For the $y^+ \geq 60$ region, a modification to the mixing length model is introduced. Influence of pressure gradient on turbulent shear stresses is limited beyond $y^+ = 60$:

$$-\overline{u'v'} = \frac{d\overline{p}}{dx}y + \frac{\tau_w}{\rho}\ , \ -\overline{u'v'} = \frac{d\overline{p}}{dx}y\frac{u_\tau}{u_\tau}\frac{\nu}{\nu} + \frac{\tau_w}{\rho}\ , \quad (4.69)$$

$$-\overline{u'v'} = \frac{\nu}{u_\tau}\frac{d\overline{p}}{dx}y^+ + \frac{\tau_w}{\rho}\ , \ \kappa^2 y^2\left|\frac{d\overline{u}}{dy}\right|\frac{d\overline{u}}{dy} = \frac{\nu}{u_\tau}\frac{d\overline{p}}{dx}60 + \frac{\tau_w}{\rho}\ , \quad (4.70)$$

$$\frac{d\overline{u}}{dy} = \frac{\sqrt{60\frac{\nu}{u_\tau}\frac{d\overline{p}}{dx} + \frac{\tau_w}{\rho}}}{\kappa y}\Bigg/\cdot\frac{\nu}{{u_\tau}^2}\ , \ \frac{du^+}{dy^+} = \frac{\sqrt{60\alpha+1}}{\kappa y^+}\ , \quad (4.71)$$

$$u^+ = \frac{1}{\kappa}\sqrt{1+60\alpha}\,ln(y^+) + u^+_{t_2}. \quad (4.72)$$

Conducted derivation of turbulent near-wall profiles shows that for $y^+ < 60$ and $y^+ \geq 60$ different expressions, (4.62) and (4.72), are being used. It is reasonable to expect that for $y^+ = 60$ they give the same value for u^+. From this condition, integration constant u^+_{t2} can be found:

$$\frac{1}{\kappa}\left[2\sqrt{1+60\alpha}+\ln\left|\sqrt{1+60\alpha}-1\right|-\ln\left(\sqrt{1+60\alpha}+1\right)\right] + u^+_{t_1} = \frac{1}{\kappa}\sqrt{1+60\alpha}\,\ln(60)+u^+_{t_2}, \quad (4.73)$$

$$u^+_{t_2} = \frac{1}{\kappa}\left[2\sqrt{1+60\alpha}+\ln\left|\sqrt{1+60\alpha}-1\right| - \ln\left(\sqrt{1+60\alpha}+1\right)-\sqrt{1+60\alpha}\,\ln(60)\right]+u^+_{t_1}. \quad (4.74)$$

The same limiting analysis as with the expression (4.62) can be used to show that (4.72) for $\alpha = 0$ reduces to standard-law-of-the-wall.

Final expressions for u^+ in inertial layer reads:

$$u^+_{log} = \begin{cases} \frac{1}{\kappa}\left[2\sqrt{1+\alpha y^+}+ln\left|\sqrt{1+\alpha y^+}-1\right|-ln\left(\sqrt{1+\alpha y^+}+1\right)\right]+u^+_{t1} & ,y^+ < 60 \\ \frac{1}{\kappa}\sqrt{1+60\alpha}\,ln(y^+)+u^+_{t2} & ,y^+ \geq 60 \end{cases}. \quad (4.75)$$

In the case of a favorable (negative) pressure gradient, there is a possibility that quantity $1+\alpha y^+$ could become negative for large y^+, giving the negative value under the square root and making the formula (4.75) unusable. In order to avoid that, lower value for $1+\alpha y^+$ needs to be limited to 0 following [1]. The same safety measure is taken for terms $\sqrt{1+60\alpha}$ and $\sqrt{1+6\alpha}$.

From the newly derived enhanced-law-of-the-wall, wall shear stress for viscous and turbulent region is obtained. Switching between them is done using the Kader blending:

$$u_\tau = u_{\tau vis}e^{\Gamma} + u_{\tau log}e^{1/\Gamma}\,,\ \frac{\tau_w}{\rho} = {u_\tau}^2, \quad (4.76)$$

$$u_{\tau vis} = \frac{\overline{u}}{u^+_{vis}}\,,\ u_{\tau log} = \frac{\overline{u}}{u^+_{log}}. \quad (4.77)$$

Menter's [4] blending method for friction velocity in this case would be inappropriate since u^+_{vis} can become negative, making $u_{\tau vis}$ negative, and blend $u_\tau = \sqrt[4]{{u_{\tau vis}}^4 + {u_{\tau log}}^4}$ would alter it to a positive value.

Modified production of turbulence kinetic energy is computed with the blended velocity gradient, using the derived formulations for viscous and logarithmic region:

$$\frac{d\overline{u}}{dy} = \left(\frac{d\overline{u}}{dy}\right)_{vis} e^{\Gamma} + \left(\frac{d\overline{u}}{dy}\right)_{log} e^{1/\Gamma}, \tag{4.78}$$

$$\left(\frac{d\overline{u}}{dy}\right)_{vis} = \frac{1}{\nu}\left(\frac{1}{\rho}\frac{d\overline{p}}{dx}y + \frac{\tau_w}{\rho}\right) \quad , \quad \left(\frac{d\overline{u}}{dy}\right)_{log} = \begin{cases} \dfrac{\sqrt{\frac{1}{\rho}\frac{d\overline{p}}{dx}y + \frac{\tau_w}{\rho}}}{\kappa y} & ,y^+ < 60 \\ \dfrac{\sqrt{60\frac{\nu}{u_\tau}\frac{1}{\rho}\frac{d\overline{p}}{dx} + \frac{\tau_w}{\rho}}}{\kappa y} & ,y^+ \geq 60 \end{cases}. \tag{4.79}$$

In Fluent [10], ω equation is solved in the wall adjacent cells, with the wall boundary condition ω_w defined as the blended value of wall adjacent cell centre:

$$\omega^+_{vis} = \frac{6}{\beta_i (y^+)^2}, \omega^+_{log} = \frac{1}{{C_\mu}^{1/2}}\left(\frac{du^+}{dy^+}\right)_{log}, \tag{4.80}$$

$$\omega^+_w = \sqrt{{\omega^+_{vis}}^2 + {\omega^+_{log}}^2}, \tag{4.81}$$

$$\omega_w = \frac{(u^*)^2}{\nu}\omega^+_w. \tag{4.82}$$

In dimensionless forms, expressions for ω_{vis} and ω_{log} are equivalent to standard ones, but transforming them to dimensioned ones is done using the empirical value u^* instead of u_τ. Also, the constant $\beta_1 = 0.075$ is replaced with a new one, $\beta_i = 0.072$.

In this study, a well-established procedure of prescribing the value for ω in the wall adjacent cells is instead adopted, for which simpler expressions are used:

$$\omega_{vis} = \frac{6\nu}{\beta_1 y^2}, \omega_{log} = \frac{1}{{C_\mu}^{1/2}}\left(\frac{d\overline{u}}{dy}\right)_{log}, \omega = \sqrt{\omega^2_{vis} + \omega^2_{log}}. \tag{4.83}$$

4.3.3 Modified Enhanced Wall Treatment

In most cases, one part of the pressure gradient is spent on accerelating the flow and the other part on ballancing the wall shear stress. If in the enhanced wall treatment, α is denoted as a parameter which excludes the part of flow acceleration, the problems of limiting the value under the root $\sqrt{1+\alpha y^+}$ in cases of large negative pressure gradients can possibly be avoided. Also, prediction in adverse pressure gradient flows should be improved. In order to test this, convective terms are included in the momentum balance (4.52):

$$\kappa^2 y^2 \frac{d\overline{u}}{dy}\left|\frac{d\overline{u}}{dy}\right| = \left(\frac{d\overline{p}}{dx} + \overline{\mathbf{u}}\cdot\nabla\overline{u}\right) y + \frac{\tau_w}{\rho}. \tag{4.84}$$

During the integration process, pressure gradient and convection terms were regarded as a constant. A justification for that assumption is provided in [14] for two non-equlibrium flow cases. Integration constant is obtained in the same manner, as with enhanced wall treatment, by matching the expression with the law of the wall $u^+ = 1/\kappa \ln(Ey^+)$ at $y^+ = 6$.

$$u^+_{log} = \frac{1}{\kappa}\left[2\sqrt{1+Ay^+} + \ln\left|\sqrt{1+Ay^+}-1\right| - \ln\left(\sqrt{1+Ay^+}+1\right)\right] + u^+_t, \tag{4.85}$$

$$u^+_t = \frac{1}{\kappa}\ln(6E) - \frac{1}{\kappa}\left[2\sqrt{1+6A} + \ln\left|\sqrt{1+6A}-1\right| - \ln\left(\sqrt{1+6A}+1\right)\right]. \tag{4.86}$$

Dimensionless parameter $A = \nu/(u^*)^3(\frac{d\overline{p}}{dx} + \overline{\mathbf{u}}\cdot\nabla\overline{u})$ includes both the pressure gradient and convective terms.

By including the convective terms, we hope that the problem of negative value appearing under the root $\sqrt{1+Ay^+}$ is avoided. Still, a limiting procedure $\sqrt{\max(0, 1+Ay^+)}$ is kept in order to ensure convergence and practical use of expression (4.85).

Limiting the influence of pressure gradient on turbulent shear stresses above $y^+ = 60$ in this wall treatment is not performed. Origin of that procedure is unknown and it is possible that in the enhanced wall treatment this is a safety measure against the negative value under the square root.

For the viscous region standard viscous-law: $u^+ = y^+$ is used instead of the expression sensitised with the pressure gradient. This is the main reason that the convergence process compared to the enhanced wall treatment is significantly improved, which is shown in the next chapter. Blending procedures for wall shear stress and production terms are adopted from the enhanced wall treatment. For ω, values are prescribed in the wall adjacent cells and simplified expressions are used.

- Wall shear stress reads:

$$u_\tau = u_{\tau vis} e^{\Gamma} + u_{\tau log} e^{1/\Gamma} \, , \; \frac{\tau_w}{\rho} = {u_\tau}^2, \tag{4.87}$$

$$u_{\tau vis} = \sqrt{\nu \frac{\overline{u}}{y}} \, , \; u_{\tau log} = \frac{\overline{u}}{u^+_{log}}. \tag{4.88}$$

- Modified production reads:

$$G = \frac{\tau_w}{\rho} \frac{d\overline{u}}{dy}, \tag{4.89}$$

$$\frac{d\overline{u}}{dy} = \left(\frac{d\overline{u}}{dy} \right)_{vis} e^{\Gamma} + \left(\frac{d\overline{u}}{dy} \right)_{log} e^{1/\Gamma}, \tag{4.90}$$

$$\left(\frac{d\overline{u}}{dy} \right)_{vis} = \frac{\overline{u}}{y} \, , \; \left(\frac{dU}{dy} \right)_{log} = \frac{\sqrt{(\frac{d\overline{p}}{dx} + \overline{\mathbf{u}} \cdot \nabla \overline{u}) y + \frac{\tau_w}{\rho}}}{\kappa y}. \tag{4.91}$$

- Specific dissipation rate reads:

$$\omega_{vis} = \frac{6\nu}{\beta_1 y^2} \, , \; \omega_{log} = \frac{1}{{C_\mu}^{1/2}} \left(\frac{d\overline{u}}{dy} \right)_{log}, \tag{4.92}$$

$$\omega = \sqrt{\omega^2_{vis} + \omega^2_{log}}. \tag{4.93}$$

4.4 Wall Treatments in `foam-extend` 3.2

In `foam-extend` 3.2, choice of ${\nu_t}^w$ is independent of the used eddy viscosity turbulence model. This value is specified as a separate boundary condition, and if the user does not specify anything, the default option based on standard wall functions is assumed:

$$\frac{\tau_w}{\rho} = \frac{{C_\mu}^{1/4} k^{1/2} \overline{u} \kappa}{\ln(E y^*)}, \tag{4.94}$$

$$\frac{\tau_w}{\rho} = (\nu + {\nu_t}^w)\frac{\overline{u}}{y}\ ,\ {\nu_t}^w = \tau_w \frac{y}{\overline{u}} - \nu = \frac{{C_\mu}^{1/4} k^{1/2} \overline{u} \kappa}{\ln(E y^*)\overline{u}} - \nu, \tag{4.95}$$

$${\nu_t}^w = \frac{{C_\mu}^{1/4} k^{1/2} y \kappa}{ln(E y^*)} - \nu = \nu \left(\frac{{C_\mu}^{1/4} k^{1/2} y \kappa}{\nu\ \ln(E y^*)} - 1 \right) = \nu \left(\frac{y^* \kappa}{\ln(E y^*)} - 1 \right). \tag{4.96}$$

Demarcation of viscous-turbulent region, y^+_{lam} is computed from the nonlinear equation $y^+_{lam} = \frac{1}{\kappa}\ln(E y^+_{lam})$ already disscused in section 4.2.2. Wall eddy viscosity ${\nu_t}^w$ for the whole near wall region is defined as:

$${\nu_t}^w = \begin{cases} 0 & , y^* \leq y^+_{lam} \\ \nu \left(\dfrac{y^* \kappa}{\ln(E y^*)} - 1 \right) & , y^* > y^+_{lam} \end{cases}. \tag{4.97}$$

Treatment of other transported variables depends on the used turbulence model.

4.4.1 $k - \varepsilon$ Model

Wall functions in `foam-extend` for the $k - \varepsilon$ model are based on standard wall functions [11]. Unlike there, averaged dissipation ε for turbulent kinetic energy is not computed and the definition of production term is also slightly altered.

- Modified production term reads:

$$G = \begin{cases} 0 & , y^* \leq y^+_{lam} \\ G_{log} & , y^* > y^+_{lam} \end{cases}, \tag{4.98}$$

$$(G_{log})_1 = \frac{\tau_w}{\rho}\left(\frac{d\overline{u}}{dy}\right)_{log} = \frac{\tau_w}{\rho}\frac{\tau_w}{\kappa\rho {C_\mu}^{1/4} k^{1/2} y} = \frac{[\,(\nu+{\nu_t}^w)\,|\nabla\overline{\mathbf{u}}_w|\,]^2}{\kappa {C_\mu}^{1/4} k^{1/2} y}. \tag{4.99}$$

$$(G_{log})_2 = \frac{\tau_w}{\rho}\left(\frac{d\overline{u}}{dy}\right)_{log} = (\nu+{\nu_t}^w)|\nabla\overline{\mathbf{u}}_w|\frac{u^*}{\kappa y} = (\nu+{\nu_t}^w)|\nabla\overline{\mathbf{u}}_w|\frac{{C_\mu}^{1/4}k^{1/2}}{\kappa y}. \tag{4.100}$$

- Dissipation rate reads:

$$\varepsilon = \frac{{C_\mu}^{3/4}k^{3/2}}{\kappa y}. \tag{4.101}$$

  From the presented derivation it can be seen that both G_{log} terms are matematically identical. They are derived from the same expression: $\tau_w/\rho(d\overline{u}/dy)_{log}$. But from a numerical view they are different due to the discretisation error. In the `foam-extend` 3.2, expression (4.99) is used in the wall functions for the $k-\varepsilon$ model.

4.4.2 $k-\omega$ SST Model

Automatic wall treatment in the case of $k-\omega$ SST model is only partially taken into account, and only for the ω term.

- Production term reads:

$$G = \begin{cases} 0 & ,y^* \leq y^+ \\ G_{log} & ,\ y^* > y^+ \end{cases}, \tag{4.102}$$

$$G_{log} = (\nu+{\nu_t}^w)|\nabla\overline{\mathbf{u}}_w|\frac{{C_\mu}^{1/4}k^{1/2}}{\kappa y}. \tag{4.103}$$

- Specific dissipation rate reads:

$$\omega = \sqrt{\omega_{vis}^2+\omega_{log}^2}, \tag{4.104}$$

$$\omega_{vis} = \frac{6\nu}{\beta 1 y^2}, \tag{4.105}$$

$$\omega_{log} = \frac{1}{{C_\mu}^{1/2}}\left(\frac{d\overline{u}}{dy}\right)_{log} = \frac{1}{{C_\mu}^{1/2}}\frac{u^*}{\kappa y} = \frac{1}{{C_\mu}^{1/2}}\frac{{C_\mu}^{1/4}k^{1/2}}{\kappa y} = \frac{k^{1/2}}{{C_\mu}^{1/4}\kappa y}. \tag{4.106}$$

In the next chapter, the presented wall treatments are tested. It is shown that for some regions on the wall, this wall treatment fails. It is assumed that the cause for that is the sharp switching behaviour of the production term and significant improvement is achieved using either (4.103) through whole wall adjacent cell, or a blended expression for generation term defined as:

$$G = G_{vis} e^{\Gamma} + G_{log} e^{1/\Gamma}. \tag{4.107}$$

For G_{log} relation (4.103) is used, and G_{vis} is formulated as:

$$G_{vis} = \nu_t \left(\frac{d\overline{u}}{dy} \right)^2 = \frac{k}{\omega_{vis}} \left(\frac{\overline{u}}{y} \right)^2. \tag{4.108}$$

This modification on the production term results in a new method, which through the later text termed as: improved wall treatment. For a production term, a blended value (4.107) is used.

Chapter 5

Validation Studies

Wall treatments described in the previous Chapter are implemented in the open-source code `foam-extend`. Currently implemented wall treatments for $k-\varepsilon$ and $k-\omega$ SST are compared with the newly introduced ones and with experimental data for two test cases, flow over NACA4412 aerofoil and flow over prolate spheroid. For both test cases, two grids are used: one grid to test the Low-Reynolds behaviour (all cell volumes in the viscous layer) and the second one with cell volumes both in the buffer and inertial layer. Wall functions for $k-\varepsilon$ model are not tested in the Low-Reynolds approach.

Both test cases were analysed using a steady state approach with the SIMPLE algorithm. For convection of velocity, the linear-upwind scheme with a limiter is used, while for the rest of convective terms, first order upwind scheme is used. Gradients and Laplacian terms are discretised with Gaussian integration with linear interpolation of cell-centered values to the faces. Additionally, for the Laplacian term, explicit non-orthogonal correction for the surface normal gradient is employed. Pressure equation is solved using the algebraic multigrid solver and all other equations are solved with the BiConjugate Gradient Stabilized method (BiCGStab) with diagonal incomplete-LU (DILU) preconditioner [34].

The naming convention of different wall treatments used in diagrams is:

- $k-\varepsilon$ standardWF: standard wall functions in `foam-extend` for $k-\varepsilon$ model, section 4.4.1,
- $k-\varepsilon$ NonEqWF: non-equilibrium wall functions for $k-\varepsilon$ model, section 4.2.2,
- $k-\omega$ SST standardWT: current implementation of wall treatment for $k-\omega$ SST model in `foam-extend`, section 4.4.2,
- $k-\omega$ SST AWT: automatic wall treatment, section 4.3.1,
- $k-\omega$ SST EWT: enhanced wall treatment, section 4.3.2,
- $k-\omega$ SST MEWT: modified enhanced wall treatment, section 4.3.3,
- $k-\omega$ SST IWT: improved wall treatment, e.g. current implementation of wall treatment for $k-\omega$ SST model with the new production term, expression 4.107.

5.1 NACA4412 Aerofoil

To validate the methods presented in this work, flow past NACA4412 aerofoil at the angle of attack of 15 degrees is investigated. Freestream velocity is set to $U_\infty = 18.4$ m/s, and the corresponding Reynolds number, based on the chord length $c = 0.25$m, is $Re_c = 3.6 \cdot 10^5$. Numerical results are compared with the experimental data for C_f and C_p from [35]. For freestream turbulence intensity, value of $I = u'/U_\infty = 0.086\%$ is taken and for turbulent viscosity, ratio $\beta = \nu_t/\nu = 5$ is used. These values are used to set the freestream boundary conditions for turbulent quantities:

$$k = \frac{1}{2}\overline{\mathbf{u}' \cdot \mathbf{u}'} = \frac{1}{2}(I \cdot U_\infty)^2, \tag{5.1}$$

$$\varepsilon = \frac{0.09k^2}{\beta\nu}, \tag{5.2}$$

$$\omega = \frac{0.09k}{\beta\nu}. \tag{5.3}$$

The given recommendation are taken from [36].

Two structured grids are used. The first one for HRN approach with the wall adjacent cells in the buffer and logarithmic region, GRID-A, and the second one with all of the wall adjacent cells in the viscous region for LRN approach, named GRID-B. The domain is extruded in the wall-normal direction approximately 50 chord lengths in order to eliminate the influence of the farfield. The height of the wall adjacent cell is 10^{-3} m for coarse mesh and 10^{-5} m for the Low-Reynolds number mesh. Both meshes have 598 points along the aerofoil surface which are clustered towards the leading and trailing edges. Table 5.1 shows quality parameters of both meshes and Figure 5.1 shows the mesh used for the LRN approach.

Table 5.1: NACA4412: mesh quality data for the GRID-A and GRID-B.

	GRID-A	GRID-B
Number of volumes	53332	94724
Max aspect ratio	92786.7	124588
Max non-orthogonality	43.75 (average: 1.11)	84.28 (average: 2.66)
Max skewness	0.428026	0.393202

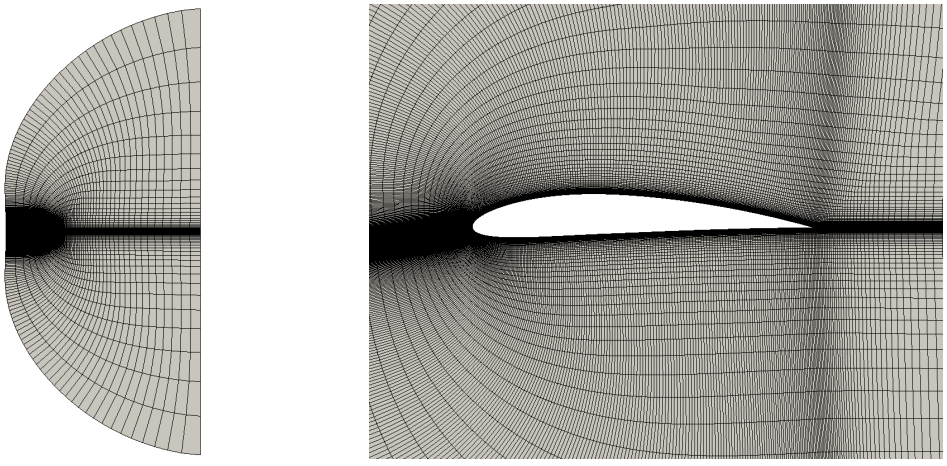

(a) **(b)**

Figure 5.1: GRID-B for LRN approach: (**a**) complete computational domain for the NACA4412, (**b**) zoomed view of the grid near the airfoil surface.

5.1.1 Results

Figures 5.2 - 5.9 show the qualitative comparison of the skin friction, pressure coefficient, y^+ and y^* between HRN and LRN approaches from which it can be seen that for LRN approach methods are in the close agreement, except for the enhanced wall treatment which for this case has bad performance. A more detailed comparison between methods is given for skin friction coefficient obtained with HRN approach, Figures 5.10 - 5.14, in which the most accurate results, obtained with the standard wall functions and non-equilibrium wall functions, are compared with the other methods. Furthermore, Figure 5.15, shows the comparison with Spalart-Allmaras turbulence model using LRN approach.

It is noted that in `foam-extend`, `yPlusRAS` utility actually calculates y^*. In this work, the proper notation is used.

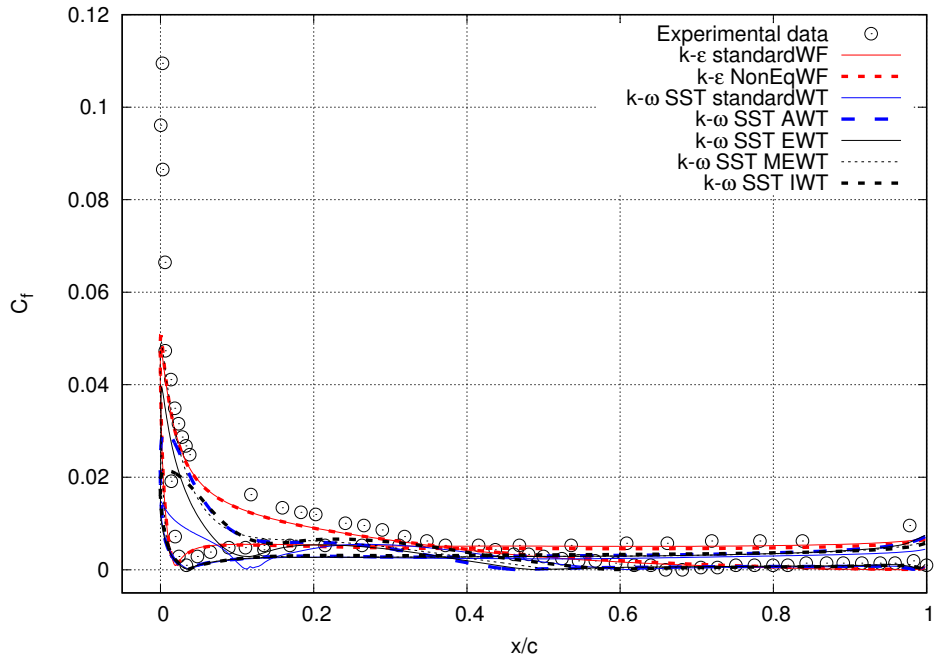

Figure 5.2: GRID-A: skin friction coefficient distribution along the NACA4412 aerofoil.

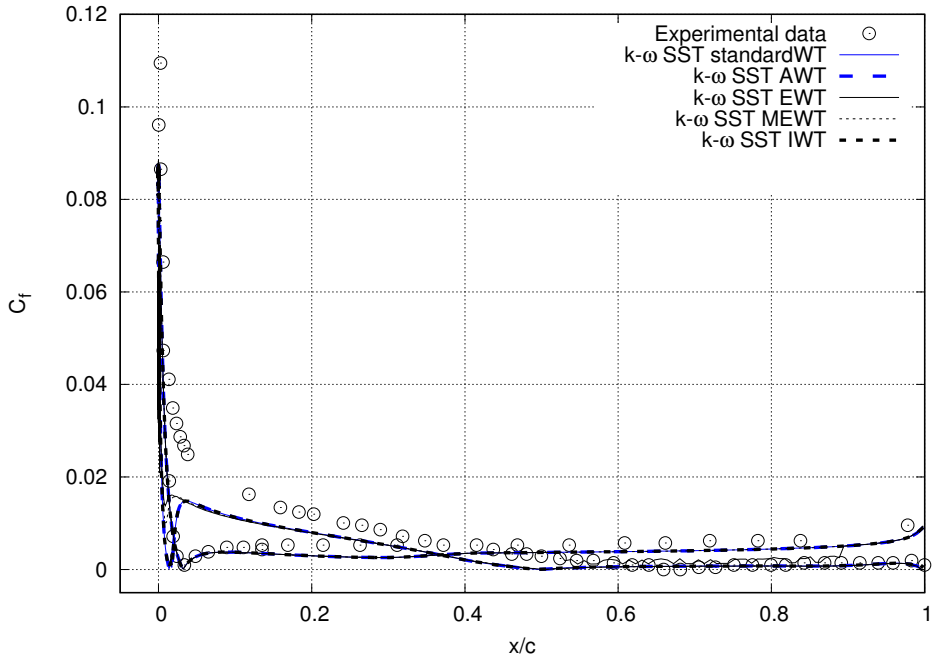

Figure 5.3: GRID-B: skin friction coefficient distribution along the NACA4412 aerofoil.

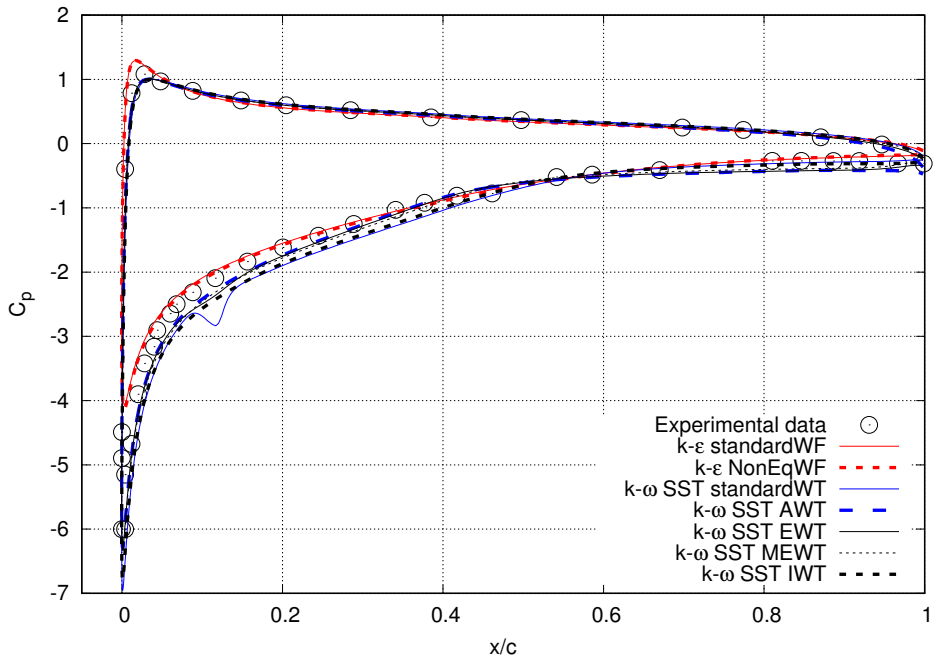

Figure 5.4: GRID-A: pressure coefficient distribution along the NACA4412 aerofoil.

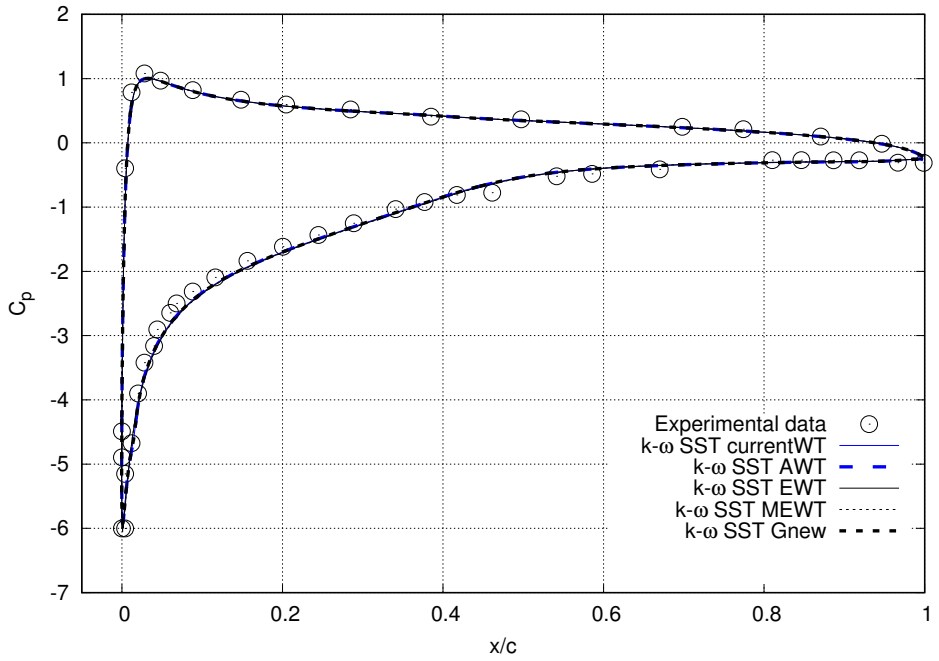

Figure 5.5: GRID-B: pressure coefficient distribution along the NACA4412 aerofoil.

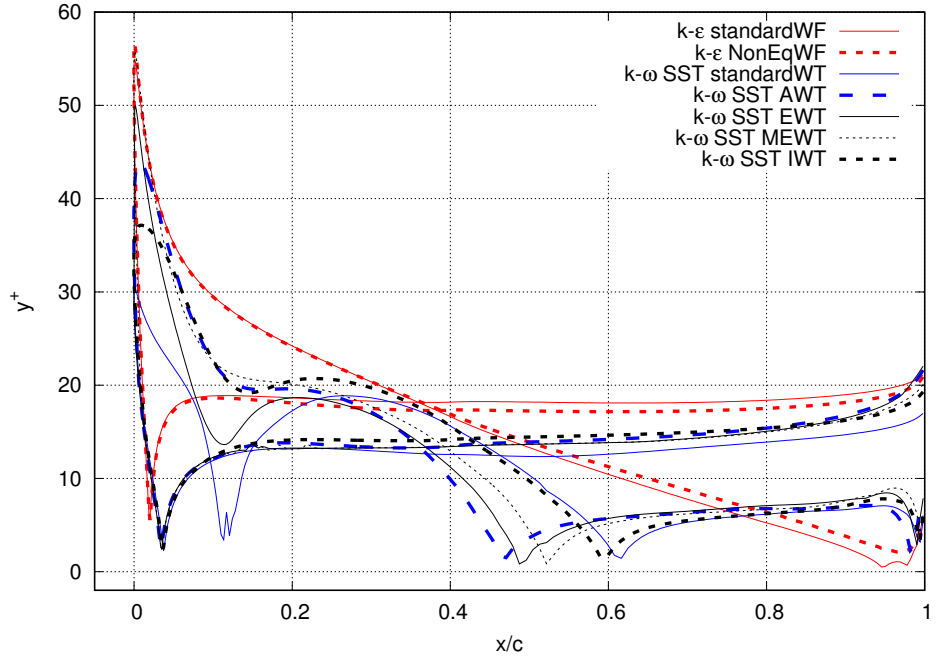

Figure 5.6: GRID-A: y^+ distribution along the NACA4412 aerofoil.

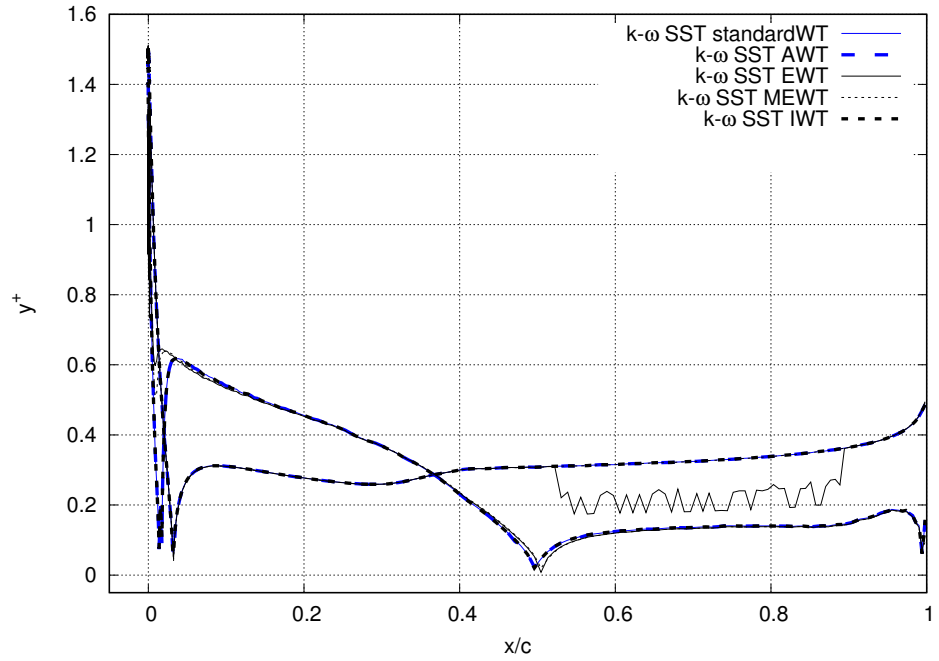

Figure 5.7: GRID-B: y^+ distribution along the NACA4412 aerofoil.

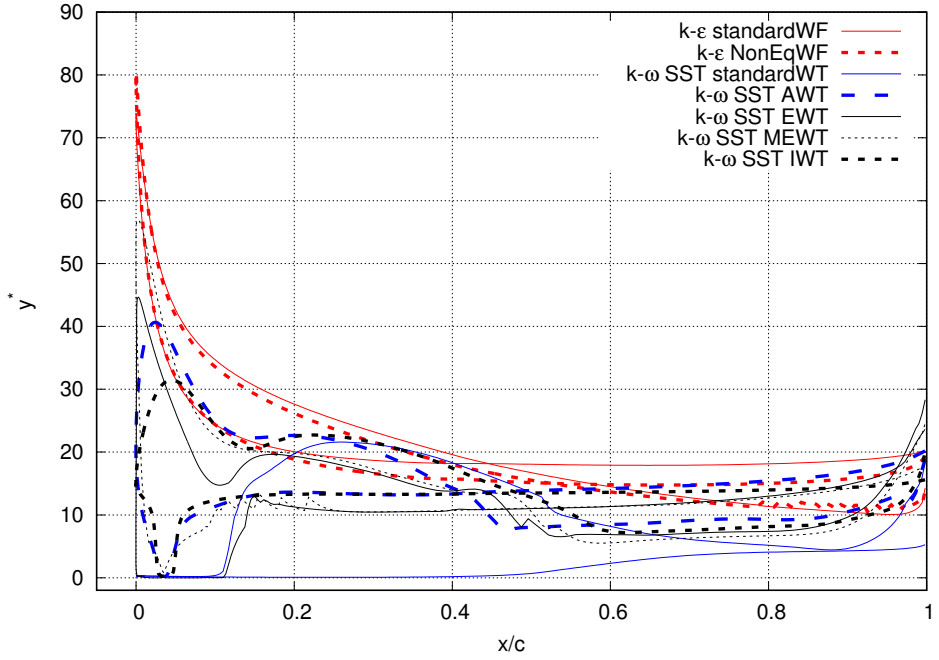

Figure 5.8: GRID-A: y^* distribution along the NACA4412 aerofoil.

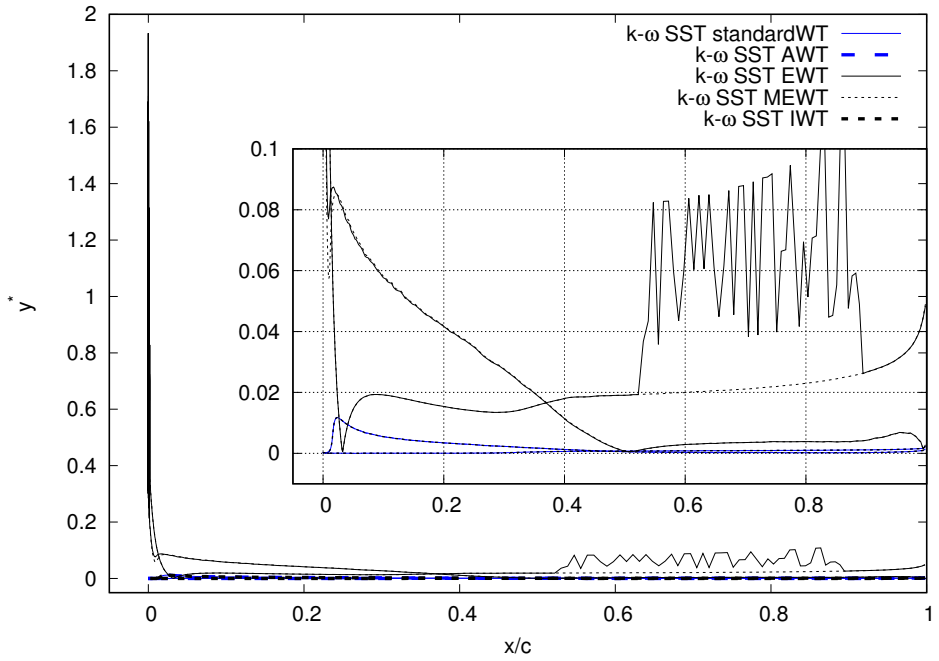

Figure 5.9: GRID-B: y^* distribution along the NACA4412 aerofoil.

A more detailed comparison of the skin friction coefficient for HRN approach is given in the following diagrams.

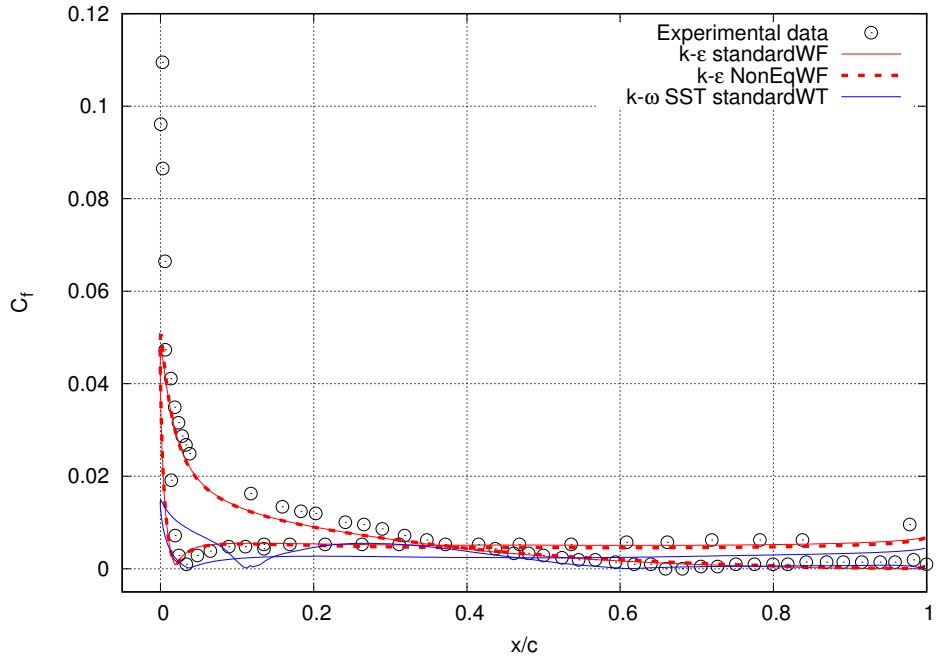

Figure 5.10: GRID-A: comparison of the current implementation of the wall treatment for $k-\omega$ SST model with the best obtained results for the NACA4412.

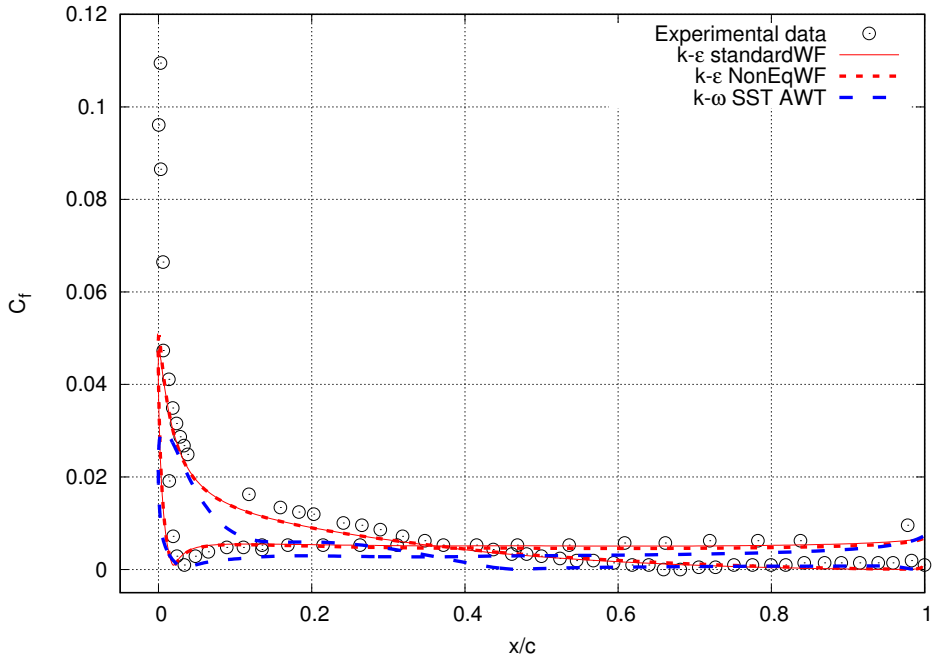

Figure 5.11: GRID-A: comparison of the automatic wall treatment with the best obtained results for the NACA4412.

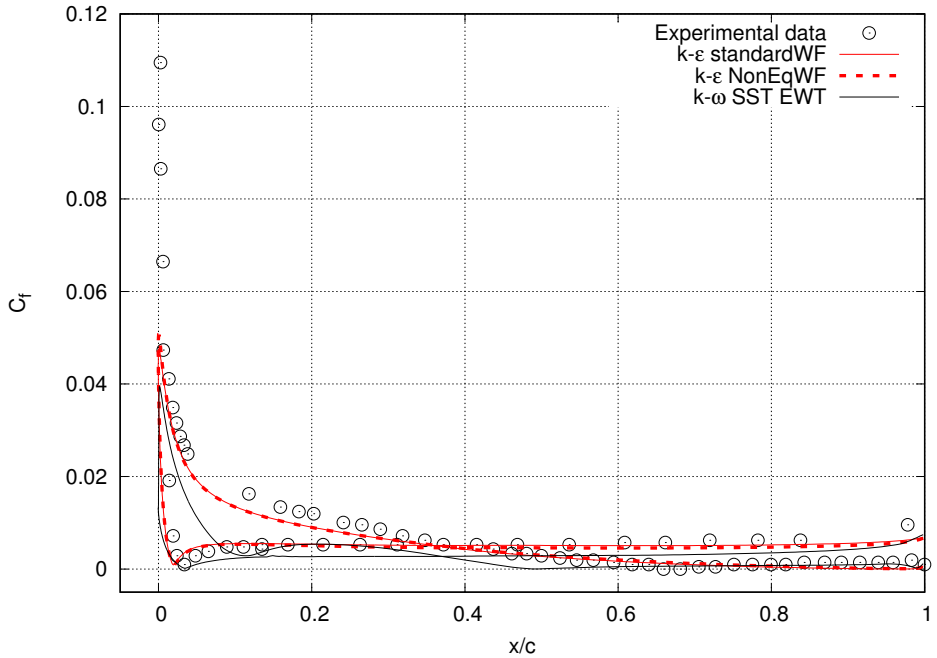

Figure 5.12: GRID-A: comparison of the enhanced wall treatment with the best obtained results for the NACA4412.

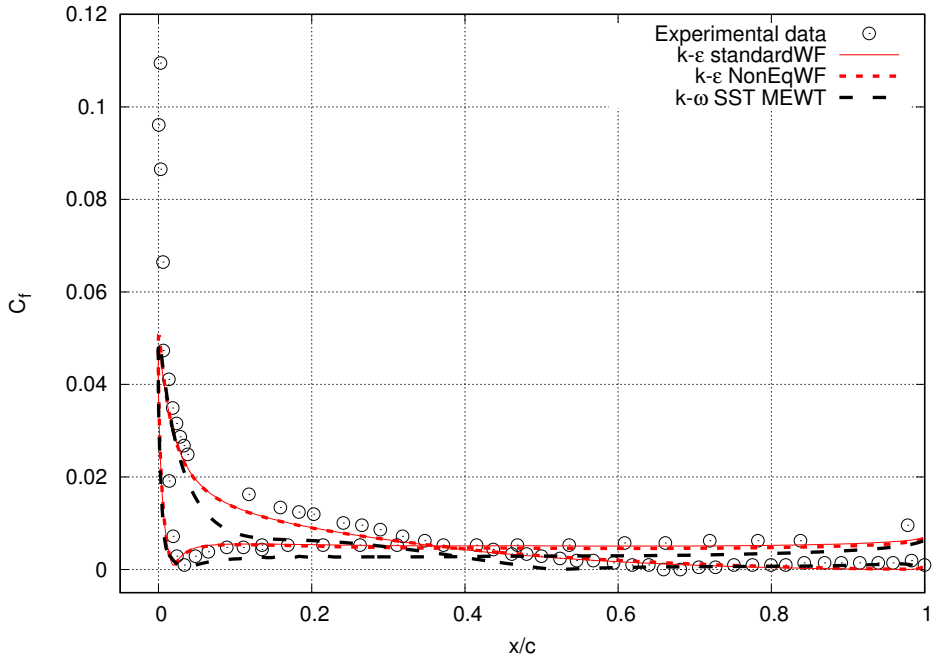

Figure 5.13: GRID-A: comparison of the modified enhanced wall treatment with the best obtained results for the NACA4412.

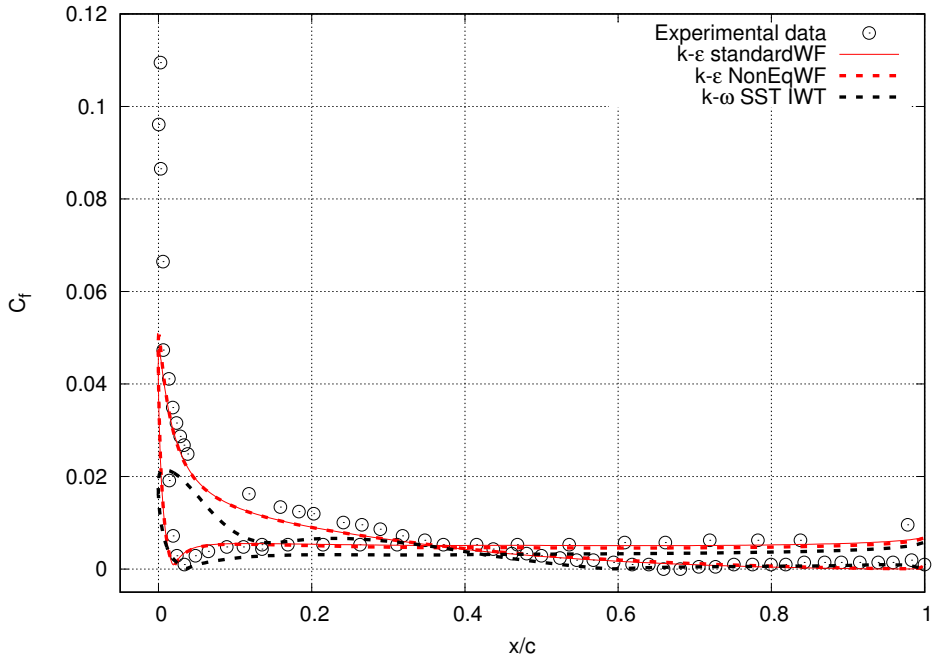

Figure 5.14: GRID-A: comparison of the improved wall treatment with the best obtained results for the NACA4412.

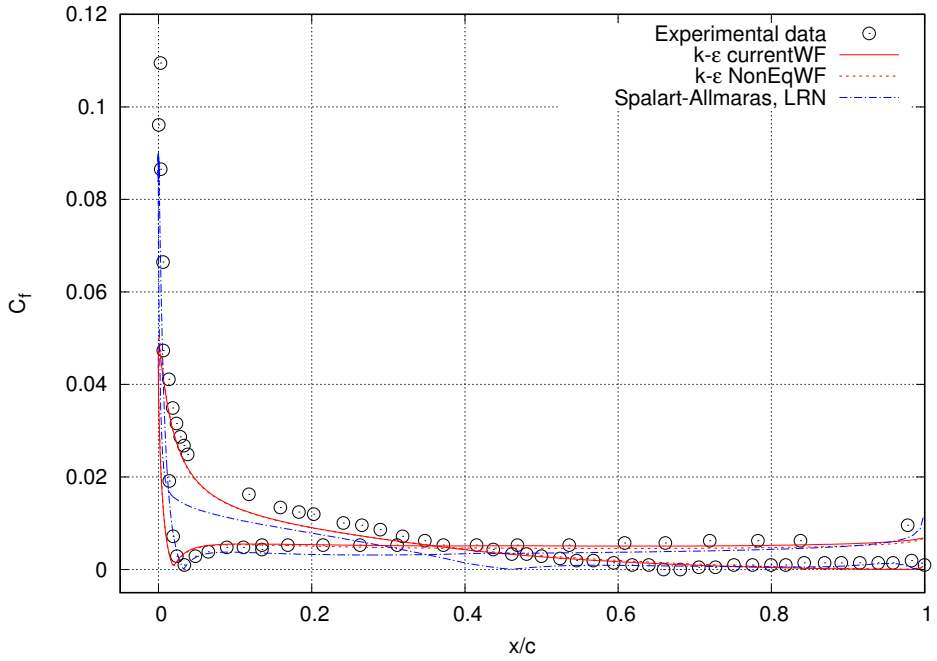

Figure 5.15: GRID-A: comparison of Spalart-Allmaras in LRN approach with the best obtained results for the NACA4412.

Figures 5.16 and 5.17 show the convergence of the drag coefficient defined as: $C_d = F/(0.5\rho U_\infty{}^2 c^2)$ where F is the magnitude of the total force acting on the aerofoil. Lastly, Figures 5.18 to 5.29 show the residual plots of all methods. Due to the slight separation at the tip of the trailing edge, full steady state solution is not obtained, except in the case of $k-\varepsilon$ model. It is noted that the results along the surface of an aerofoil are not affected by this.

The highly oscillating behaviour of the drag coefficient and residuals of enhanced wall treatment (Fig. 5.17 and 5.27) is present only in the LRN approach and replacing the pressure sensitised formulation for the viscous layer: $u^+ = y^+(1+0.5\alpha y^+)$ with the standard one: $u^+ = y^+$ solved this problem. The oscillating behaviour in the residuals in the case of non-equlibrium wall functions (Fig. 5.19) is something that should be further investigated as in the next test case, this method performed relatively well.

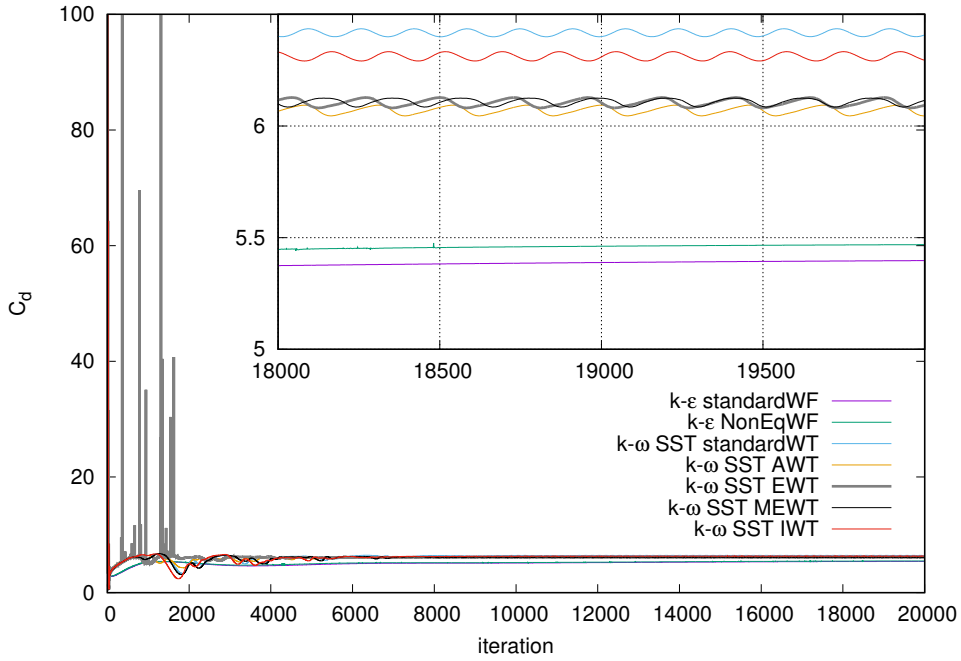

Figure 5.16: GRID-A: convergence of the drag coefficients for the NACA4412 aerofoil.

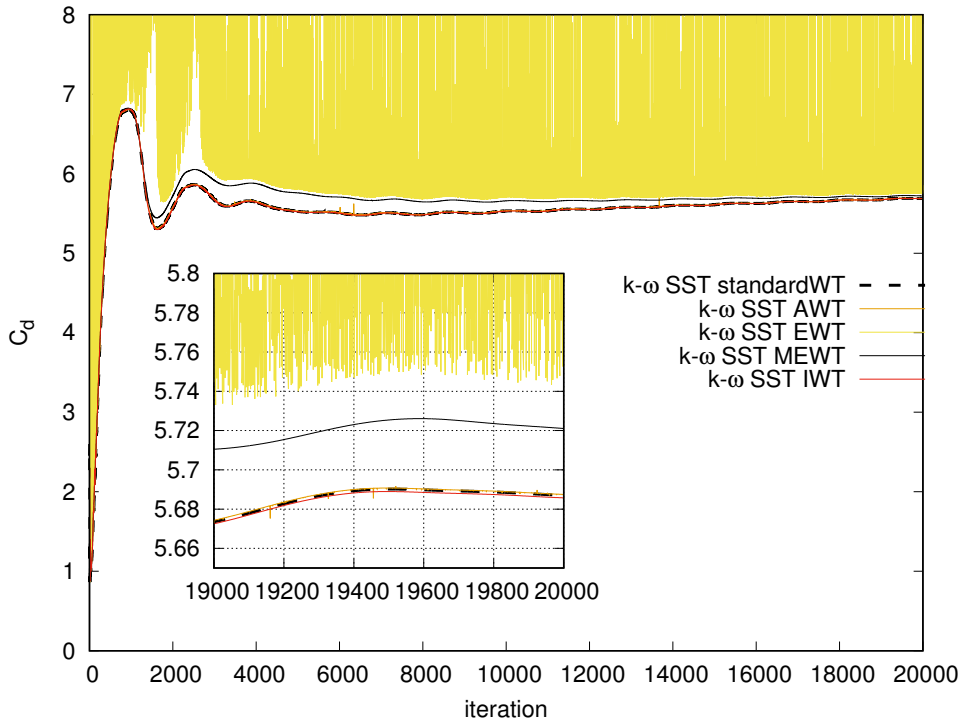

Figure 5.17: GRID-B: convergence of the drag coefficients for the NACA4412 aerofoil.

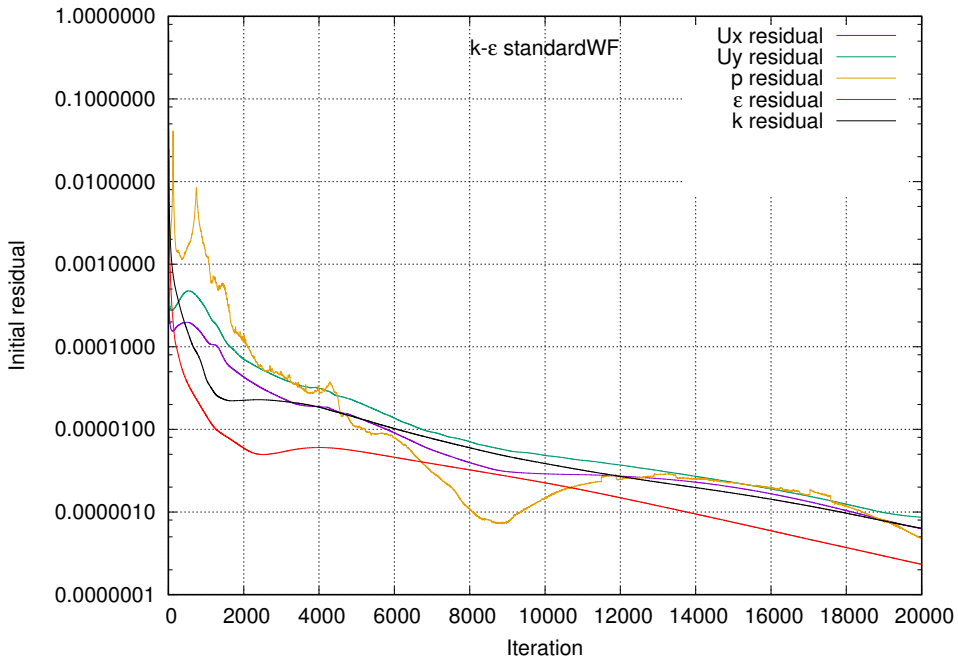

Figure 5.18: GRID-A: residual plot of the standard wall functions for the $k-\varepsilon$ model for the NACA4412.

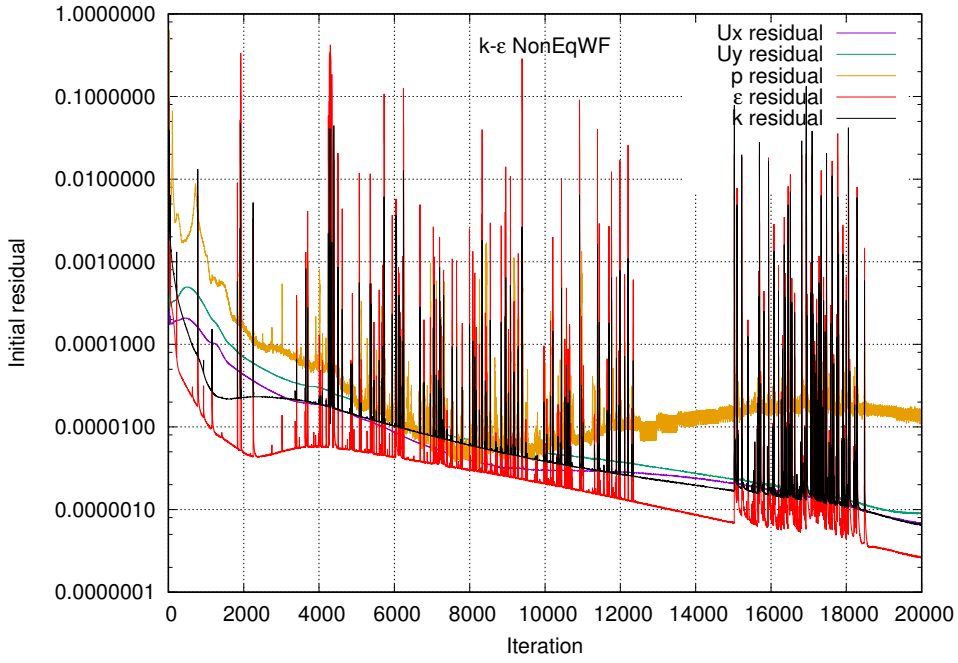

Figure 5.19: GRID-A: residual plot of the non-equilibrium wall functions for the $k-\varepsilon$ model for the NACA4412.

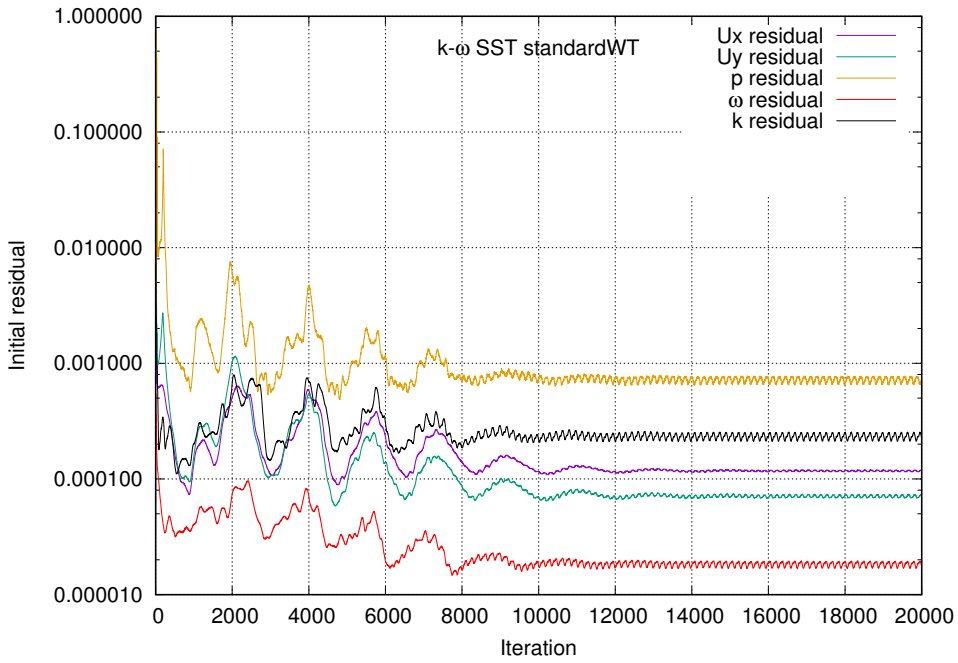

Figure 5.20: GRID-A: residual plot of the current wall treatment for the $k-\omega$ SST model for the NACA4412.

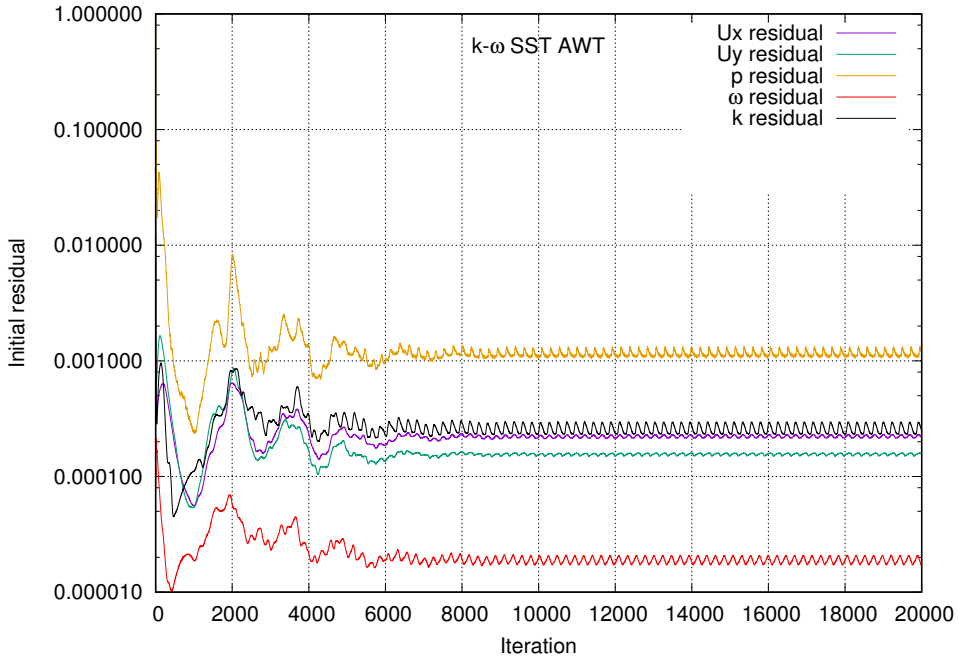

Figure 5.21: GRID-A: residual plot of the automatic wall treatment for the $k-\omega$ SST model for the NACA4412.

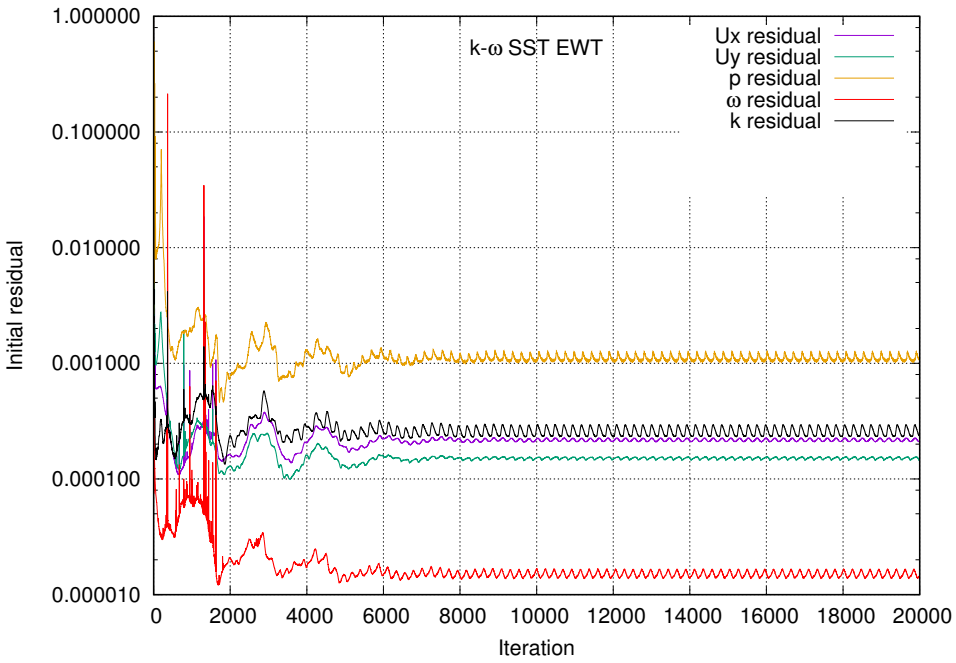

Figure 5.22: GRID-A: residual plot of the enhanced wall treatment for the $k-\omega$ SST model for the NACA4412.

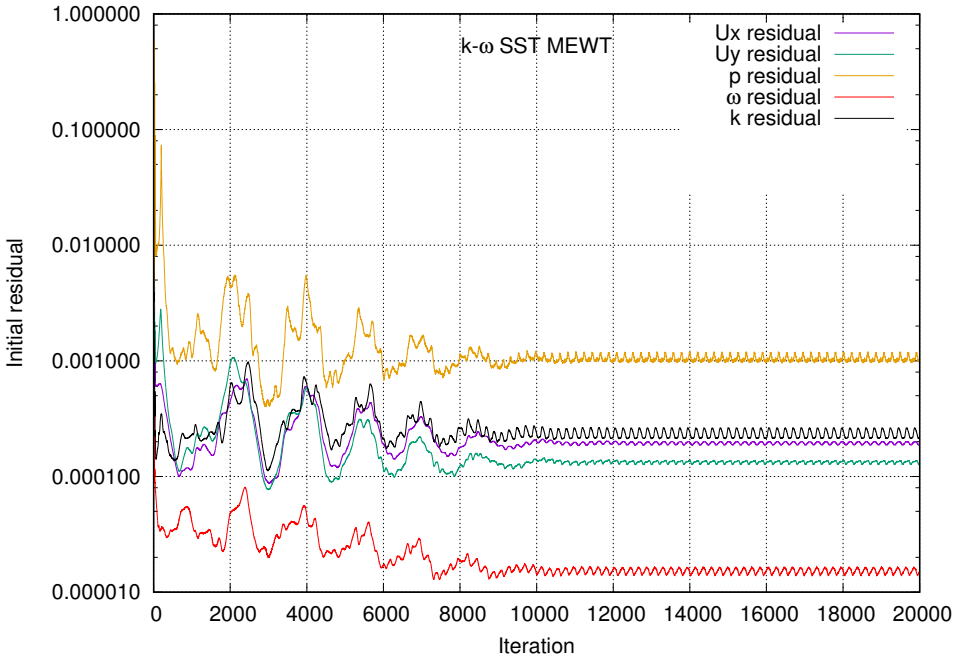

Figure 5.23: GRID-A: residual plot of the modified enhanced wall treatment for the $k-\omega$ SST model for the NACA4412.

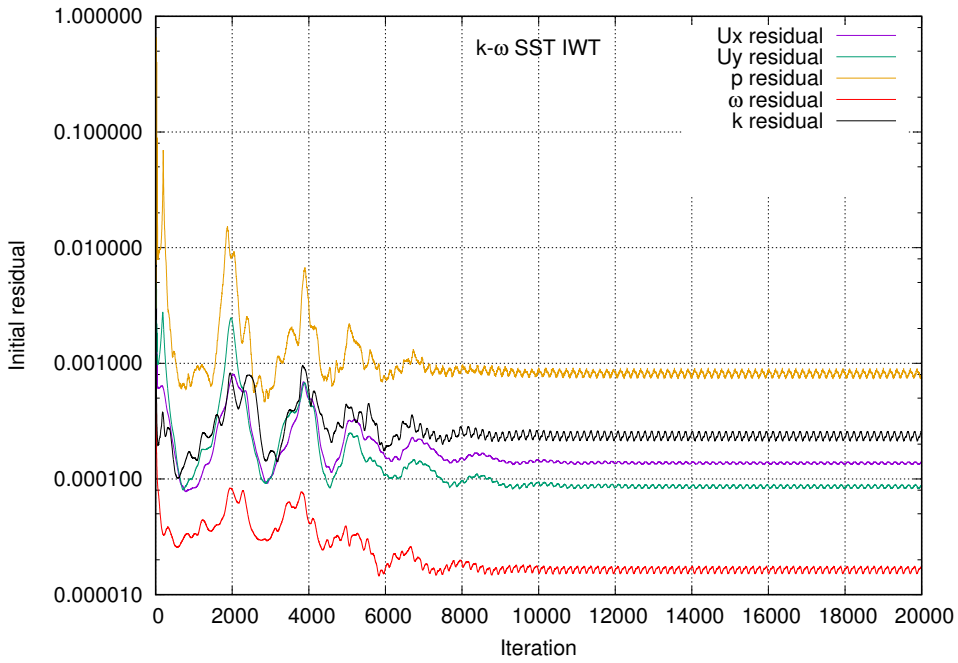

Figure 5.24: GRID-A: residual plot of the improved wall treatment for the $k-\omega$ SST model for the NACA4412.

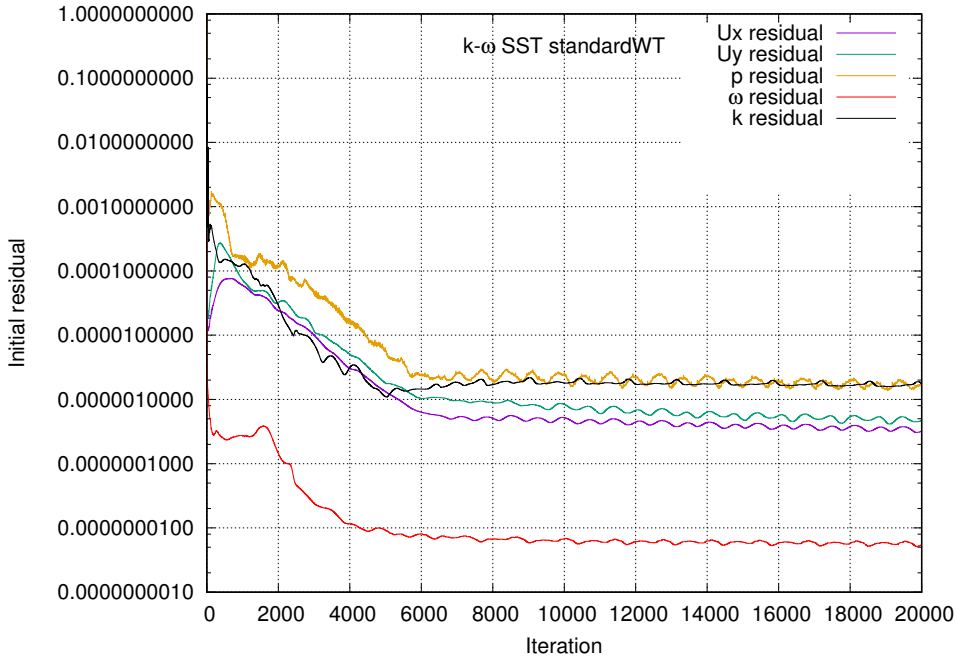

Figure 5.25: GRID-B: residual plot of the current wall treatment for the $k-\omega$ SST model for the NACA4412.

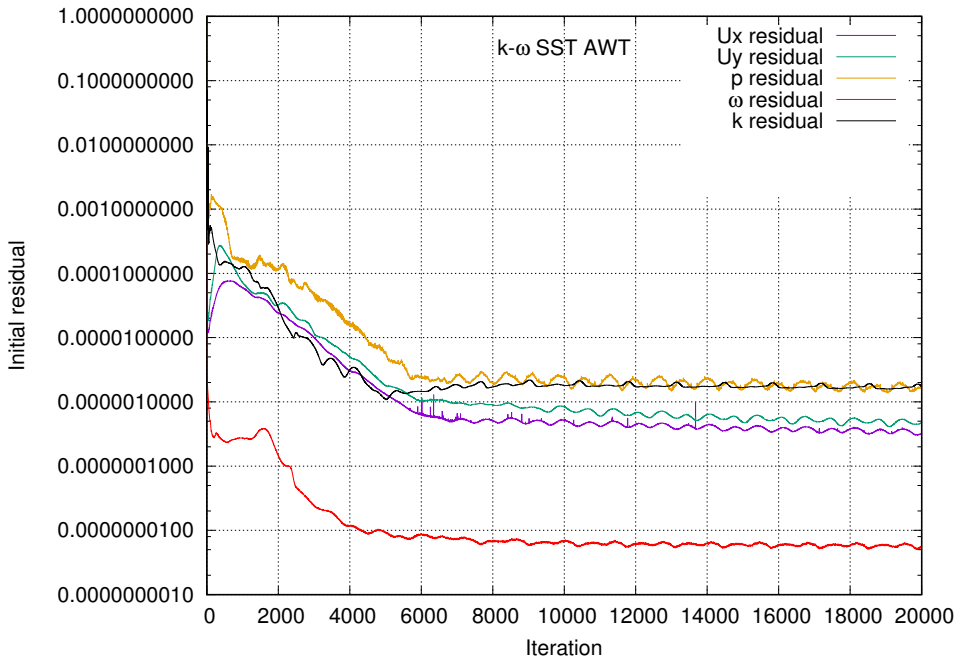

Figure 5.26: GRID-B: residual plot of the automatic wall treatment for the $k-\omega$ SST model for the NACA4412.

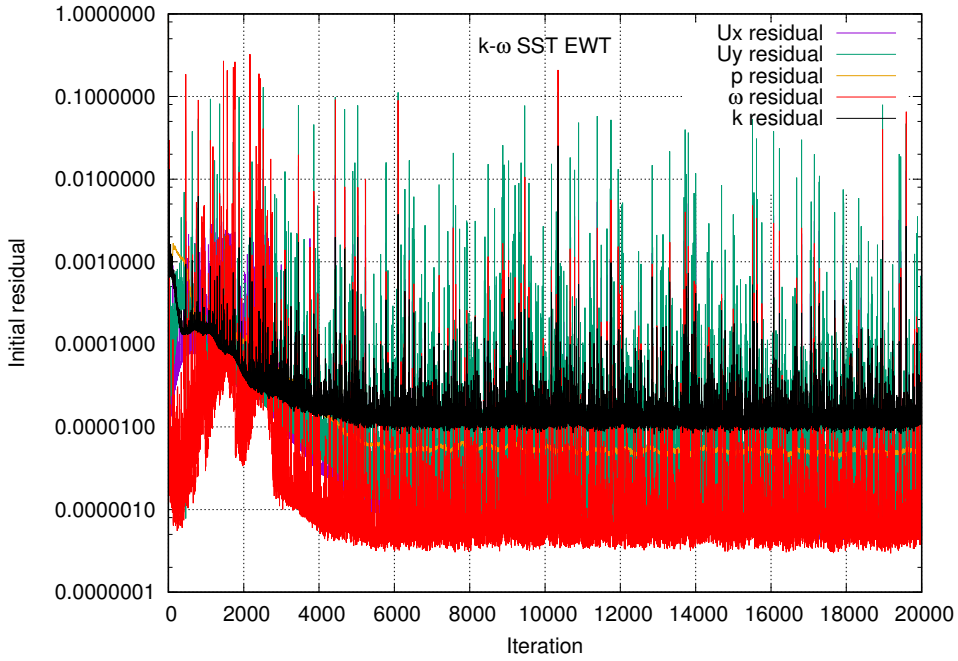

Figure 5.27: GRID-B: residual plot of the enhanced wall treatment for the $k-\omega$ SST model for the NACA4412.

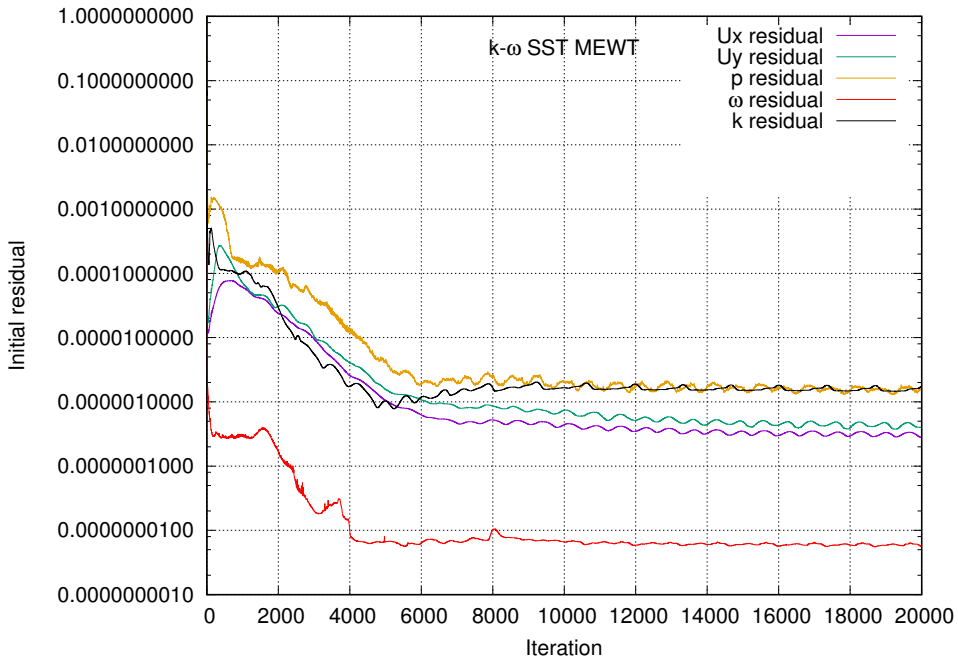

Figure 5.28: GRID-B: residual plot of the modified enhanced wall treatment for the $k-\omega$ SST model for the NACA4412.

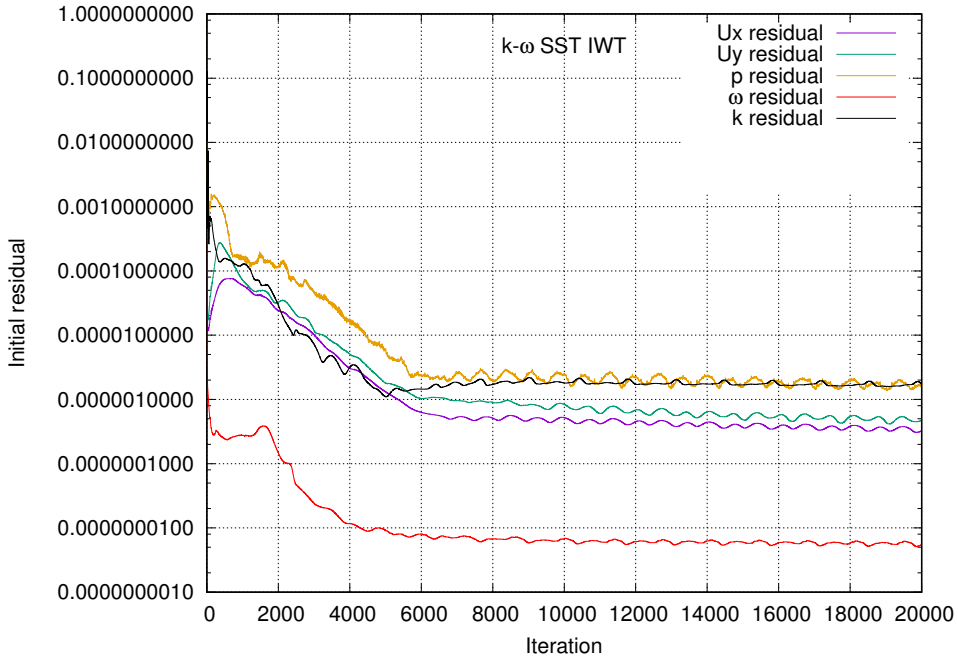

Figure 5.29: GRID-B: residual plot of the improved wall treatment for the $k-\omega$ SST model for the NACA4412.

From the presented results, it can be concluded that the calculated pressure distribution mainly depends on the near-wall grid spacing.The skin friction, which also depends on the grid resolution, additionally depends on the turbulence model and the choice of the wall treatment.
Comparing the results of skin friction coefficient from the HRN and LRN approach, it can be noticed that HRN approach around the leading edge follows the trends of the experimental data much more accurately that LRN approach. As if the formulation of the near-wall turbulence, mixing-length formulation, is in much better agreement with the physics than the formulation of $k-\omega$ SST turbulence model itself. Additionally, results for skin friction of the Spalart-Allmaras turbulence model (Fig. 5.15) are particularly interesting. Spalart-Allmaras is in much better agreement with the HRN approach than with the LRN formulation of the $k-\omega$ SST model.
The best results for skin friction in HRN approach are obtained by the $k-\varepsilon$ model, both with the standard and non-equilibrium wall functions. However, wall functions of the $k-\varepsilon$ model are not able to predict the sharp peak of the pressure coefficient at the stagnation point, which in the end results with the lower drag, Figure 5.16.
Of all of the presented wall treatments of $k-\omega$ SST model, modified enhanced wall treatment gives the best results and current implementation the worst.

In [35], much better agreement with the experimental data is presented. Moreover, results perfectly match the experimental data. But there, different turbulence models are tested, RNG $k-\varepsilon$, $k-\varepsilon$ realisable and RSM model for which the author [35] notes to have a superior performance for flows with strong streamline curvature. In our results, $k-\omega$ SST model fails exactly in this region, around leading edge of an aerofoil.

5.2 Prolate Spheroid

Analysis of the flow field around a 6:1 prolate spheroid, $L = 1.37$ m long, at 10 degrees angle of attack is performed. Reynolds number based on the long-axis of the prolate spheroid is set to $Re_L = 4.2 \cdot 10^6$. Results are compared with the experimental data [37] for skin friction coefficient given in circumferential direction along prolate spheroid at at cross-sections: $x/L = 0.6$ and $x/L = 0.772$. Experiment was performed by fixing an onset of transition at $x/L = 0.2$ which in simulation is modelled by setting the ${\nu_t}^w = 0$ up to the trip location. For lowering the computational demands, symmetry boundary condition is used. This also improves convergence, as the symmetry itself imposes additional averaging on the flow. For the freestream eddy viscosity ratio a value of $\beta = 5$ is taken, and turbulence intensity is set to $I = 0.03$ based on experimental data.

In the study, two structured grids are used, First named as GRID-A for HRN approach and second, GRID-B for LRN approach. Both of them have 157 points along the surface major axis and in the circumferential direction 71 points. Points are additionally clustered towards the sampling regions, $x/L = 0.6$ and $x/L = 0.772$. The height of the wall adjacent cells for GRID-A is 10^{-3} and $5 \cdot 10^{-5}$ for GRID-B. The far-field boundary for both grids is distanced approximately 9 m from the surface of the prolate spheroid. In figure 5.30, the grid used in the LRN approach is show, and figure 5.31 shows the defined coordinate system at cross-sections $x/L =$const. Mesh quality parameters are listed in Table 5.2.

Table 5.2: Prolate spheroid: mesh quality data for the GRID-A and GRID-B.

	GRID-A	GRID-B
Number of volumes	907920	883820
Max aspect ratio	866.92	3356.36
Max non-orthogonality	5.25 (average: 0.87)	34.86 (average: 1.20)
Max skewness	0.324575	0.393202

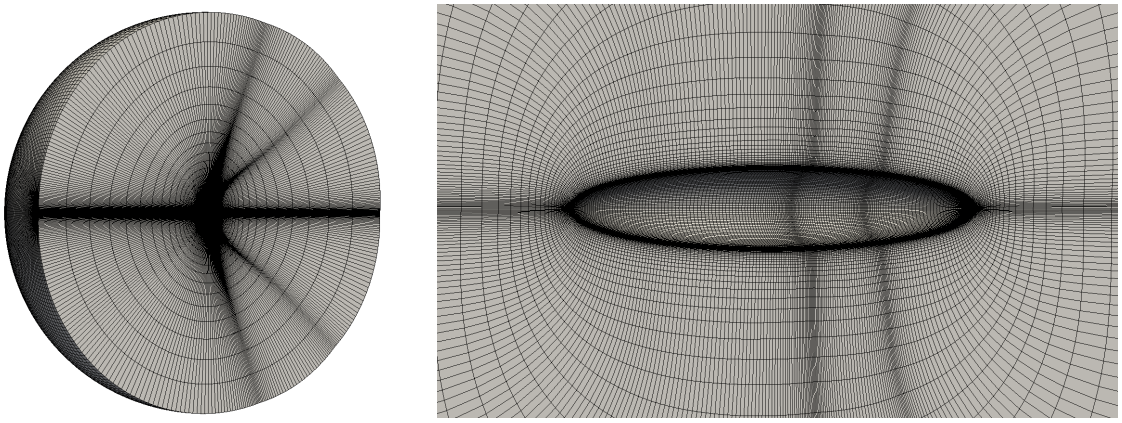

(a) **(b)**

Figure 5.30: GRID-B for LRN approach: **(a)** Complete computational domain for the prolate spheroid, **(b)** close view of the near-wall grid.

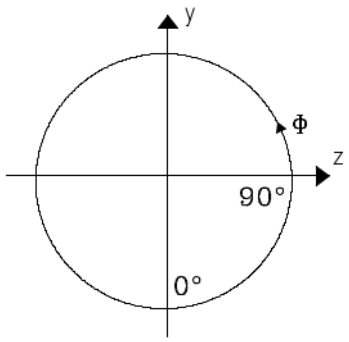

Figure 5.31: Coordinate system for cross-sections $x/L = \text{const}$.

5.2.1 Results

Results for the prolate spheroid are presented in the same manner as for NACA4412. Figures 5.44 to 5.33 show the skin friction coefficient at two cross-sections, $x/L = 0.6$ and $x/L = 0.772$ and corresponding values of y^+ and y^*. From presented, it can be seen that on LRN approach all methods perform relatively the same. For the case of HRN approach, standard wall function of $k-\varepsilon$ model and the current wall treatment of $k-\omega$ SST model deviate significantly from the results of other methods, Fig. 5.33 and 5.39. For the wall treatment of $k-\omega$ SST model, currently implemented in `foam-extend`, testing showed that the method fails on coarser grids in cases of lower velocity gradients which in the end are responsible for

the production of turbulent kinetic energy, expression (3.35). The production term is defined with a sharp switching behaviour(4.102) and the flow with a lower velocity gradients in the end result with the similar sharp switching behaviour in results of the skin friction coefficient, y^+ and y^*. This can be seen in Fig. 5.33, 5.35 and 5.37. Replacing the expression for production (4.102) with the blended value (4.107), which results in the improved wall treatment method, greatly improves results. To further illustrate this, Figure 5.32 shows the distribution of the skin friction coefficient along the surface of the prolate spheroid obtained with the improved wall treatment, for both HRN and LRN approaches in comparison to results obtained with the wall treatment currently in `foam-extend` on HRN approach.

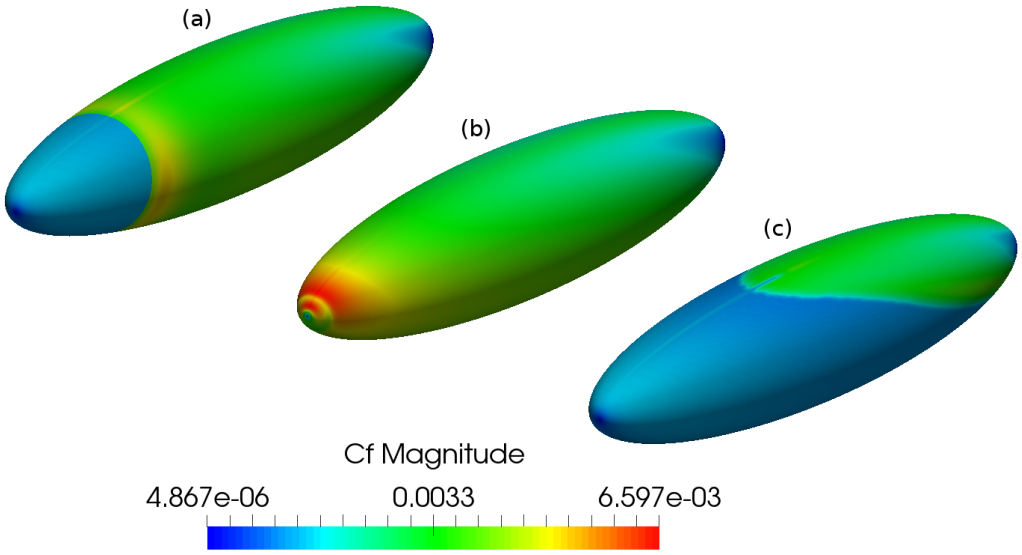

Figure 5.32: Skin friction distribution for the prolate spheroid: **(a)** improved wall treatment-HRN approach, **(b)** improved wall treatment-LRN approach, **(c)** wall treatment in `foam-extend`-HRN approach.

Sharp switching behaviour in the production term (4.98) in the case of standard wall functions for $k-\varepsilon$ model is not pronounced in this tests. The author believes that the reason for this is the well-known large non-physical over-production of the turbulent kinetic energy of $k-\varepsilon$ model at the impingement point.

The rest of the results are given in the following diagrams.

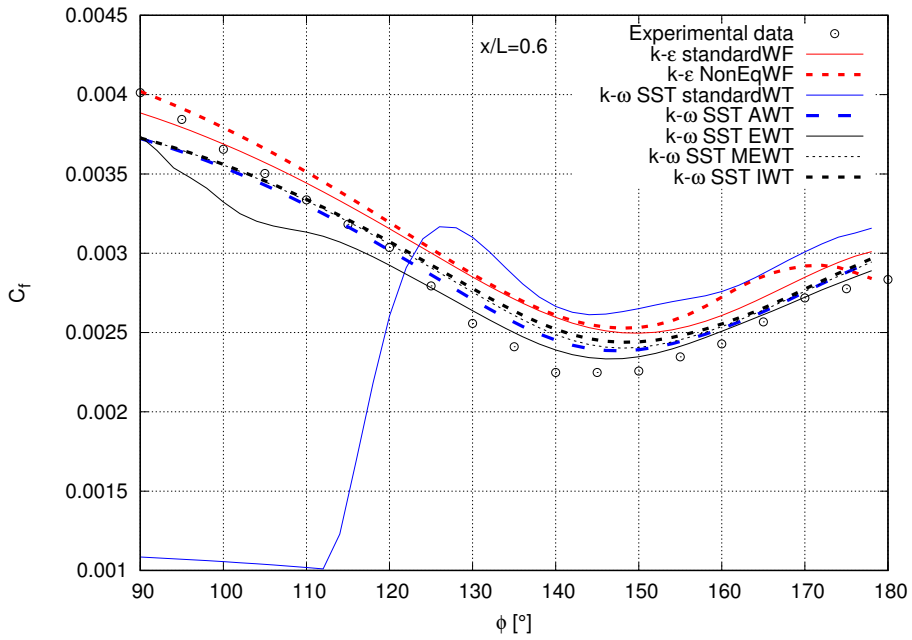

Figure 5.33: GRID-A: skin friction coefficient distribution on the prolate spheroid at $x/L = 0.6$.

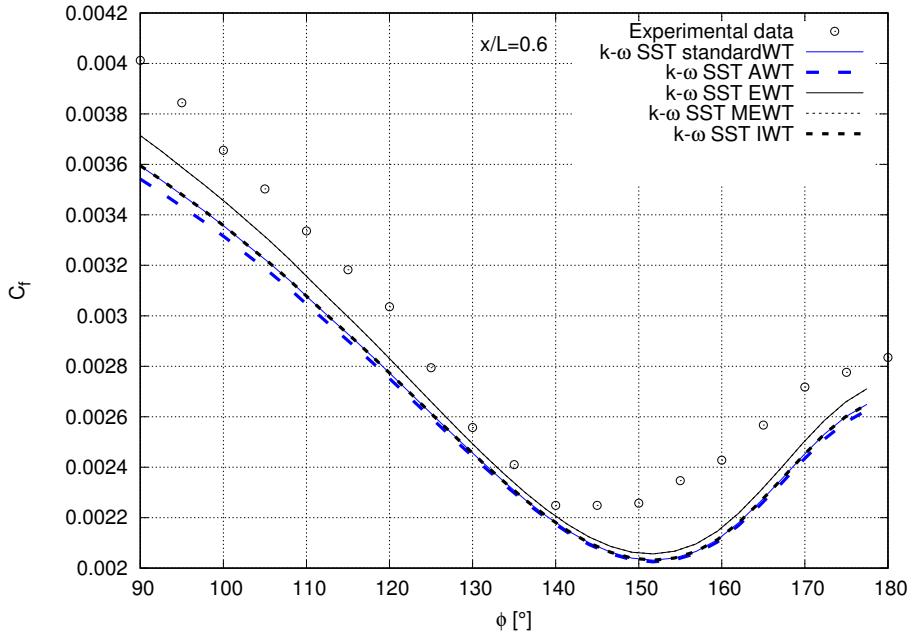

Figure 5.34: GRID-B: skin friction coefficient distribution on the prolate spheroid at $x/L = 0.6$.

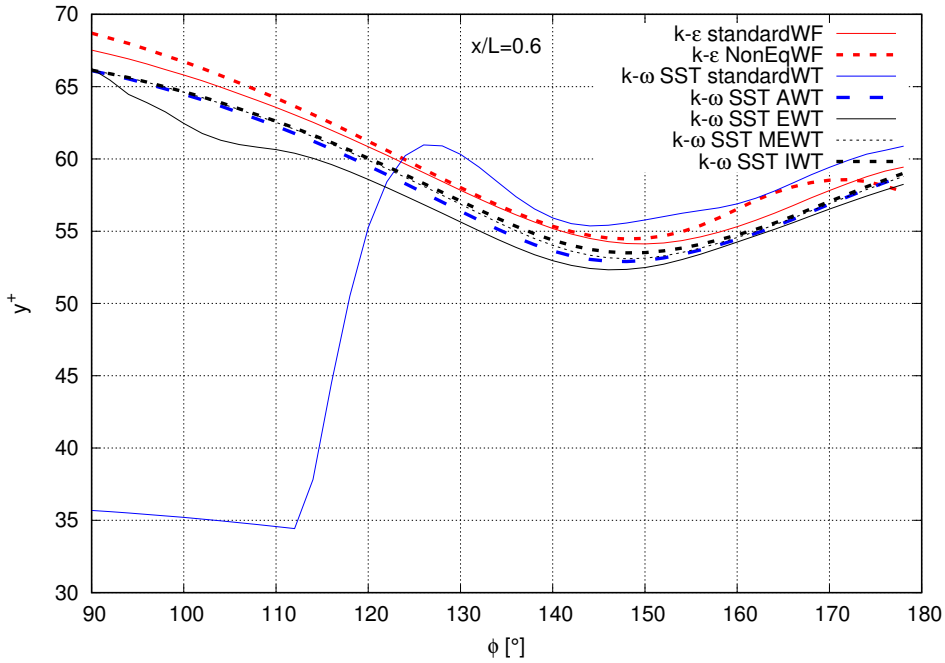

Figure 5.35: GRID-A: y^+ distribution on the prolate spheroid at $x/L = 0.6$.

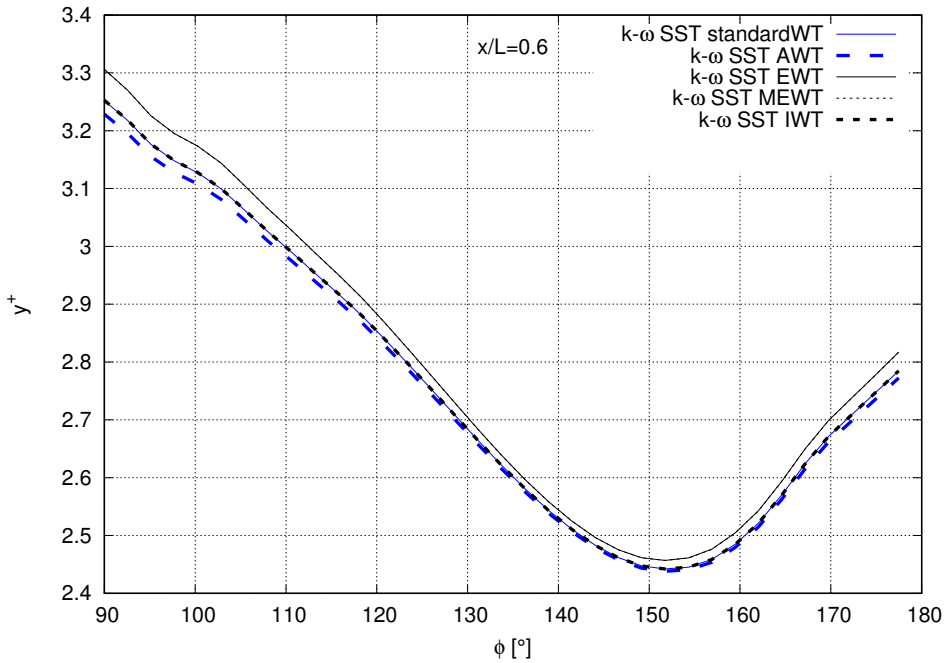

Figure 5.36: GRID-B: y^+ distribution on the prolate spheroid at $x/L = 0.6$.

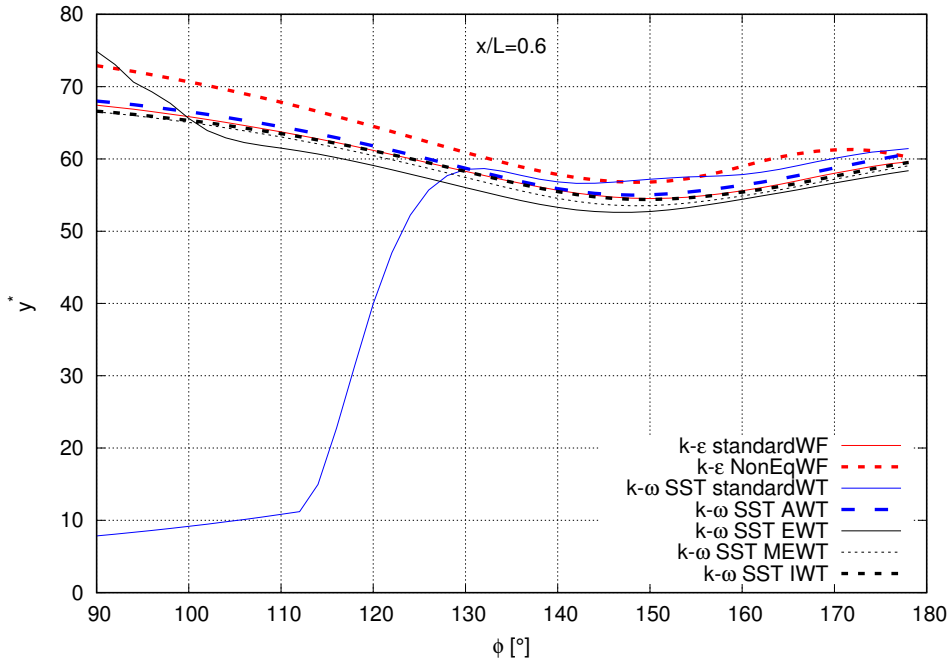

Figure 5.37: GRID-A: y^* distribution on the prolate spheroid at $x/L = 0.6$.

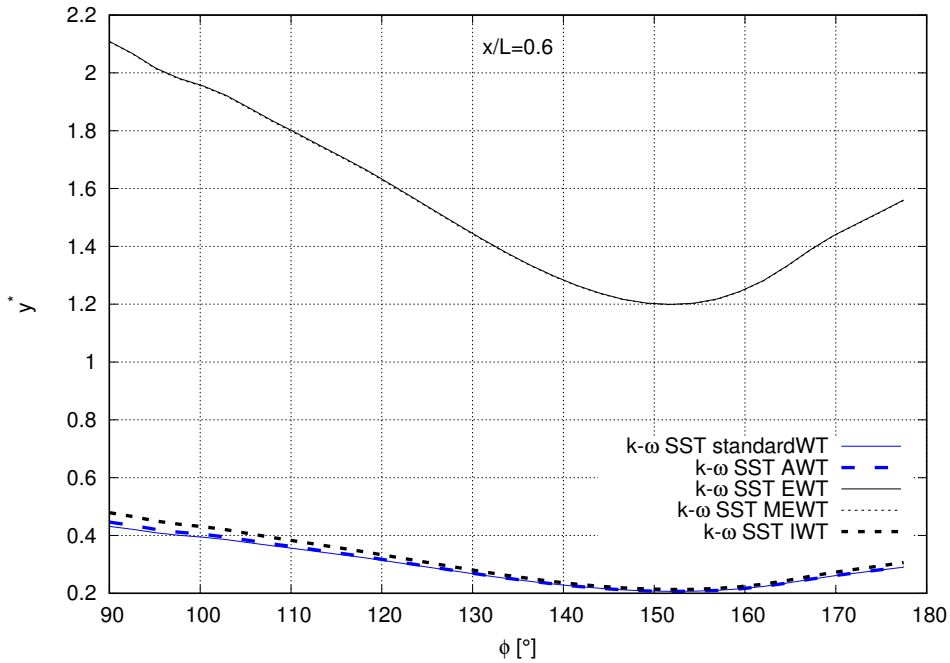

Figure 5.38: GRID-B: y^* distribution on the prolate spheroid at $x/L = 0.6$.

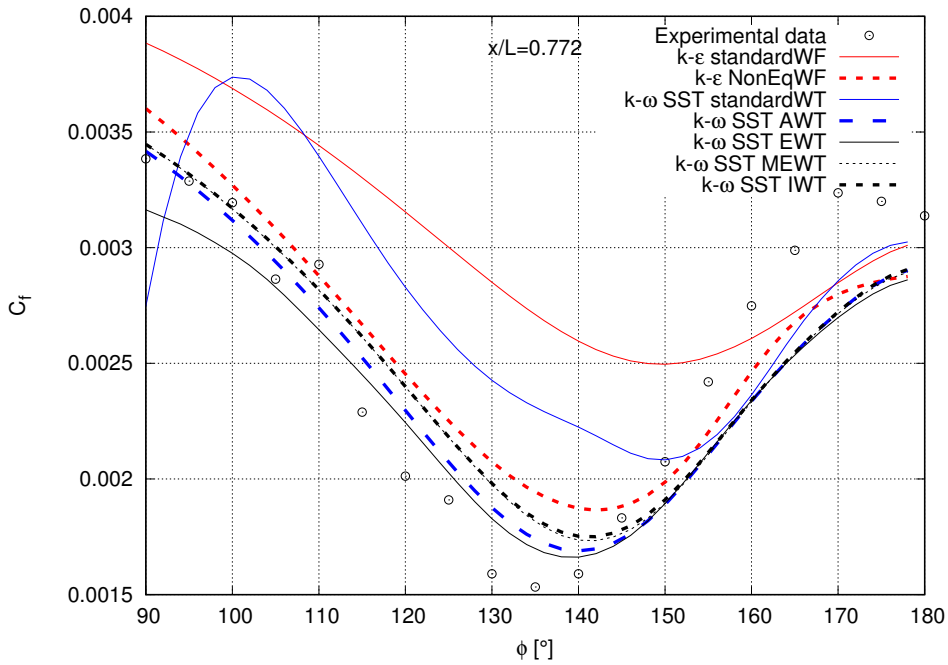

Figure 5.39: GRID-A: skin friction coefficient distribution on the prolate spheroid at $x/L = 0.772$.

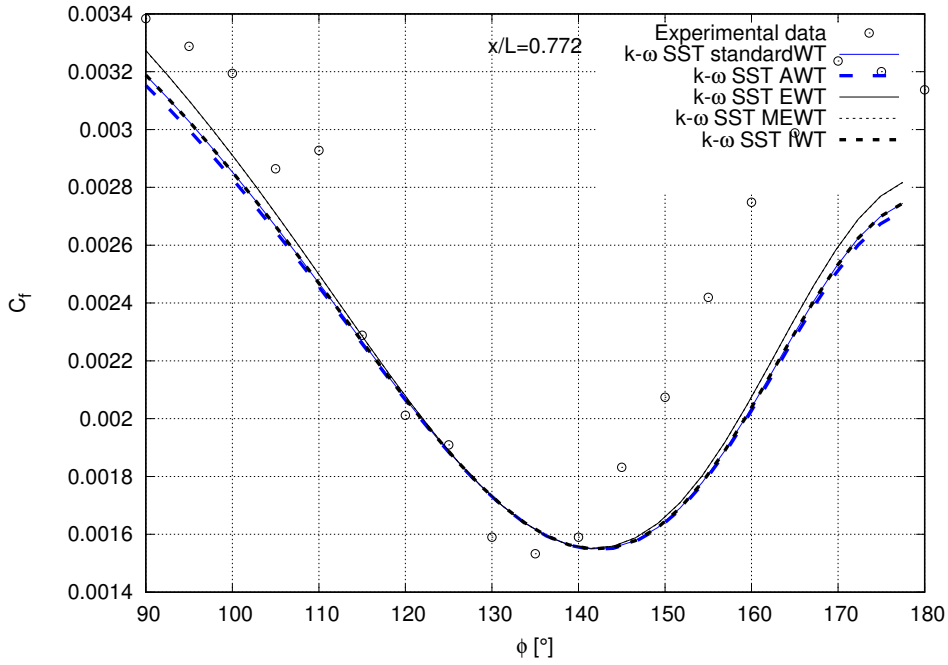

Figure 5.40: GRID-B: skin friction coefficient distribution on the prolate spheroid at $x/L = 0.772$.

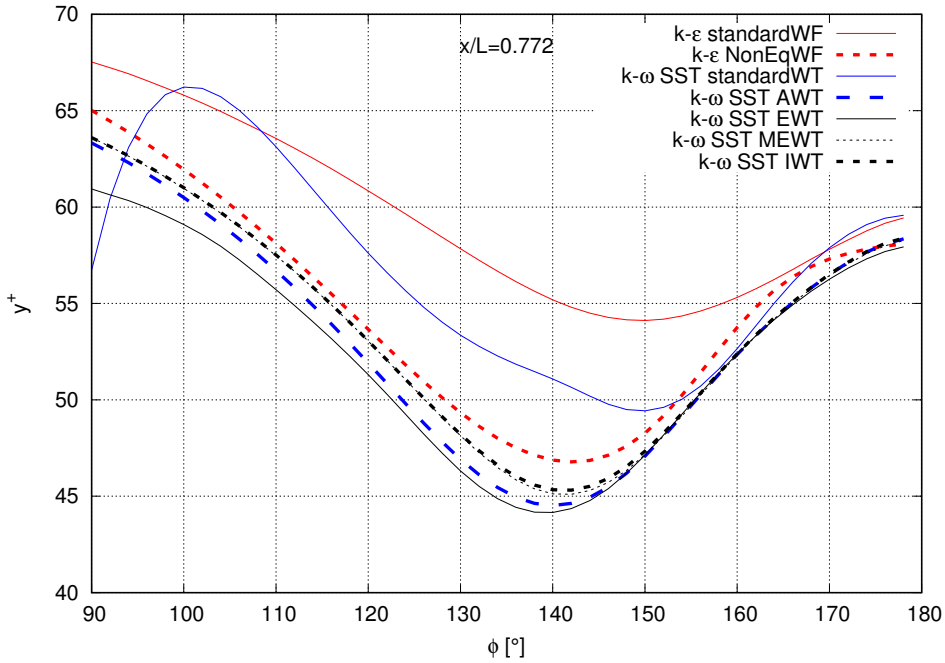

Figure 5.41: GRID-A: y^+ distribution on the prolate spheroid at $x/L = 0.772$.

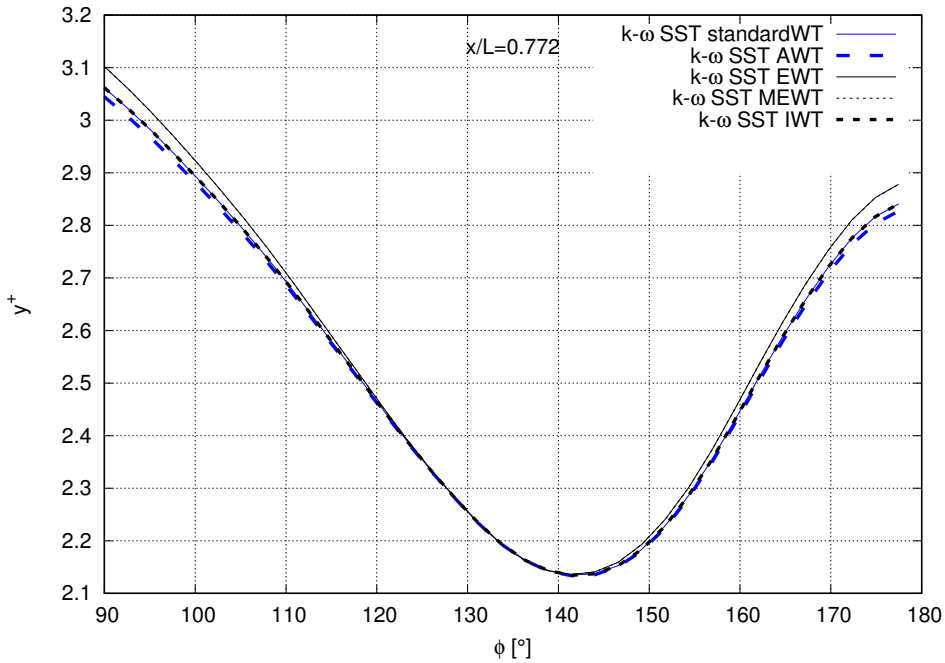

Figure 5.42: GRID-B: y^+ distribution on the prolate spheroid at $x/L = 0.772$.

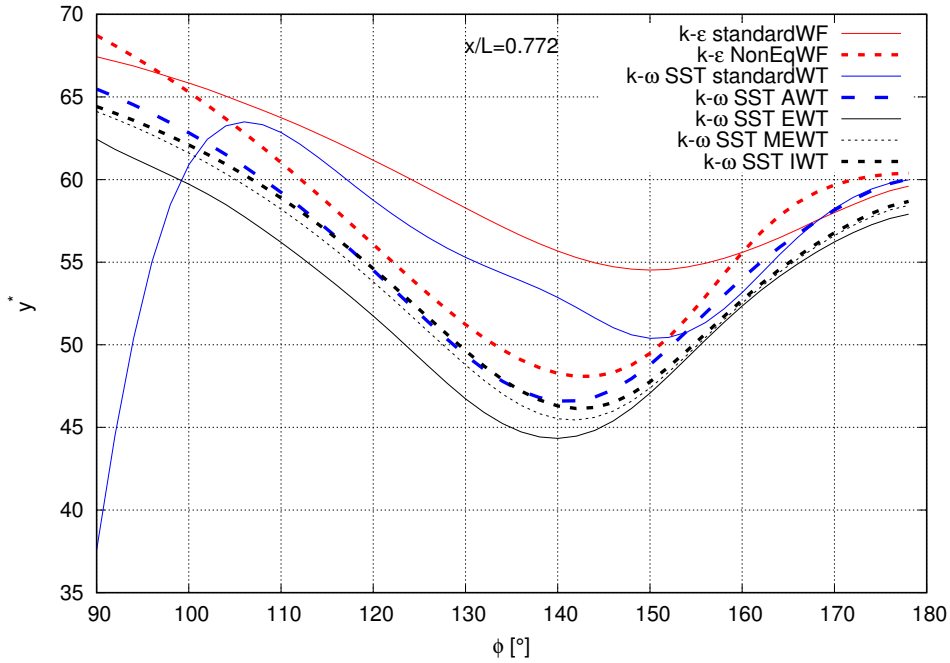

Figure 5.43: GRID-A: y^* distribution on the prolate spheroid at $x/L = 0.772$.

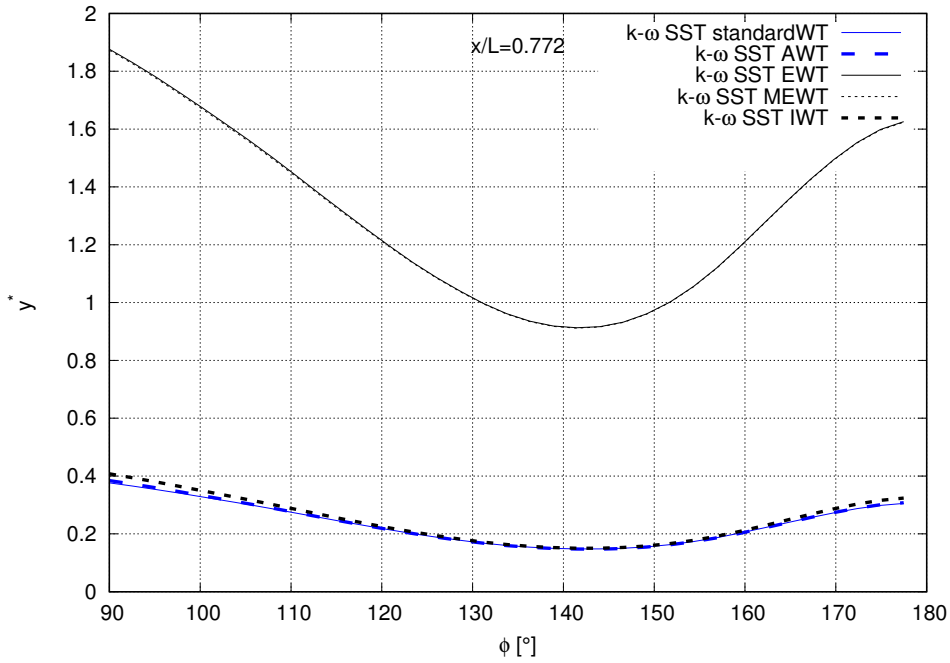

Figure 5.44: GRID-B: y^* distribution on the prolate spheroid at $x/L = 0.772$.

For this test case, drag coefficient is defined as $C_d = F/0.5\rho U_\infty{}^2 L^2$ and its convergence rate can be seen in Figures 5.45 and 5.46. For both the HRN and the LRN approach, results are in a close agreement, except for the enhanced wall treatment, with an oscillating behaviour in the LRN

approach. Residual plot of all methods is shown on Figures 5.47 to 5.58. From the presented results it can be seen that in the case of the prolate spheroid, oscillating behaviour in residuals of the non-equilibrium wall functions is not present(Fig. 5.48). As already mentioned, this requires further analysis.

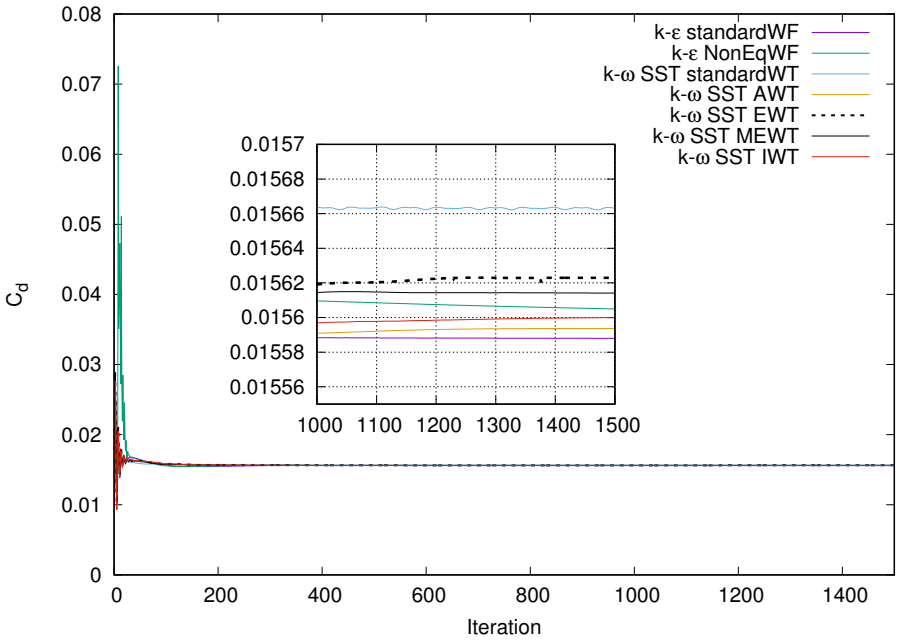

Figure 5.45: GRID-A: convergence of the drag coefficients for the prolate spheroid.

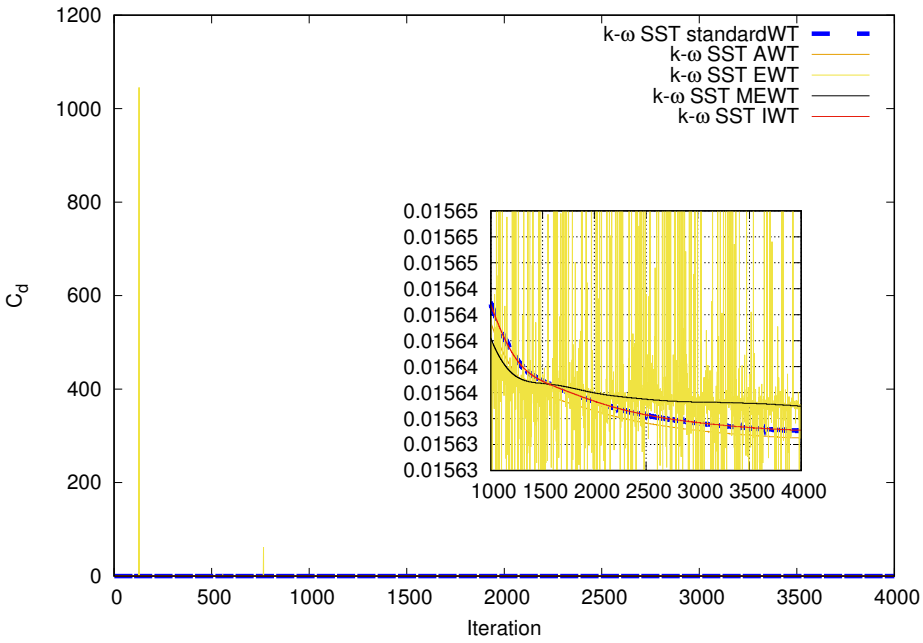

Figure 5.46: GRID-B: convergence of the drag coefficients for the prolate spheroid.

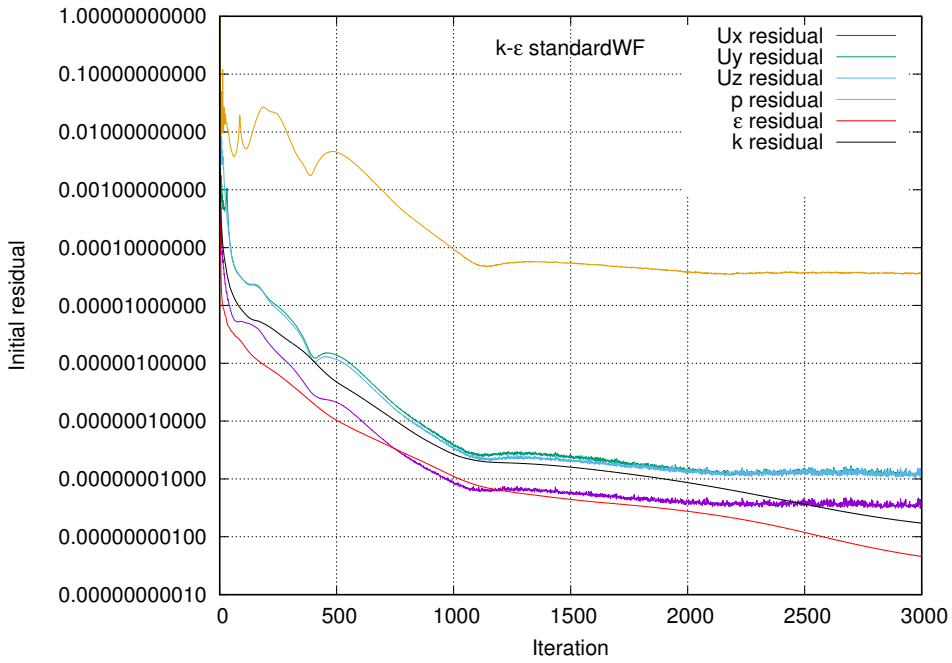

Figure 5.47: GRID-A: residual plot of the standard wall functions for $k-\varepsilon$ for the prolate spheroid.

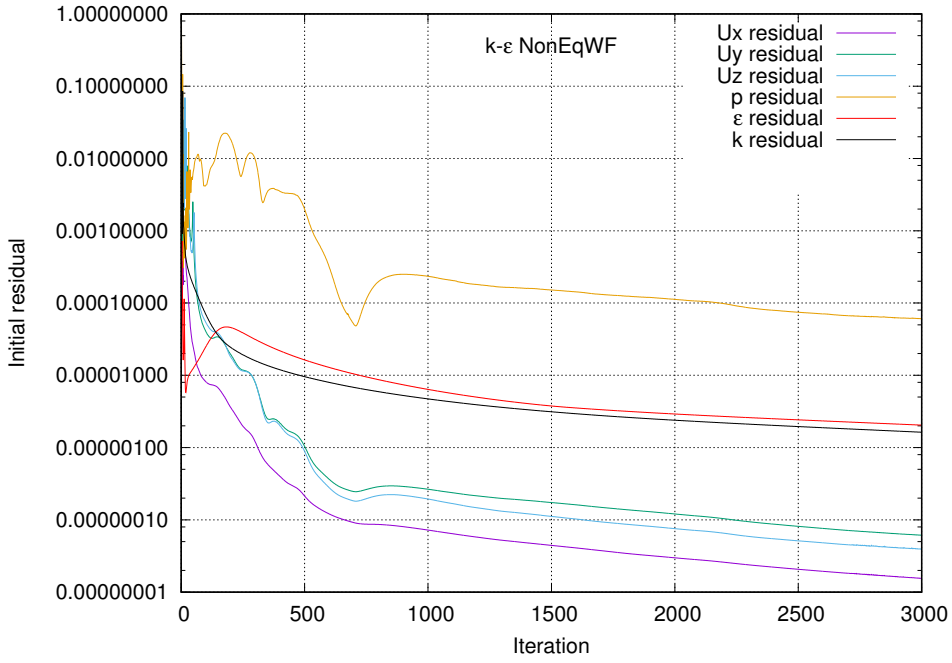

Figure 5.48: GRID-A: residual plot of the non-equilibrium wall functions for $k-\varepsilon$ model for the prolate spheroid.

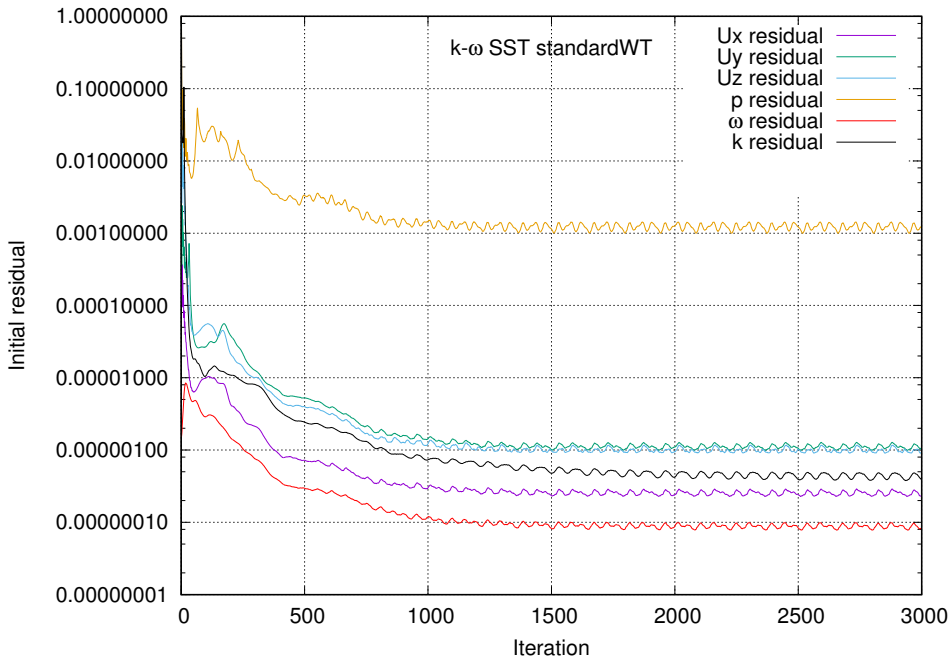

Figure 5.49: GRID-A: residual plot of the current wall treatment for $k-\omega$ SST model for the prolate spheroid.

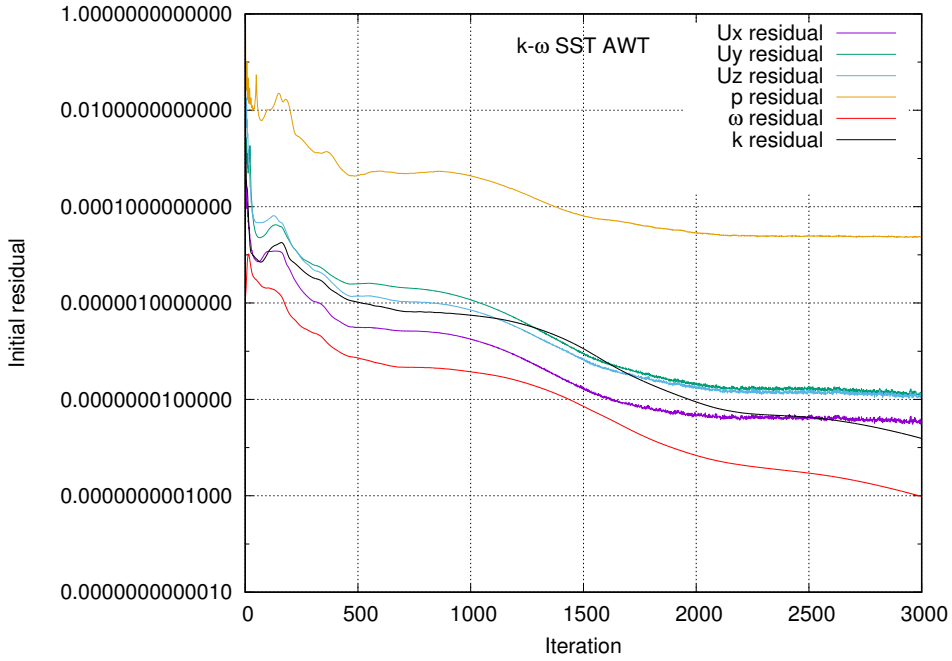

Figure 5.50: GRID-A: residual plot of the automatic wall treatment for $k-\omega$ SST model for the prolate spheroid.

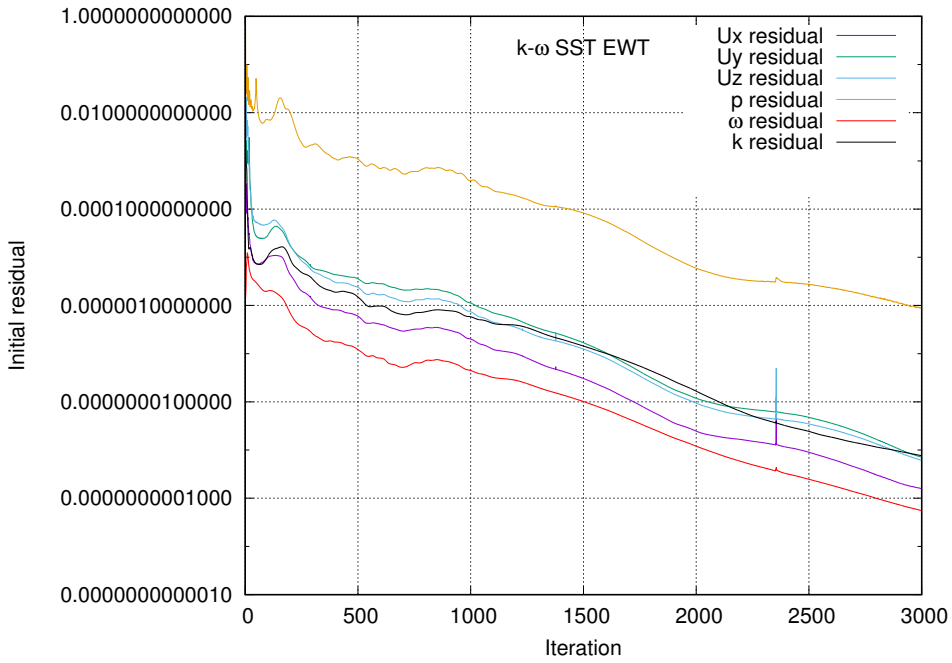

Figure 5.51: GRID-A: residual plot of enhanced wall treatment for $k-\omega$ SST model for the prolate spheroid.

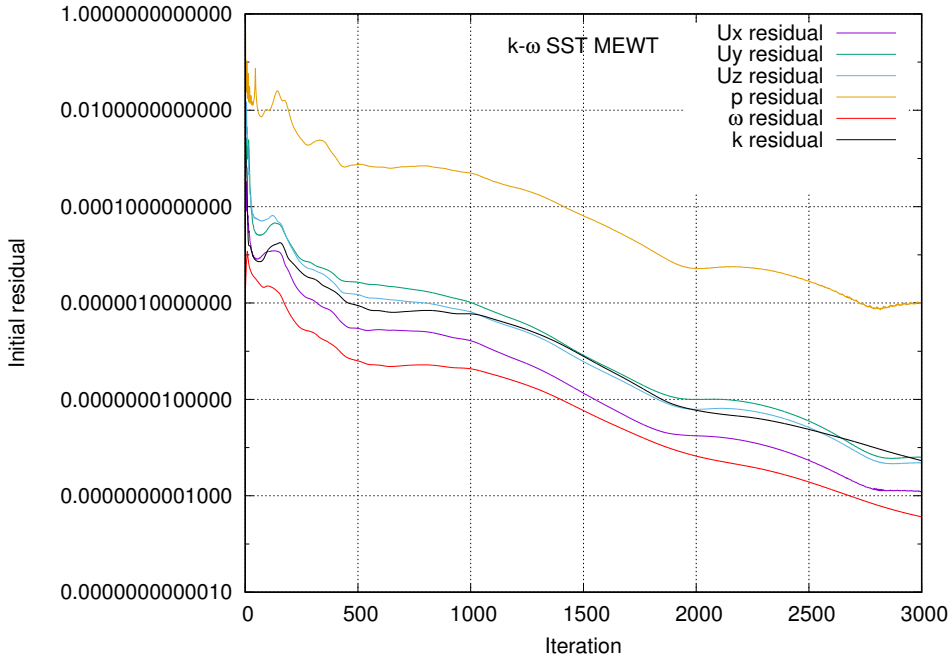

Figure 5.52: GRID-A: residual plot of modified enhanced wall treatment for the $k-\omega$ SST model for the prolate spheroid.

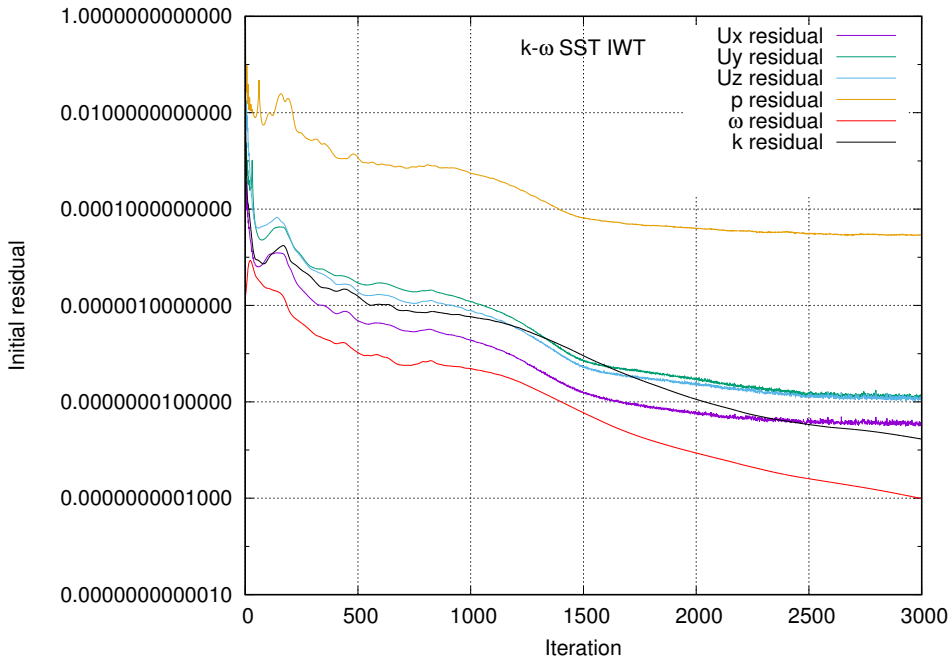

Figure 5.53: GRID-A: residual plot of the improved wall treatment for $k-\omega$ SST model for the prolate spheroid.

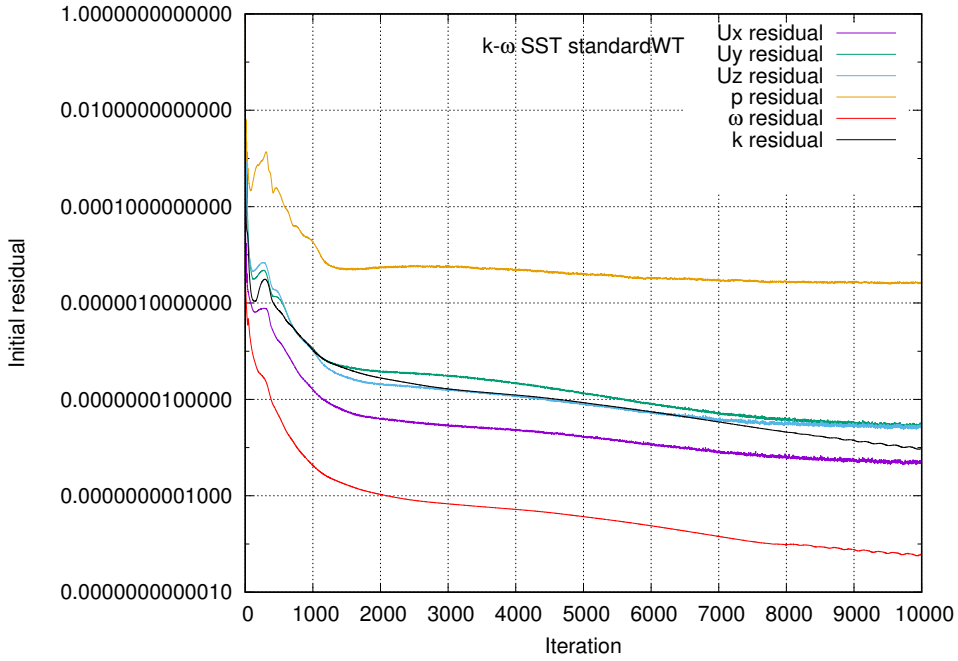

Figure 5.54: GRID-B: residual plot of the current wall treatment for $k-\omega$ SST model for the prolate spheroid.

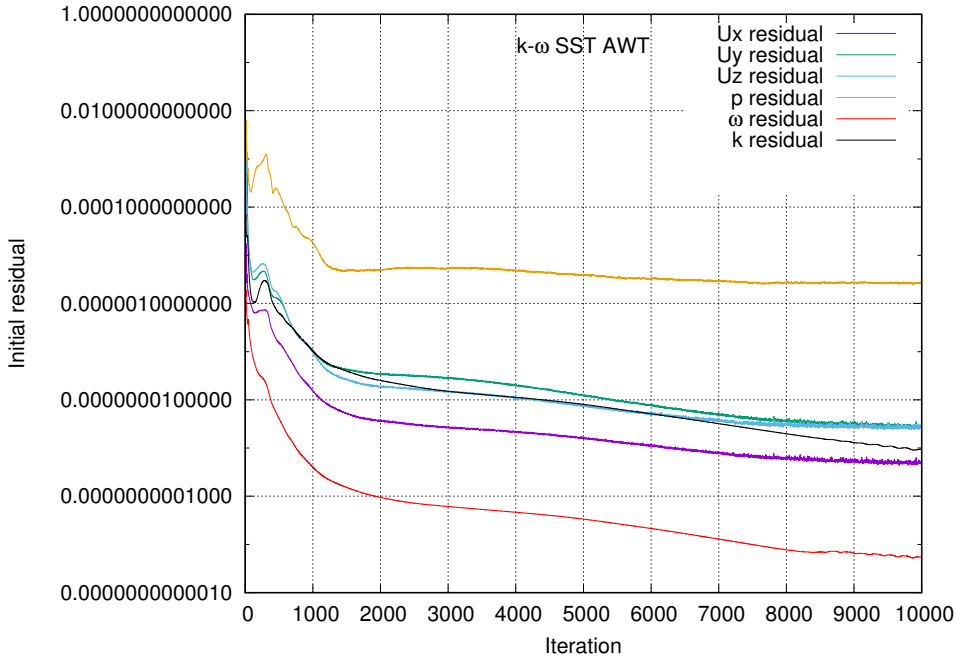

Figure 5.55: GRID-B: residual plot of the automatic wall treatment for $k-\omega$ SST model for the prolate spheroid.

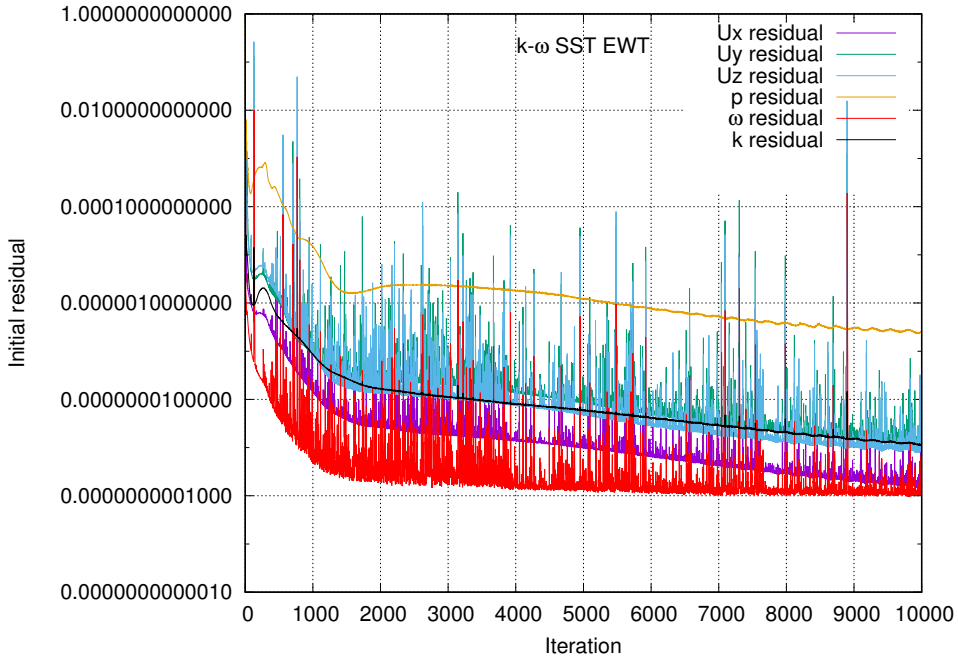

Figure 5.56: GRID-B:residual plot of enhanced wall treatment for $k-\omega$ SST model for the prolate spheroid.

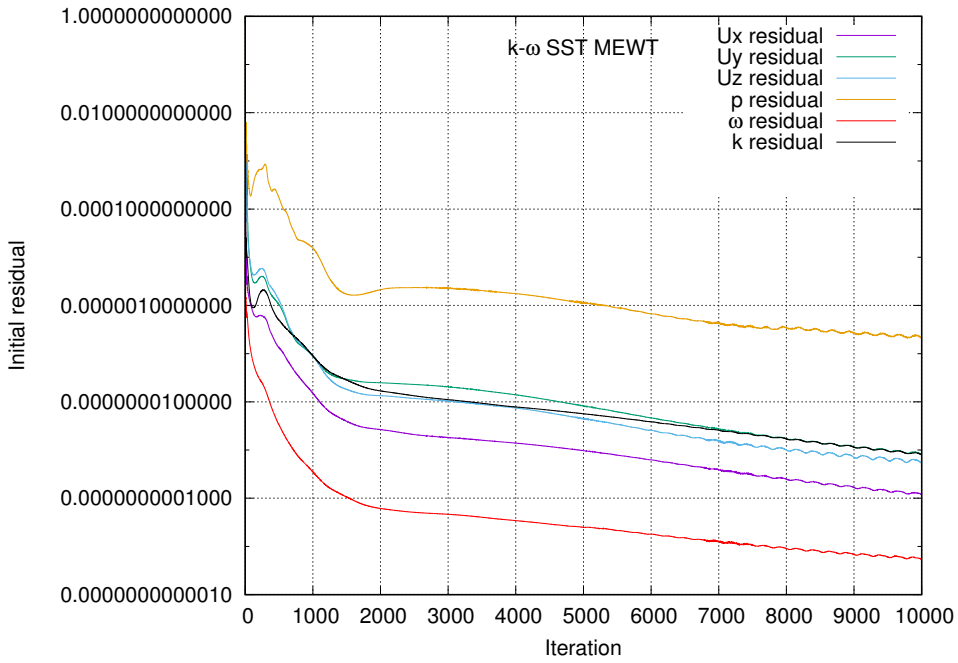

Figure 5.57: GRID-B: residual plot of modified enhanced wall treatment for the $k-\omega$ SST model for the prolate spheroid.

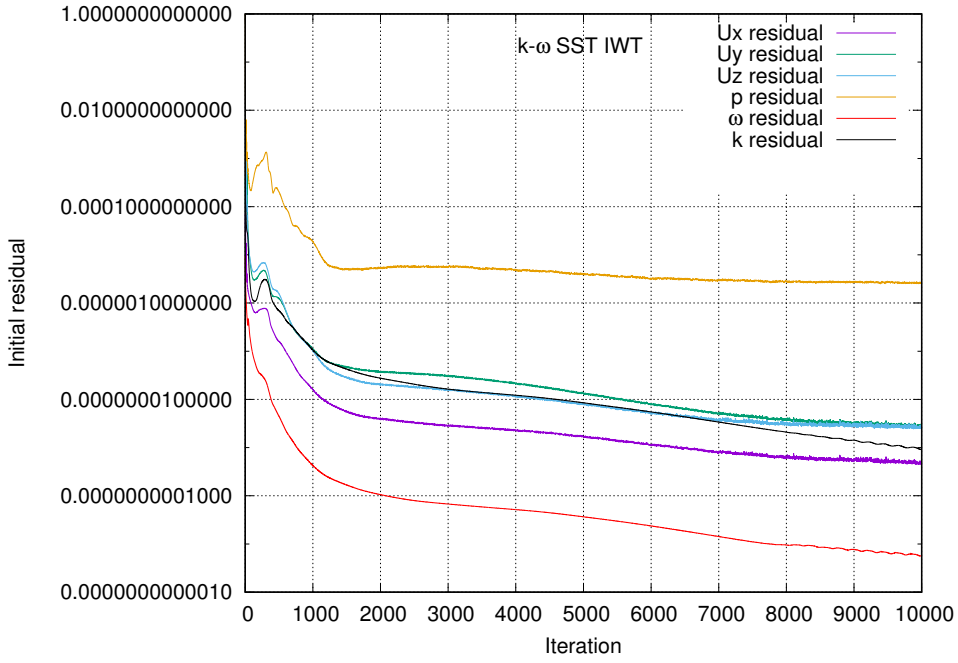

Figure 5.58: GRID-B: residual plot of the improved wall treatment for $k-\omega$ SST model for the prolate spheroid.

Flow over prolate spheroid is a particularly challenging task for any turbulence model [24], especially for RANS. The main goal here is to test how the assumptions of wall-parallel two-dimensional flow and mixing-length hypothesis hold in a case of a three-dimensional flow. Additionally, a concern is whether the turbulence model itself (LRN approach) is able to resolve this flow field. Following diagrams, Fig 5.59 and 5.60, make this comparison of HRN and LRN approach with experimental data for skin friction for modified enhanced wall treatment. As it can be seen, in some regions results of HRN approach are in a better agreement with the experimental data than results of LRN approach.

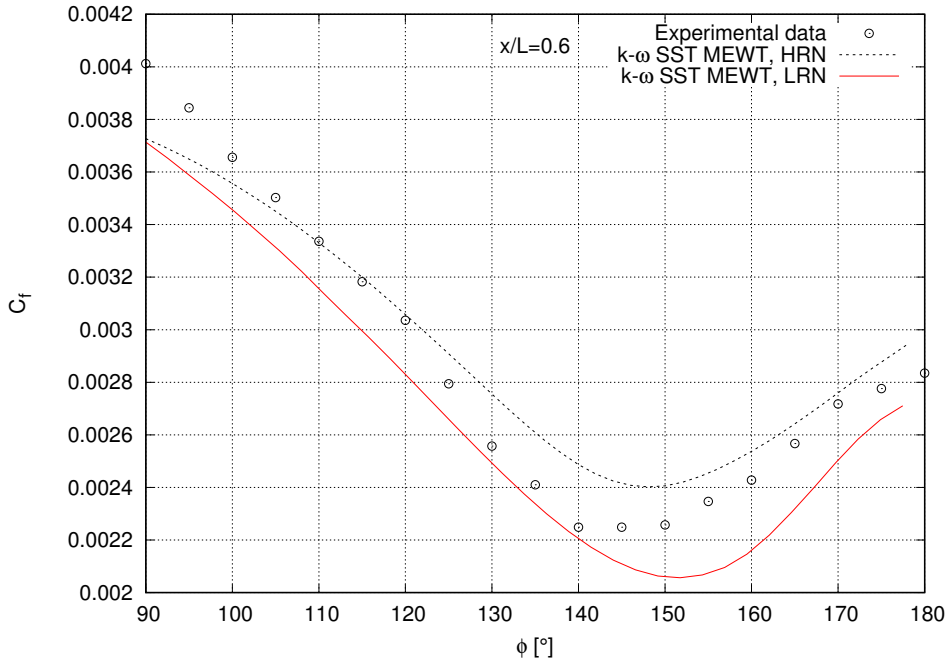

Figure 5.59: Comparison of the skin friction coefficient for the modified enhanced wall treatment for HRN and LRN approach with the experimental data at $x/L = 0.6$.

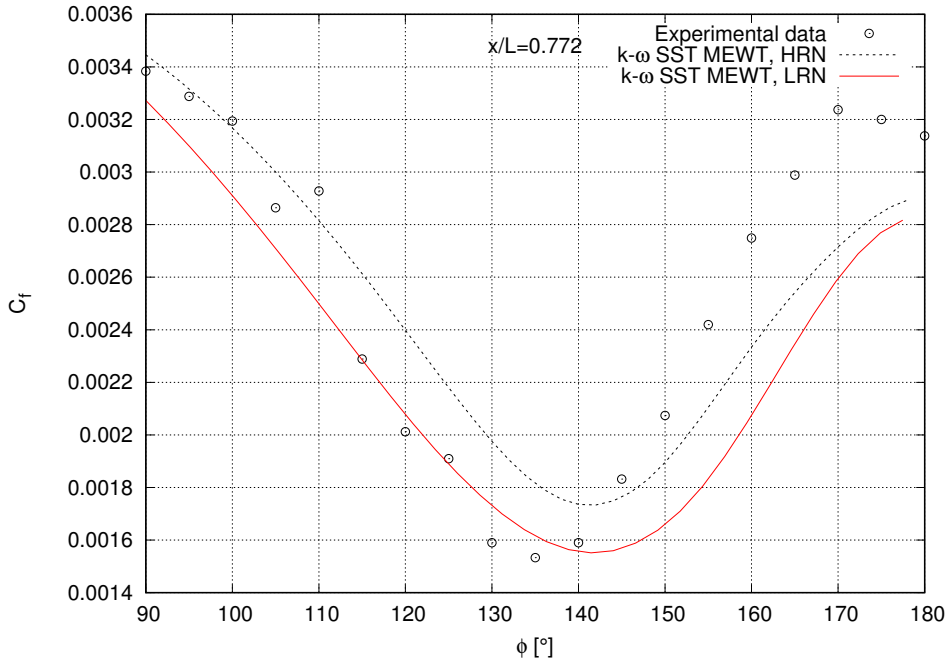

Figure 5.60: Comparison of skin friction for $k-\omega$ SST MEWT for the HRN and LRN approach with experimental data at $x/L = 0.772$.

Chapter 6

Benchmarking the Wall Functions and Wall Treatments

The previous chapter tested various methods for wall functions and wall treatments. The results are given in a context of an accuracy of obtained results when compared to experimental data and stability of convergence process. This chapter covers the analysis of the performance of wall functions and wall treatments in terms of a computational time. Tables 6.1 - 6.4 contain the time of each method needed to perform 500 iteration cycles (SIMPLE loops). This is found to be sufficient for the relative change in the total force F_{rel}, between two successive iterations $(\text{i}-1)$ and (i), to drop below 0.1% (see Fig. 6.1 - 6.4).

$$F_{\text{rel}} = \frac{|F_{\text{i}} - F_{\text{i}-1}|}{F_{\text{i}-1}}. \tag{6.1}$$

Furthermore, computational times in tables are given relative to the current implementation of the wall treatment for $k-\omega$ SST model. Computational time of enhanced wall treatment is not taken into account due to already shown high oscillations in forces and residuals of this method. All simulations are performed on a single-core desktop PC with an Intel Core i7-4820K CPU @ 3.70GHz with 16 GB of DDR3 memory.

In the case of the NACA4412 aerofoil, almost all methods show an increase in computational time, Tables 6.1 and 6.2. The highest one is for the modified enhanced wall treatment which in section 5.1 showed the best agreement with experimental data of all wall treatments for $k-\omega$

SST turbulence model. Differences in computational time are less pronounced for LRN approach, with the maximum increase being 5%, again for the modified enhanced wall treatment. Non-equilibrium wall functions for the $k-\varepsilon$ model are the only ones that resulted in lower computational time.

Table 6.1: GRID-A: computational time for the NACA4412

	Computational time	Relative computational time
$k-\varepsilon$ currentWF	102 s	1.11
$k-\varepsilon$ NonEqWF	89 s	0.97
$k-\omega$ SST currentWT	92 s	1
$k-\omega$ SST AWT	92 s	1
$k-\omega$ SST MEWT	103 s	1.12
$k-\omega$ SST Gnew	94 s	1.02

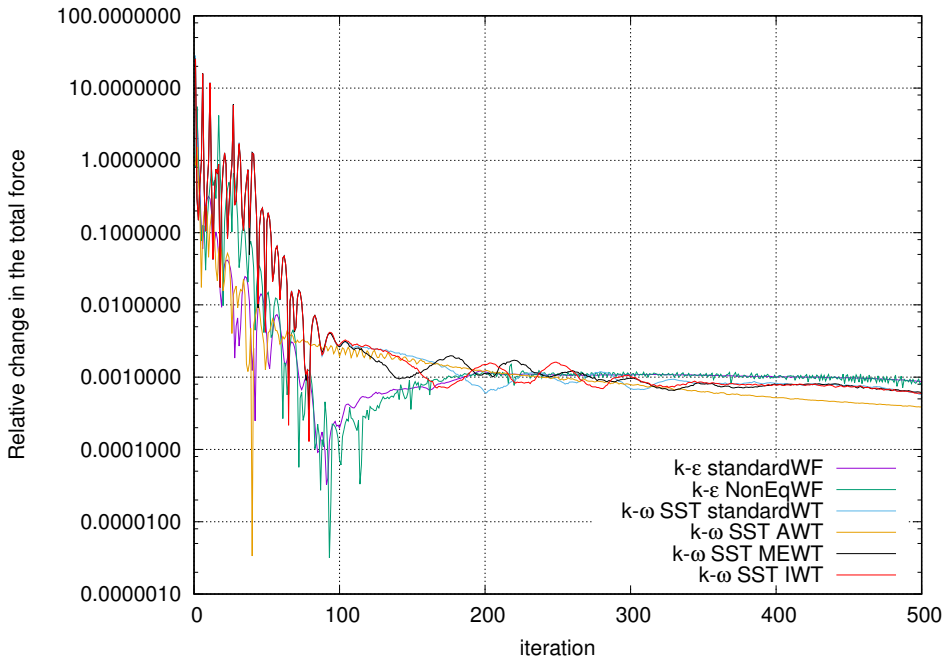

Figure 6.1: GRID-A: relative change in the total force for the NACA4412.

Table 6.2: GRID-B: computational time for the NACA4412

	Computational time	Relative computational time
$k-\omega$ SST currentWT	391 s	1
$k-\omega$ SST AWT	398 s	1.02
$k-\omega$ SST MEWT	410 s	1.05
$k-\omega$ SST Gnew	394 s	1.01

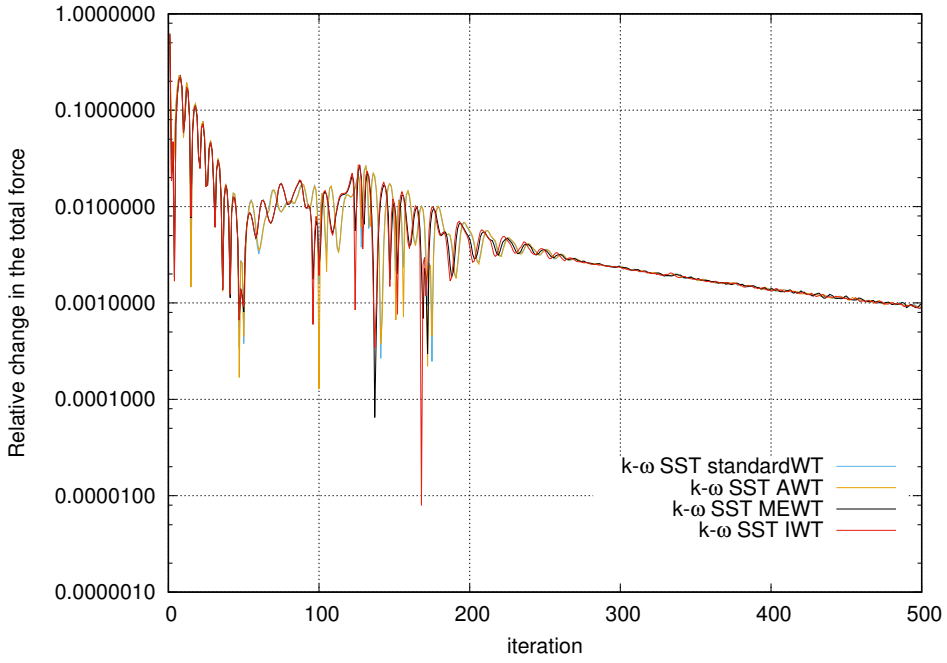

Figure 6.2: GRID-B: relative change in the total force for the NACA4412.

In the case of the prolate spheroid, different performance to the one obtained for the NACA4412 is achieved. Compared to the current implementation of the wall treatment in `foam-extend` for the $k-\omega$ SST model, all methods have a much lower computational time, Tables 6.3 and 6.4 , especially for HRN approach. The only exception here are the non-equilibrium wall functions which still performed faster, but only marginally. Once again, it is interesting to point out the performance of the improved wall treatment. Replacing the sharp switching behaviour of production term with the blended value, not only improved the predictions of skin friction

in HRN approach but also resulted in a four-time lower computational time compared to the previous formulation.

Table 6.3: GRID-A: computational time for the prolate spheroid

	Computational time	Relative computational time
$k-\varepsilon$ currentWF	2147 s	0.23
$k-\varepsilon$ NonEqWF	9040 s	0.97
$k-\omega$ SST currentWT	9343 s	1
$k-\omega$ SST AWT	2044 s	0.22
$k-\omega$ SST MEWT	3432 s	0.37
$k-\omega$ SST Gnew	2360 s	0.25

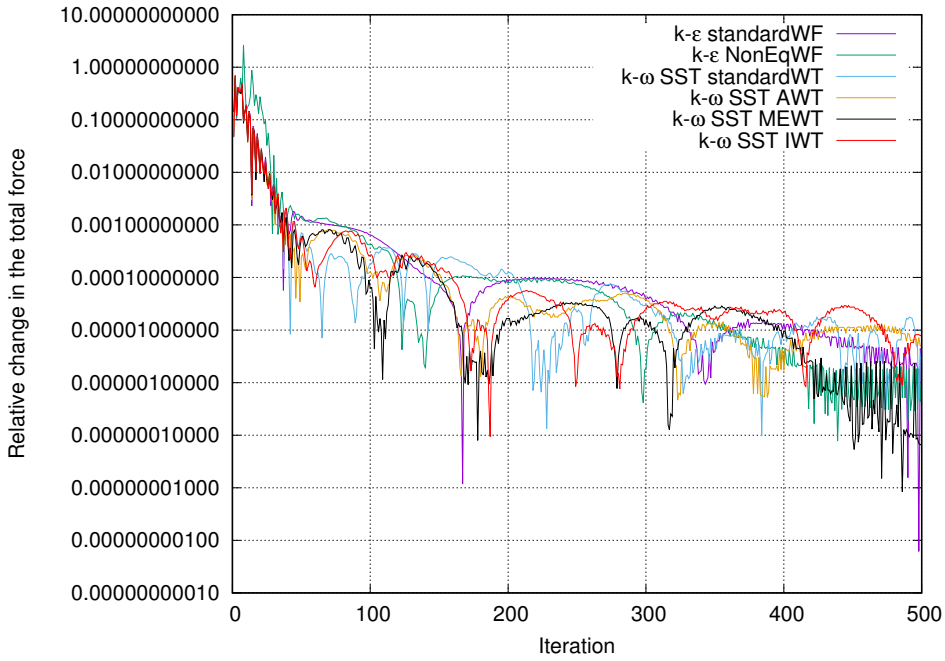

Figure 6.3: GRID-A: relative change in the total force for the prolate spheroid.

Table 6.4: GRID-B: computational time for the prolate spheroid

	Computational time	Relative computational time
$k-\omega$ SST currentWT	2582 s	1
$k-\omega$ SST AWT	1963 s	0.76
$k-\omega$ SST MEWT	2275 s	0.88
$k-\omega$ SST Gnew	1954 s	0.76

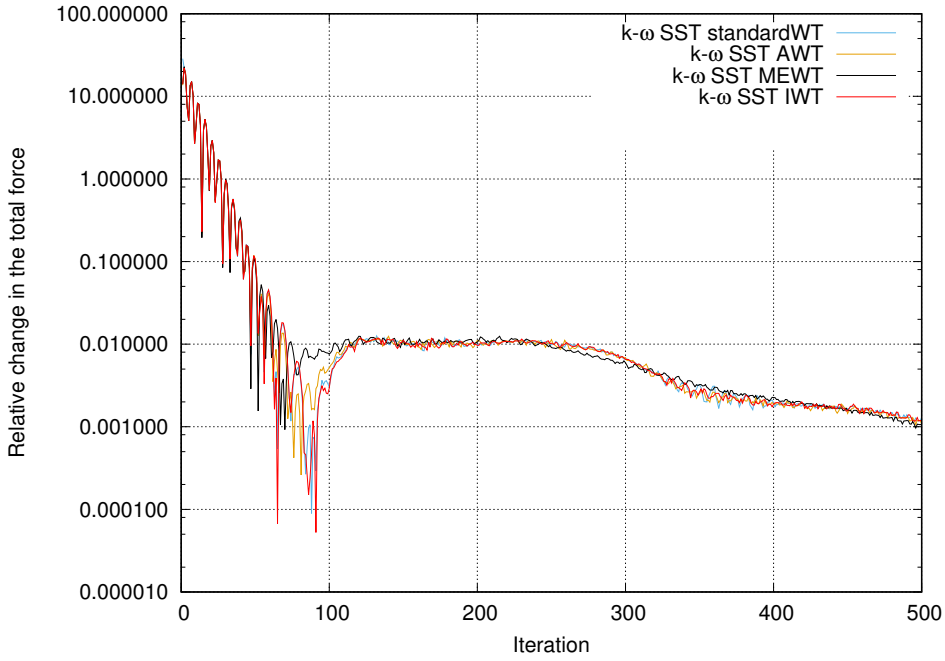

Figure 6.4: GRID-B: f relative change in the total force for the prolate spheroid.

Chapter 7

Conclusion

Wall functions and wall treatments for two-equation models, $k-\varepsilon$ [10] and $k-\omega$ SST [9] [1] [10], are presented, discussed and implemented in `foam-extend`. Newly implemented ones are tested against the current implementation in `foam-extend`. For the validation, two test cases are used, flow over NACA4412 and flow over 6:1 prolate spheroid.

Testing showed that the new implementations can serve as a good replacement for the ones currently in `foam-extend`. And although the results are not matching available experimental data perfectly, an improvement over current implementation of wall functions is clear. Additionally, a conclusion is reached that currently used wall treatment for $k-\omega$ SST model in `foam-extend` fail in regions of relatively low-velocity gradients when used in HRN approach. Furthermore, it is emphasised that in order to make a final conclusion, further testing should be conducted. For the present moment, testing showed that the non-equilibrium wall function for $k-\varepsilon$ models implemented in `foam-extend` improves accuracy and that they should be preferred to current ones. But, there is still a need to investigate strange oscillating behaviour in residuals in the case of flow past the NACA4412 aerofoil. For $k-\omega$ SST model, the choice falls on modified enhanced wall treatment which in the case of NACA4412 resulted in much greater accuracy compared to other methods and especially compared to the current implementation of wall treatments in `foam-extend`.

Bibliography

[1] G. H. White, F. M.; Christoph, "A simple theory for the two-dimensional compressible turbulent boundary layer," *Journal of Basic Engineering*, vol. 94, 1972.

[2] W. Jones and B. Launder, "The prediction of laminarization with a two-equation model of turbulence," *International Journal of Heat and Mass Transfer*, vol. 15, 1972.

[3] B. E. Launder and B. I. Sharma, "Application of the energy-dissipation model of turbulence to the calculation of flow near a spinning disc," *Letters in Heat and Mass Transfer*, vol. 1, 1974.

[4] F. Menter and T. Esch, "Elements of industrial heat transfer prediction," *16th Brazilian Congress of Mechanical Engineering (COBEM)*, Nov. 2001.

[5] F. R. Menter, M. Kuntz, and R. Langtry, *Ten Years of Industrial Experience with the SST Turbulence Model*. Begell House, Inc., 2003.

[6] A. Hellsten, "Some improvements in Menter's k-omega SST turbulence model. Fluid Dynamics and Co-located Conferences, American Institute of Aeronautics and Astronautics," 1998.

[7] D. C. Wilcox, *Turbulence modeling for CFD*. DCW Industries, Inc, 1993.

[8] S.-E. Kim and D. Choudhury, "A near-wall treatment using wall functions sensitized to pressure gradient," *Separated and complex flows- 1995*, pp. 273–280, 1995.

[9] Ansys, *ANSYS CFX-Solver Theory Guide*.

[10] Ansys, *ANSYS FLUENT Theory Guide*.

[11] B. Launder and D. Spalding, "The numerical computation of turbulent flows," *Computer Methods in Applied Mechanics and Engineering*, vol. 3, no. 2, pp. 269 – 289, 1974.

[12] C. C. Chieng and B. E. Launder, "On the calculation of turbulent heat transport downstream from an abrupt pipe expansion," *Numerical Heat Transfer*, vol. 3, no. 2, pp. 189–207, 1980.

[13] T. Craft, A. Gerasimov, H. Iacovides, and B. Launder, "Progress in the generalization of wall-function treatments," *International Journal of Heat and Fluid Flow*, vol. 23, pp. 148–160, 4 2002.

[14] M. Popovac and K. Hanjalic, "Compound wall treatment for rans computation of complex turbulent flows and heat transfer," *Flow, Turbulence and Combustion*, vol. 78, no. 2, p. 177, 2007.

[15] T. Craft, A. Gerasimov, H. Iacovides, and B. Launder, *Development and application of a new wall-function strategy*. 2001.

[16] T. J. Craft, S. E. Gant, H. Iacovides, and B. E. Launder, "Development and application of a new wall function for complex turbulent flows," *ECCOMAS*, 2001.

[17] O. J. Hinze, *Turbulence*. New York : McGraw-Hill Book Company, 1975., 2nd edition ed., 1975.

[18] T. Cebeci, *Analysis of turbulent flows*. Elsevier, 2nd rev. and expanded ed ed., 2004.

[19] R. B. Bird, W. E. Stewart, and E. N. Lightfoot, *Transport phenomena*. J. Wiley, 2nd, wiley international ed ed., 2002.

[20] J. L. L. Thomas B. Gatski, M. Yousuff Hussaini, *Simulation and modelling of turbulent flows*. Icase/Larc Series in Computational Science and Engineering, Oxford University Press, USA, 1996.

[21] G. A. Holzapfel, *Nonlinear Solid Mechanics: A Continuum Approach for Engineering*. Wiley, 1st ed., 2000.

[22] Wikipedia, "Navier-Stokes existence and smoothness- Wikipedia, the free encyclopedia." [Online; accessed 11-February-2017].

[23] S. B. Pope, *Turbulent Flows*. Cambridge University Press, 2000.

[24] Z. Xiao, Y. Zhang, J. Huang, H. Chen, and S. Fu, "Prediction of separation flows around a 6:1 prolate spheroid using rans/les hybrid approaches," *Acta Mechanica Sinica*, vol. 23, 08 2007.

[25] D. Randall, "Reynolds averaging," 2016.

[26] Z. Virag, M. Šavar, and I. Džijan, "Mehanika fluida ii." University Lectures, 2015.

[27] F. R. Menter, "Two-equation eddy-viscosity turbulence models for engineering applications," *AIAA Journal*, vol. 32, 08 1994.

[28] J. Bredberg, "On Two-equation Eddy-Viscosity Models," tech. rep., Chalmers University of Technology, Department of Thermo and Fluid Dynamics, 2001.

[29] L. Davidson, "An introduction to turbulence models," 2015.

[30] H. K. Versteeg and W. Malalasekera, *An introduction to computational fluid dynamics - the finite volume method*. Prentice Hall, 2nd ed., 2007.

[31] J. H. Ferziger and M. Peric, *Computational Methods for Fluid Dynamics*. Springer, 3rd ed., 2002.

[32] F. Moukalled, L. Mangani, and M. Darwish, *Fluid Mechanics and Its Applications, The Finite Volume Method in Computational Fluid Dynamics Volume 113*, vol. 10.1007/978-3-319-16874-6. 2016.

[33] F. R. Menter, J. C. Ferreira, T. Esch, and B. Konno, "The SST Turbulence Model with Improved Wall Treatment for Heat Transfer Predictions in Gas Turbines. In: Proceedings of the international gas turbine congress, Tokyo, IGTC2003-TS-059," 2003.

[34] Y. Saad, *Iterative methods for sparse linear systems*. Society for Industrial and Applied Mathematics, 2nd ed ed., 2003.

[35] O. Badran, R. Quadros, and F. Aldudak, "Two-equation turbulence models for turbulent flow over a naca 4412 airfoil at angle of attack 15 degree."

[36] ESI, "Guidelines for specification of turbulence at inflow boundaries." [Online; accessed 15-February-2017].

[37] DEPARTMENT OF AEROSPACE AND OCEAN ENGINEERING- Virginia Polytechnic Institute and State University, "Steady Flow Over a 6:1 Prolate Spheroid."